POLITECNICO DI TORINO

Master's degree course in Aerospace Engineering

Master's Degree Thesis

Study of the docking and collision avoidance manoeuvres for a CubeSat with a Mothercraft.

Supervisors:

Prof. Sabrina Corpino

Prof. Fabrizio Stesina

Candidate:

Caterina Speranza

Academic year 2020-2021

A mio nonno

Abstract

In January this year, 143 SmallSats were launched into orbit in a single launch by a dedicated SpaceX mission, setting a new record that shows the importance that small satellites play in the new space economy. Among the small satellites, CubeSats are revolutionising the space market with their low cost, fast delivery and mission versatility. The number of technology demonstrators in which they are involved is growing, but rendezvous and docking operations are still a very challenging topic for CubeSats.

Rendezvous and Docking (RVD) manoeuvres require high performance on relative position and velocity between Chaser and Target and relative attitude, accuracy at the final point, time to complete the manoeuvres and control effort. Moreover, the fundamental constraints derive from the safety aspects that imposed constrained trajectories. Advanced guidance and control strategies can improve the confidence level in the success of the manoeuvres also in presence of uncertainties and disturbances introduced by a technological limitations and the harshness of the space environment. One of the most promising solutions for the trajectory control is the Nonlinear Model Predictive Control (NMPC). The advantages of this technique for the rendezvous and docking problem are: 1) the possibility to constrain the input, the state and output imposing boundaries whose violation is prevented and the capability to jointly define an optimal guidance strategy and the feedback command allowing the spacecraft to follow this strategy. Constraints or penalties on fuel consumption, time to capture and safety conditions of the manoeuvre can be introduced. NMPC can drive some variables to their optimal set points (i.e. the relative position and attitude can be optimized to meet the soft docking requirements) while others can be held within imposed ranges (i.e. the velocity can be regulated with specific profiles). The prediction of the future states leads to the definition of an optimal trajectory. For the MPC design in this research, a reference tracking optimization criterion is introduced in order to assign a higher importance to the capability of the controller to track the desired values.

This thesis proposes solutions of guidance and control strategies to perform a docking operation between a 12U CubeSat and a Mothercraft with Space Rider characteristics safely even in presence of one failure of the propulsion system and ensuring a high control authority for collision avoidance manoeuvres in case of violation of the safety rules.

The designed strategies are verified using a detailed model and a robust simulation architecture built in the MATLAB/Simulink© environment with the support of System Tool Kit©. This architecture includes: Disturbance Torques include all the torques due to Aerodynamics Drag, the Solar Pressure, Gravitational Gradient, residual magnetic dipole, and the sloshing of the fuel in the tank while the Aerodynamics drag is considered as disturbance external force. For the purpose of the simulations, translational and rotational dynamics are coupled.

The thesis assesses the capabilities of a Model Predictive Controller to control the Chaser trajectory and develops a control that allows Collision Avoidance Manoeuvres to be performed if the constraints imposed on the trajectory are violated or if failures occur. Regarding the Model Predictive Controller, it provides an excellent capability to lead the Chaser to achieve the docking port with the required accuracy in terms of final position and approaching velocity both in nominal and in non-nominal conditions. Moreover, robustness analysis of the performance is completed showing how the achieved results show that a relevant

margin exists between the majority of performances and the required values ensuring the capability of the system to work properly in presence of all the uncertainties. Concerning Collision Avoidance Manoeuvres, a classical approach modelled on the strategies used for the International Space Station has been handled. It is based on an open loop control strategy that provides a departure of the Chaser from the docking axis to achieve a safe point from which the approach can be retried. The performance has been evaluated for manoeuvres beginning at different distances from the Target in nominal, off-nominal and safety violation events. Moreover, possible further strategies for future improvements have been presented.

Sommario

List of figures

List of tables

Abbreviations

RVD	Rendezvous and Docking
CAM	Collision Avoidance Manoeuvre
S/C	Spacecraft
GNC	Guidance Navigation & Control
SROC	Space Rider Observer Cube
NMPC	Nonlinear Model Predictive Control
LQR	Linear Quadratic Regulator
PD	Proportional Derivative
SMPC	Stochastic Model Predictive Control
LVLH	Local Vertical Local Horizontal
PWM	Pulse Width Modulation
CoM	Centre of Mass
MIMO	Multiple Inputs Multiple Outputs
CWH	Clohessy–Wiltshire-Hill
FMEA	Failure Mode and Effects Analysis
EOP	Early Operations Phase
SROC	Space Rider Observer Cube
DOF	Degree Of Freedom
ADCS	Attitude Determination and Control System

1 Introduction

CubeSats is gaining the attention of major players in the space field [1]. According to Allied Market Research, the space market share for CubeSats was valued at US$ 184.11 million in 2020 and is expected to grow by 15.1% until 2027 [26]. The low cost and quick schedule due to the fixed body size (CubeSat units U), their modularity and integrability and the rise of miniaturized technologies such as propulsion systems, optical cameras, off-the-shelf components etc., can enable important capabilities such as manoeuvres in Earth orbit or interplanetary, formation flight, close inspection, proximity operations and many more.
In addition, their small size simplifies placement on the launcher, increasing launch opportunities and thus reducing launch costs, and allowing several satellites from the same constellation to be released at the same time.
One of the most challenging mission is the inspection and monitoring of orbiting spacecraft/targets, such as the International Space Station [2], the Lunar Gateway [3], operative [[3]] and not operative [[4]] big spacecraft. In these missions the spacecraft must avoid any possible collision with the target that corresponds to:

1) keeping its trajectory outside a safety ellipse during the inspection phase [6].
2) ensuring safe passive trajectories in case of misbehaviour or off-nominal conditions
3) move away from the target in case of risk of collision with quick manoeuvres.

In the context of rendezvous and docking operations, the retrieval to a mothercraft of a CubeSat has never been done before because of stringent safety constraints that affect the requirements on position and attitude accuracy and the ability to perform collision avoidance manoeuvres.
The major technological challenges for docking are the relative navigation between Chaser and Target supported by vision-based information and sensor-fusion through advanced algorithms for determination [7], [8] the strategies to favour the identification of the docking port [9] , the coupling mechanisms [10], and the control system (especially for manoeuvres very close to the Target), realised through advanced controllers, precise propulsion systems and actuators that guarantee the right level of accuracy. In particular, the last few metres before docking are crucial because the margin of error is reduced, and this is worsened by the reduced dimensions of spacecraft, the requirements to be met by the mating mechanism and the technology of small satellites which does not provide the same performance as that used for bigger satellites.

One way to improve the confidence level in the success of the docking phase is to adopt an effective strategy to control the relative distance between Target and Chaser. In this regard, the problem related to the docking manoeuvres is deepened in literature for big satellites [[10]], [0], [0], and the docking of spacecraft with the ISS is almost a “routine” operation both for cargo and manned vehicles [0], [[14]], [[15]]. From the analysis of the solutions for big spacecraft is possible to identify how the robustness of the control and the manoeuvre authority together with the execution time and, in case, the control effort are fundamental aspects that the controller must satisfy.
The range of controller for docking of big spacecraft is large and includes optimal, robust, and adaptive control laws. In [[16]], the authors study controllers based on Linear Quadratic Regulator (LQR) and Proportional Derivative (PD) Control and present an analysis that compares different guidance trajectories evaluated though time execution of the manoeuvre, fuel consumption, mating accuracy but they do not provide the optimality of the results. Adaptive control laws for spacecraft rendezvous and docking under measurement uncertainty, such as systematic bias, or some stochastic disturbances, are proposed in [[17]]. In [[18]], authors show an optimized state dependent MPC that integrates a pulse width pulse frequency

modulation model: the results highlight a good accuracy at the final state minimizing the control efforts and approaching time. Authors in [20] give a complete overview of the manoeuvre and control capabilities for the capture of a non-rotating and of a rotating target, using a Model Predictive Controller (MPC) but limiting the study to planar manoeuvres. Other possible solution is the Model Predictive Controller with the tuning based on the tracking reference system optimization, as demonstrate in [21] in a docking manoeuvre with a non-cooperative target. Authors in [22] demonstrate how the MPC controller successfully manages the docking phase handling constraints on state vector and control vectors.
However, the docking of small satellites is never performed in orbit now and the control problem is a relative new topic. Authors in [23] present the determination and control strategy for CPOD mission, but no further details are provided on the adopted techniques. Authors in [24] present an H-infinity controller taking care the robust stability and performance through the mu-synthesis. Authors in [25] propose and validate on a test-bench a sampling-based stochastic model predictive control (SMPC) algorithm with off-line determination of the controller weights for discrete-time linear systems subject to both parametric uncertainties and additive disturbances.

The present thesis has the objective to propose the best control strategies for the docking phase between a CubeSat and a mothercraft, such as Space Rider. The controller design is mainly based on a Model Predictive Control, tuned in order to support both nominal and off-nominal manoeuvres. The controller is developed on a linear-dynamics while all the analyses, made through simulations, are conducted using a non-linear model that includes also environmental disturbance, coupling of the rotational and translational dynamics, and uncertainties on the system parameters. It is demonstrated that the lateral misalignment at the mating point is lower than 0.02 m is achieved, the approaching velocity is lower than 0.05 m/s and the lateral velocity is deeply lower than 1 mm/s. The entire manoeuvre is completed in less than 10 minute and with a reduced control effort. Moreover, the achieved results show that a margin exists between the performance and the required values ensuring the capability of the system to work properly in presence of all the uncertainties and confirm the robustness of the controller. Moreover, the capabilities of the controller in off-nominal conditions are verified. Off-nominal conditions can occur both for errors in the trajectory tracking that would lead to unsafe approaches and can be caused by failures of the onboard system (i.e. the propulsion system). Simulation runs demonstrate the capability both to conclude the docking manoeuvre when one failure on the thrusters occurs and to complete collision avoidance manoeuvres when the approach constraints are violated, conducting the CubeSat in a passive safe point two kilometres away from the target.

The thesis is organized as follow: The first chapter introduces the state of the art of the topics covered and the objectives of the work. is concerned with a review of literature relating to rendezvous and docking and introduces the SROC mission, the case study of the thesis project, and its requirements for the mission phases covered. The third deals with the mathematical models used and the theoretical foundations behind them. The third chapter shows the results of the simulations relating to the two topics covered (Fine-tuning of the controller to meet requirements and CAM). Finally, the conclusions summarize the work, the objectives achieved and the future steps.

2 CubeSat Rendezvous and Docking

2.1 Rendezvous and Docking

Rendezvous and Docking (RVD) operations between two spacecraft consist of a series of orbital manoeuvres and controlled trajectories that allow for a soft approach between two satellites up to a desired relative separation (Rendezvous) that can be followed by a further approach ending in controlled physical contact (Docking). The classic approach is to control the orbit of one of the two spacecraft which is the active vehicle (usually called Chaser), which reaches the orbit of the passive vehicle (called Target) and follows a series of manoeuvres that bring it at an ever-smaller distance from the Chaser until physical contact is achieved if operations include docking. To enable this to happen, the Chaser is equipped with a Guidance, Navigation & Control (GNC) system responsible of controlling the states of the vehicle in order to allow the entry into docking interface.

Given the progressive approach of the two vehicles, any state (position, velocity, attitude and angular velocities) of the chasing vehicle outside the nominal limits of the approach trajectory could lead to a collision with the target. Therefore, all approach trajectories should meet the following two conditions:

- They should be intrinsically safe, i.e. they should ensure no collision with the target, even in the event of loss of thrust or control capability at any point on the trajectory.
- If the previous condition cannot be achieved, a collision avoidance manoeuvre must be possible at any point on the trajectory.

A rendezvous mission can be divided into a number of phases: launch, phasing, far range rendezvous, close-range rendezvous and mating, described in the Figure 1. Each of these phases must comply with specific requirements that become increasingly stringent as the Chaser approaches the target. The phasing is the reduction of the orbital phase angle between the Chaser and Target, and it ends with the acquisition of the 'entry gate' (or 'trajectory gate') which shall satisfy a set of margins for position and velocity values at a certain range. The 'gate' (or 'aim point') will be on the target orbit, or very close to it, and represents the beginning of the far-range relative rendezvous operations. The major objective of the far-range rendezvous phase is the reduction of trajectory dispersions; therefore, its major tasks are the acquisition of the target orbit, the reduction of approach velocity and the synchronisation of the mission timeline. At the end of this phase, the Chaser reaches a point near the target in which it can stay indefinitely at zero Delta-V cost, and this point can be a hold point, or a forward and backward drifts below or above the target orbit, or an elliptical motion with the mean orbital height equal to the target orbit. The close-range rendezvous phase includes the closing, which is the reduction of the relative distance, and the final approach, which consists on the achievement of the mating conditions. This phase is safety critical and because of the resulting relative trajectory, pure tangential thrust manoeuvres are rarely used while radial approaches are preferred. Radial approach starts from a hold point and precedes flying around the target. The final approach depends on the docking system and shall fulfil the requirements of attitude and relative position and velocity. The mating includes capture, which is the prevention of escape of capture interfaces and the attenuation of shock and residual motion, and the achievement of rigid structural connection.

In the present study the last two phases, close-range rendezvous and docking, are discussed.

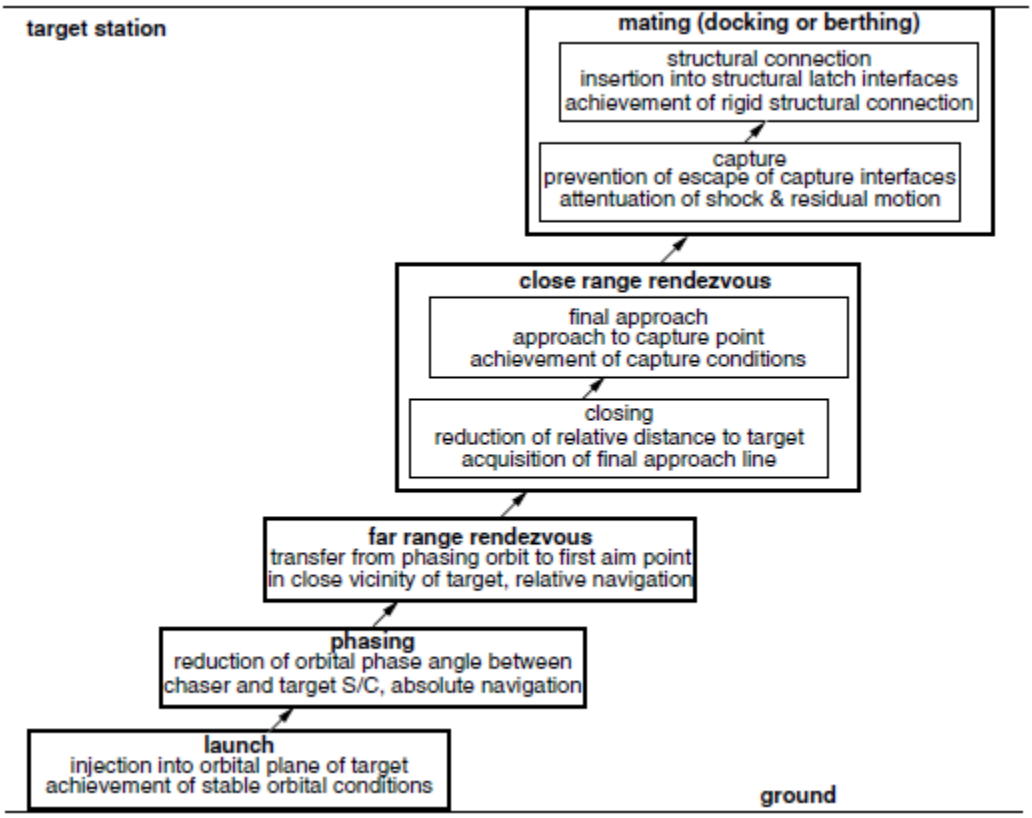

Figure 1 Rendezvous Phases (Reference to [27])

Attention should be directed to: errors outside and inside the plane, the synchronisation of the mission up to capture with external constraints (ground station coverage, lighting conditions, etc.), both the space and ground segments of both vehicles must be ready from closing to mating.

The rendezvous process may be interrupted due to contingencies in the Chaser or target. In this case, the Chaser should be able to move to a holding point at a safe distance, where it can wait for the resolution of the contingencies concerning the target until the approach can be resumed or identify its own and resolve it if possible. The mission strategy must, therefore, take account of these manoeuvres. This point may be, for example, the point from which the closing trajectory begins or a safer point at a greater distance.

The types of trajectories used for the final approach are straight line controlled closed loop trajectories or quasi-straight-line trajectories realised by a multitude of small jumps. The first type requires autonomous control systems while the latter is more convenient for manned controlled approaches, since fixed thrust pulses can be commanded. During the last few metres, straight-line approaches are recommended both because of the limited field of view of the rendezvous sensors and because the docking interfaces must fit into each other along their axes of symmetry.

During operations, the attitude of the vehicle must be based on:

- the range of action of the optical sensors towards the target;
- the range of the antennas for communication with the ground stations, which must monitor the progress of the entire approach phase;

- the need to point the solar panels towards the sun to obtain the necessary energy supply.

Another important constraint, especially if optical sensors are used, is lighting conditions. The final stages of docking must be synchronised with the occurrence of adequate light conditions. An alternative would be artificial lighting, but this is limited by the available electrical power. All these constraints can lead to restricted windows in the timeline in which the final approach and acquisition can take place and it will be seen in the following paragraphs that this is a cause of requirements in the case study under consideration.

2.2 CubeSat Definition

SpaceX's record of January 2021 for a single launch of 143 SmalSats gives an idea of the importance that this class of spacecraft is gaining in the space field. Thanks to current technology and recent investments in the fields of microelectronics, micropropulsion, remote communications and the increased use of commercial off-the-shelf (COTS) components, small satellites are taking over the space market scenes, thanks to the low cost and adaptability to different missions that recent technologies make possible.

Depending on their mass, several subcategories of small satellites can be identified as follows:

- Minisatellite: 150 - 500 kg
- Microsatellite: 10 - 150 kg
- Nanosatellite: 1 - 10 kg
- Picosatellite: 0.01 - 1 kg
- Femtosatellite: 0.001 - 0.01 kg

A CubeSat is a cube-shaped SmallSat with a modular structure, consisting of one or more units. Each unit has dimensions of 10 cm × 10 cm × 10 cm and the current state of the art suggests the availability of CubeSats ranging from 1U (one unit) to 24U (24 units). The CubeSat concept was proposed by Prof. Jordi Puig-Suari (California Polytechnic State University) and Prof. Bob Twiggs (Stanford University) in 1999 for educational purposes, but due to their modularity and integrity recently space agencies and private investors in the field are investing in its development. Until now, missions involving CubeSat have been technology demonstrators.

The European Space Agency (ESA), in particular, has been using CubeSat since 2013 is involved in CubeSat missions such as: GOMX-3, a 3-unit CubeSat mission to demonstrate aircraft ADS-B signal reception and geostationary telecommunication satellite spot beam signal quality using an L-band reconfigurable software defined radio payload; GOMX-4, a 6-unit CubeSat mission to demonstrate inter-satellite links and propulsion technologies; QARMAN, a 3-unit CubeSat mission to demonstrate re-entry technologies; SIMBA, a 3-unit CubeSat mission to measure the Total Solar Irradiance and Earth Radiation Budget climate variables; Picasso, a 3-unit CubeSat mission to measure Stratospheric Ozone distribution, Mesospheric Temperature profile and Electron density in the ionosphere; and others will follow such as: RadCube, a 3-unit CubeSat mission to demonstrate miniaturised instrument technologies; PRETTY, a 3-unit CubeSat mission to demonstrate the technique of GNSS Reflectometry at low grazing angles for altimetry

In 2018, nasa also launched a Mars Cube One MarCO cubesat mission, a 6U cubesat. Both MarCO-A and MarCO-B were able to fly over Mars, transmitting data back to Earth from Insight as it landed on Mars. It

also plans to launch a microwave oven-sized CubeSat weighing just 55 pounds this year to serve as the first spacecraft to test a unique elliptical lunar orbit as part of NASA's Cislunar Autonomous Positioning System Technology Operations and Navigation Experiment (CAPSTONE). As a precursor to Gateway, CAPSTONE will help reduce the risk to future spacecraft by validating innovative navigation technologies and testing the dynamics of this halo-shaped orbit.

The Politecnico di Torino is the first universities in Italy to participate in a CubeSat mission thanks to the CubeSat Polito Team with whose collaboration this thesis work has been carried out. The Team, born in 2008 as a student team, is involved in the study, design and development of small platforms, and in particular CubeSat, for research purposes, scientific missions and technology demonstration with the partnership of ESA and ASI. In 2012 it launched EST@R-I, a 1U CubeSat created for educational purposes with the aim of demonstrating an active 3-axis ADCS (Attitude Determination and Control Subsystem) technology, including an inertial measurement unit. And in 2016 EST@R-II was launched, a 1U CubeSat developed for demonstrating the autonomous active attitude control capabilities based on magnetic actuation. Among the various missions carried out by the Team, this thesis falls within the context of the SROC project.

2.3 Case of study: SROC

The case study of this thesis project is the Space Rider Observer Cube SROC mission of the CubeSat Team of Politecnico di Torino, scheduled for late 2023. SROC is a 12U CubeSat mission capable of performing on-site observations of Space Rider, the new space transportation system developed by Thales-Alenia for ESA. SROC will be part of Space Rider's Cargo Bay, will be released at 400 km altitude, perform walking safe ellipse trajectory to observe it and finally dock to re-enter the cargo.

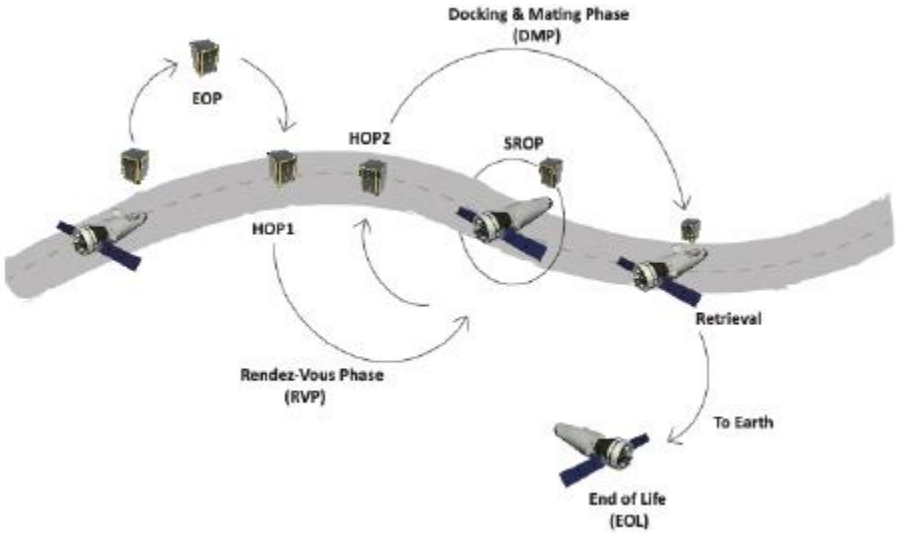

Figure 2 SROC Mission

The SROC mission phases are reported in Figure 2 SROC Mission, it is divided into the following phases:

- Deployment Phase: SROC is deployed from the DARM system inside the Space Rider cargo bay;
- Early Operations Phase: the duration may vary, between the best case of 5 days and the worst of 10 days;

- Hold Point Phase 1: the first hold point is needed to stop the drift away motion after EOP;
- Rendezvous Phase: the goal is to reduce the distance between SROC and Space Rider, after the free drift during the EOP phase, and to achieve the relative position to start the observation phase. Two different strategies are developed to accomplish this task and they will be explained in detail later;
- SR Observation phase: this phase is divided into different scenarios that are repeated several times, according to the number of desired observations. This phase is composed by:
    - WSE insertion: SROC performs a manoeuvre to enter the WSE which, thanks to the contribution of the atmospheric drag, will advance along the positive InTrack direction allowing the observation of Space Rider in total passive safety;
    - SR observation: SROC passively maintains its motion in the WSE to observe Space Rider, guaranteeing the payload operating range;
    - Free Flight: after the observation period, SROC continues its motion without manoeuvring to allow the downlink with ground stations;
    - Approach: SROC manoeuvres to approach again SR and to start another observation cycle. This scenario is not performed for the last observation cycle, where instead a Hold Point trajectory is executed;
- Hold Point Phase 2: the second hold point is needed to stop the drift away motion after the last free flight segment and prepare for docking;
- Docking & Mating Phase: the last phase is composed by three different segments to perform the mating with Space Rider:
    - Fly Around: SROC exits the Hold Point trajectory to approach Space Rider along the radial direction;
    - Close Approach: SROC stops its relative motion w.r.t. Space Rider and reduces the distance between the two spacecraft;
    - Mating: SROC manoeuvres to mate with Space Rider.

The present study discusses the manoeuvring strategies for the last 50 m of the trajectory which fall into the last two phases of the Docking & Mating Phase: the Close Approach Phase from 50 m to 30 m and the Mating Phase from 30 m to the physical contact at 0 m.

Safety significantly influences SROC mission and system design. The only examples of similar missions available to date are related to the CubeSats deployed from the International Space Station (ISS) and the visiting vehicles to the ISS. For the development of the first iteration of the SROC mission design, the safety strategy aims to avoid any collision with the Rider (which means that: the SROC demonstrator mission must not compromise the SR vehicle and its mission) and is based on the following concept (minimum risk philosophy):

- Several "volumes", in the form of ellipsoids, are built around the Space Rider. These ellipsoids delimit different zones where the SROC CubeSat is to be used in different ways and where certain capabilities are required. Decision points must be defined for the transition from one zone to the adjacent one.
- Take advantage of the safe free drift trajectory approach, i.e. SROC trajectories must be safe in a passive mode, whenever possible.
- A collision avoidance system must be integrated into the CubeSat design, which must tolerate at least one failure, and be fully autonomous (i.e. independent of ground operations) or semi-autonomous

(to be defined in later design phase). (to be defined in the subsequent design phase, pending also requirements and/or constraints from the requirements and/or constraints from the Space Rider project).

2.4 Objectives and Requirements

Previous work [6] has focused first on a preliminary mission analysis in which the docking phase was treated as a series of radial boosts such as in Figure 3, and then on the implementation of a 6 DOF orbital simulator dedicated to the docking phase in order to simulate the trajectory in the last 50 m in detail.

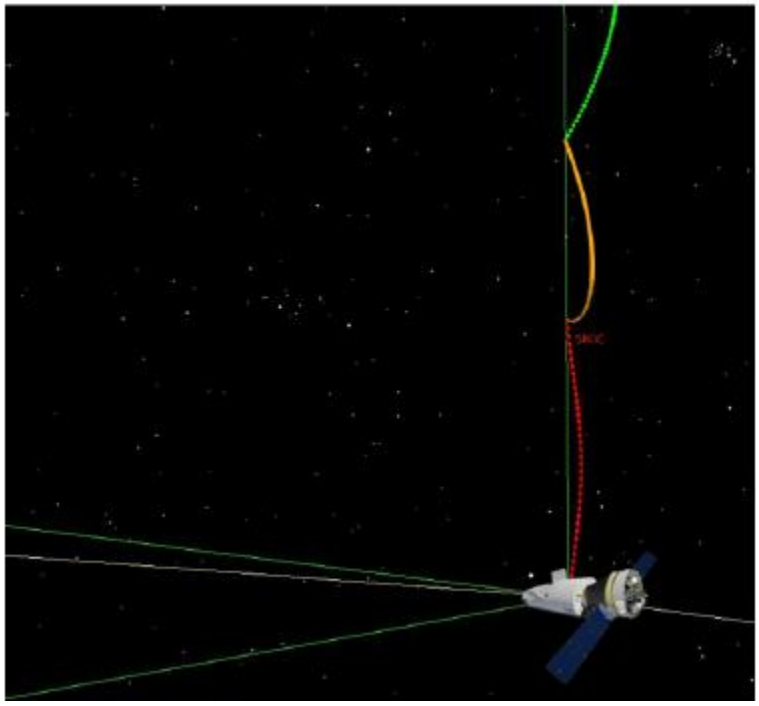

Figure 3 Docking and Mating Phase in STK previous analyses

External disturbances, errors due to sensor bias or imperfect thruster orientation, the coupling between translational and rotational dynamics, the Guidance and Control system for position and attitude and the actuating system for position and attitude are included in the simulator. The mathematical models and the structure of the GNC used will be described in Chapter 3.

The previous paragraph showed the importance of safety in the SROC mission, particularly during the last stages of docking. Any mission that involves the capture of a target must meet requirements that ensure collision avoidance. In this regard, this thesis has focused on the guidance and control of the satellite, in order to improve the position control based on nonlinear model predictive control (reference section 3.6) so that the requirements are met and the study of collision avoidance strategies so that the Chaser, in the event of a malfunction, can safely move away from the target. Therefore, the necessary strategies to make the pre-existing system compatible with the SROC requirements have been studied, in particular the objectives achieved are:

- Improvement of the trajectory control system, so that the nominal trajectory meets the requirements in terms of lateral misalignment and axial and lateral velocities. The attitude control system already verified them.
- Verification of the robustness of the control system for the nominal case and in the case of a failure and development of strategies to compensate for the resulting moment.
- Verification of compliance with the requirements by switching off the thrusters in the last few metres to avoid fouling the other payloads of the mothercraft with exhaust plumes.
- Identification of collision possibilities and development of strategies to avoid them.

The requirements to be met at the end docking, i.e. at the start of coupling, are:

1. Lateral misalignment of less than 0.02 m must be respected;
2. Axial velocity (along negative R-bar axis, see Chapter 2 for reference frame) at contact of less than 0.05 m/s must be respected at the end of docking;
3. Lateral velocity (along V-bar and H-bar axes) at contact of less than 0.001 m/s must be respected at the start of coupling;
4. Overall duration of closing and mating of 10 minutes.

Regarding the eventuality of failure, failures of the propulsion system have been treated, the requirement to be respected is:

5. Be able to perform docking even with one failure.

The requirements on CAM are that the system must be able to perform manoeuvres that:

6. Move the Chaser away without collision until a point where the approach can be retried at least 2 km along the negative V-bar axis (see Chapter 2 for the reference frame);
7. Be passive safe for a period of time at least 24 hr;

Table 1 SROC Docking and CAM Requirements

End Docking Requirements	
Lateral misalignment	< 0.02 m
Axial Velocity	< 0.05 m
Lateral velocity	< 0.001 m
Overall duration	10 min
CAM Requirements	
Final distance from Target	2 km
Passive Safety Period	24 hr

Requirements 1., 2. and 3. are related to the docking mechanism still under study. Requirement 4. comes from the analyses preceding this thesis work [6] and is due to the fact that during docking, especially in the closing and mating phases, the Chaser must be in good illumination conditions in order to exploit the information of all the sensors, including the cameras that may work in the visible spectrum and which play a fundamental role during relative navigation. Requirement 6) comes from the fact that the Target having a

lower ballistic coefficient, i.e. a higher resistance, will decay faster than the Chaser, causing the Chaser to move in time to a higher position (negative R-bar direction) behind the Target [27]. Therefore, it is safer for both S/C if the Chaser performs the escape manoeuvre by moving away towards the negative V-bar axis (the V-bar axis corresponds to the direction of motion of the Target).

3 Mathematical Modelling

This chapter aims to illustrate the theoretical foundations on which the thesis work is based and their implementation using the MATLAB-Simulink® calculation software.

After a brief outline of the reference systems used, the dynamics and kinematics model of the S/C, the environment model and the disturbances introduced are discussed. The GNC system is then described, in particular the theory behind the design of the controller used for the trajectory: the Nonlinear Model Predictive Control and how it has been set up, ending with the model used for the thrusters.

3.1 Reference Frames

In chapter 1 RVD operations are introduced and it is mentioned that the typical approach is to have an active satellite (the Chaser) tracking the passive one (the Target). it is useful to study such an approach using a local reference system. In the study of docking manoeuvres, we have chosen to consider the LVLH as the local system for the reasons that will be discussed below. In high-precision manoeuvres such as Rendezvous but especially docking manoeuvres, it is also necessary to know the relative attitude of the Chaser with respect to the Target. This is usually studied in the body axis system, a system integral with the vehicle but with axis orientation that changes according to the mission or mission phases considered. The two reference systems adopted are explained in detail below.

3.1.1 Local Vertical Local Horizontal Frame

The reference system adopted for the study of close approach and docking is the Local Vertical Local Horizontal (LVLH) system. It is used to describe the motion of an orbiting body relative to the centre of the earth. This reference frame is useful in the case of relative trajectories because in the context of relative motion can be considered quasi-inertial. The system is defined as follows:

- The origin of the system is the COM of the S/C;
- The z axis points along the nadir vector;
- The y axis pointing along the negative orbit normal, in the direction opposite to the spacecraft's orbital angular velocity;
- The x axis completes the right-handed triad and has a direction equal to that of motion.

The LVLH x, y and z axes, shown in Figure 4 are also called V-bar, H-bar and R-bar. The current mission baseline envisages docking on negative R-bar. In particular, the close approach starts at 50m on negative R-bar and ends at 30m, at which distance the mating starts up to 0m. The manoeuvres discussed in the next chapters are designed in the LVLH system having a centre in the Target COM.

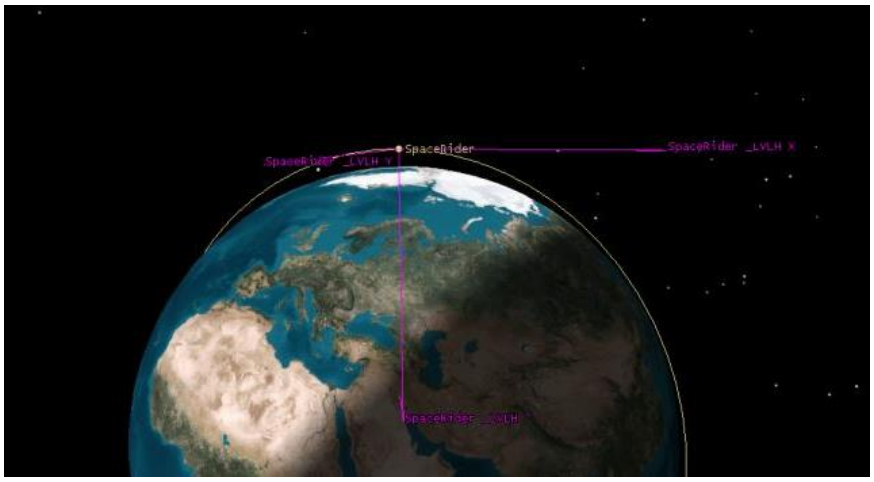

Figure 4 LVLH reference frame

3.1.2 Radial-InTrack-CrossTrack Frame

The system Radial-InTrack-CrossTrack (RIC) Frame, also called Hill's frame, is a system similar to the LVLH. The Hill's frame also has its origin in the centre of the spacecraft mass, the first axis is the radial outwards direction (Radial), the second axis is the direction of the orbital velocity vector (InTrack) and the third one completing the triad is the orbital angular momentum direction (CrossTrack). This system is shown in Figure 5 important for the equations of motion that will be used, the Hill's equations, as we will see in the paragraph 3.4. Both the frames are compared and shown in Figure 6, together with the absolute position, velocity and angular momentum, assuming a circular orbit for the leader spacecraft.

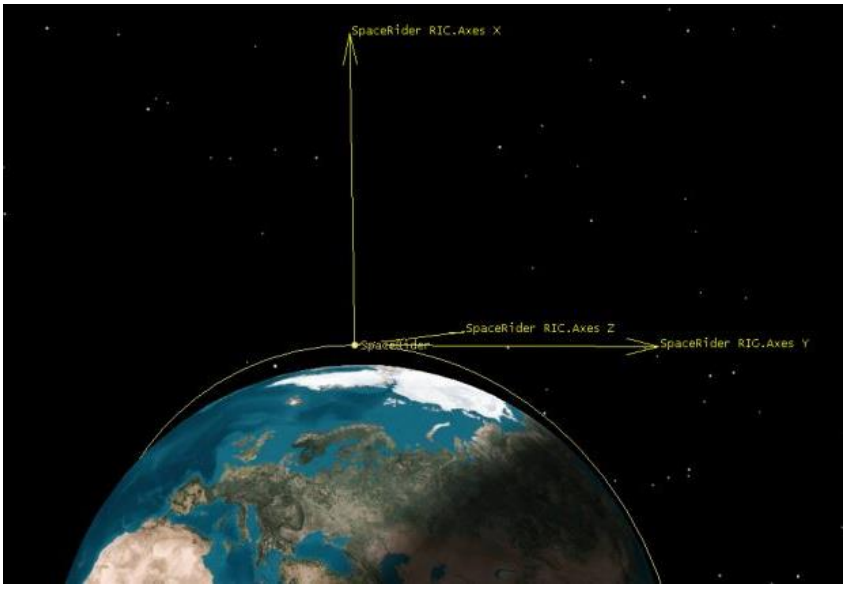

Figure 5 RIC Reference Frame

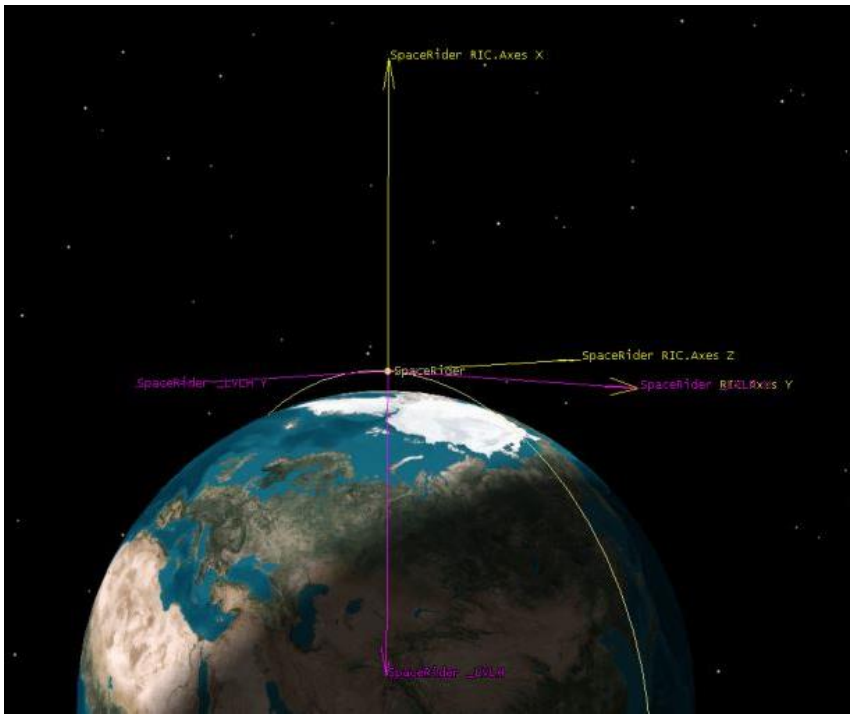

Figure 6 Comparison between RIC and LVLH Reference Frame

3.1.3 Body Frame

The body reference system is used to describe all rotations of the spacecraft. Due to the variation of the COM of the vehicle during manoeuvres, it has axes that do not refer to the physical geometry of the vehicle but depend on the mission strategy. In the present case, one has:

- The z-axis points in the opposite direction to the docking axis (R-bar) and it is chosen in this way because on the normal face there are sensors relating to the proximity navigation phases;
- The y-axis is the one whose normal face is the one with the largest surface area of solar panels;
- The z-axis completes the tern.

The coordinate transformation from the LVLH system is always possible knowing the azimuth α_z, elevation α_y and roll α_x angles. It is shown below:

$$\begin{bmatrix} x_{body} \\ y_{body} \\ z_{body} \end{bmatrix} = \begin{bmatrix} 1 & 0 & 0 \\ 0 & \cos\alpha_x & sin\,\alpha_x \\ 0 & -\sin\alpha_x & cos\,\alpha_x \end{bmatrix} \cdot \begin{bmatrix} -sin\,\alpha_y & 0 & cos\,\alpha_y \\ 0 & 1 & 0 \\ cos\,\alpha_y & 0 & sin\,\alpha_y \end{bmatrix} \cdot \begin{bmatrix} cos\,\alpha_z & sin\,\alpha_z & 0 \\ -sin\,\alpha_z & cos\,\alpha_z & 0 \\ 0 & 0 & 1 \end{bmatrix} \cdot \begin{bmatrix} x_{LVLH} \\ x_{LVLH} \\ x_{LVLH} \end{bmatrix}$$

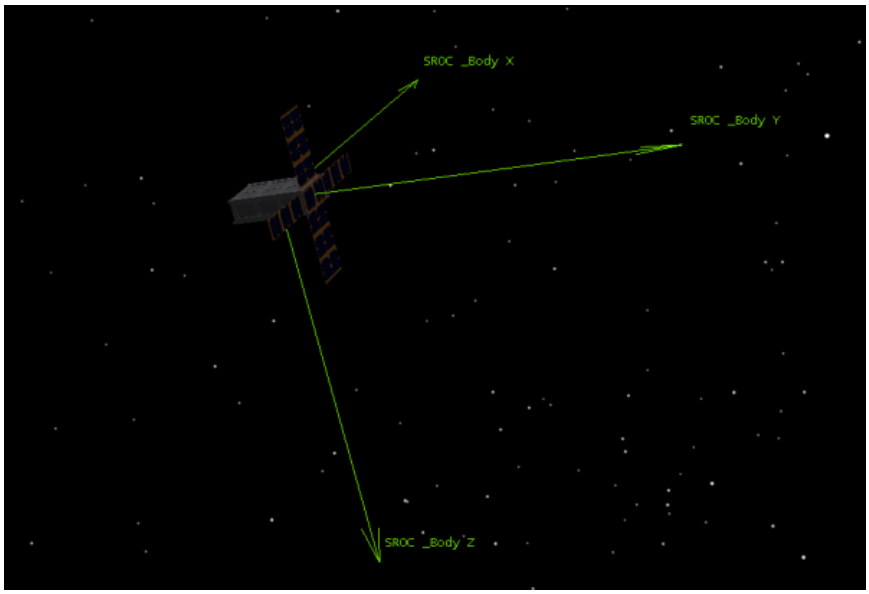

Figure 7 Body reference frame

3.2 GNC Model

The GNC is the subsystem that has the main task in the execution RVD manoeuvres. It is responsible for determining the relative position and attitude, providing guidance to the controller and controlling the S/C. Below are the main functions of the GNC which will be explained in detail in the following paragraphs.

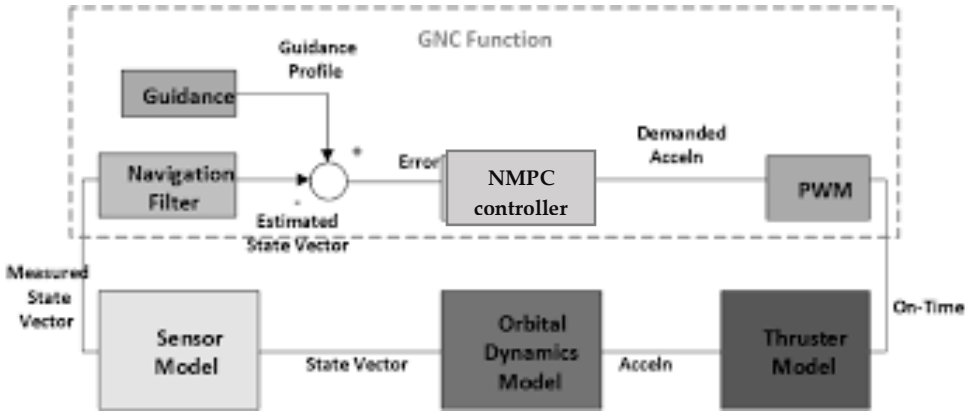

Figure 8 GNC generic model

3.2.1 Guidance

Guidance is the reference for trajectory and attitude. It can be of different types (Artificial Potencial Field, Impulsive, etc.). In the case under study, the orbital controller only needs to be referred to the desired point at which it wants to arrive, it will therefore be of type [0;0;0]. For the attitude it corresponds to the reference quaternion [1 0 0].

3.2.2 Controller

Control is the most important part of the GNC. Both because it is responsible for ensuring the accuracy of the position and attitude which is fundamental in a delicate manoeuvre such as Docking. But also because the orbit controller is the most innovative part of the subsystem. This uses an Nonlinear Model Predictive Control (NMPC) that has few applications in the space world, but because of its generality (relative to the fact that it can adapt to plants described by non-linear equations that do not have to respect many hypotheses) and robustness, it is beginning to spread in this field. The special feature of SROC GNC is the presence of two NMPC type controllers, one controlling the trajectory from 50 m to 15 m and one controlling from 15 m to contact (i.e. 0 m). This ensures better performance and lateral misalignment in the order of a centimetre.

3.2.3 Plant

The Plant is the heart of the GNC. It has within it the mathematical models that simulate the roto-translational motion of the S / C. Translational motion is studied in relative reference (see section 2.3) and is described by the CWH equations described in section 2.3. Rotational motion is described by Euler's equation. To the forces and moments involved are added the most influential environmental disturbances to the operational altitude (i.e. 400 km).

3.2.4 Actuation Subsystem

The actuation system is responsible for translating the control output generated by the controller into physical forces. It must therefore take into account the limits and characteristics of the real propulsion system.

3.3 Translational Motion

During the last stages of Rendezvous and during Docking, the relative navigation mode starts and therefore it is interesting to know the distance of the Chaser to the Target, it is convenient to use a local reference system. The Hill equations can be written in either the LVLH or the RIC system, because they are often the system with the axes rotated between them as seen in the section 3.2.1. If the orbits are circular, the relative motion is described by the Hill equations listed below:

$$\ddot{x} = 2\omega\dot{z} + \frac{1}{m_c}F_x$$

$$\ddot{y} = -\omega^2 y + \frac{1}{m_c}F_y$$

$$\ddot{z} = -2\omega\dot{x} + 3\omega^2 z + \frac{1}{m_c}F_z$$

In which ω is the mean motion n of the Target orbit ($n = \sqrt{\frac{\mu}{a^3}}$ with a semi-major axis of the orbit and μ Earth's gravitational constant and m_c is the mass of the Chaser. These equations are written in the RIC system (i.e. the Hill Frame) and are those implemented by the simulation model. However, since it is a lesser-known system than LVLH all the graphs in the Chapter - have been reported in the LVLH system.

This is a system of differential equations that can be solved performing the Laplace transformation and then obtain the time domain solution through the inverse Laplace transformation. The equations derived from this method represent a linearisation of the Hill equations and are called Clohessy–Wiltshire-Hill (CWH) equations. Perturbative forces may be added to the equations, but in the form of accelerations. There will be a dedicated the Paragraph 3.5. The simulative model of the system is as follows:

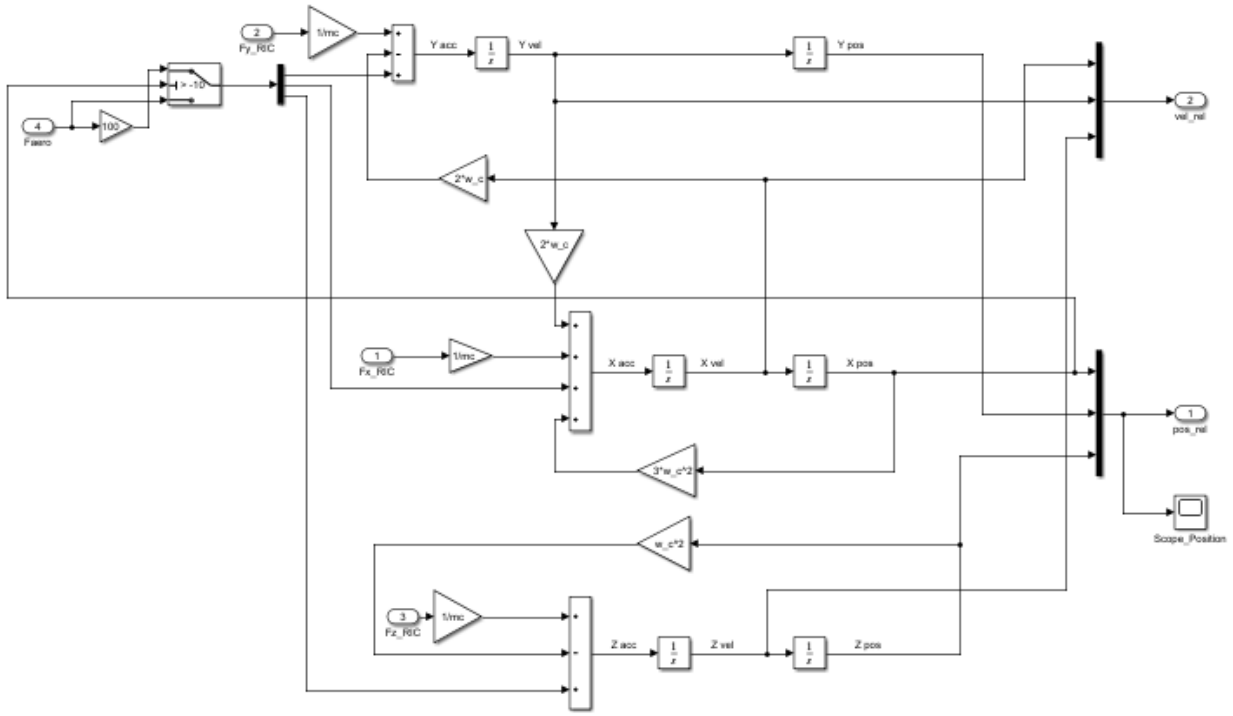

Figure 9 CWH equations in Simulink model

Considering the classical equations corresponding to the state and output time responses in the space of states:

$$\dot{x}(t) = A\bar{x}(t) + Bu(t)$$

$$y(t) = C\bar{x}(t) + Du(t)$$

In which $u(t) \in \mathbb{R}^{3x1}$ is the control input and $\bar{x}$ is the state vector:

$$\bar{x} = \begin{bmatrix} x \\ y \\ z \\ \dot{x} \\ \dot{y} \\ \dot{z} \end{bmatrix}$$

Compared to the model discussed above, the matrices are:

$$A = \begin{bmatrix} 0 & 0 & 0 & 0 & 0 & 0 \\ 0 & 0 & 0 & 0 & 0 & 0 \\ 0 & 0 & 0 & 0 & 0 & 0 \\ 3n^2 & 0 & 0 & 0 & 2n & 0 \\ 0 & 0 & 0 & -2n & 0 & 0 \\ 0 & 0 & -n^2 & 0 & 0 & 0 \end{bmatrix}$$

$$B = \begin{bmatrix} 0 & 0 & 0 \\ 0 & 0 & 0 \\ 0 & 0 & 0 \\ 1 & 0 & 0 \\ 0 & 1 & 0 \\ 0 & 0 & 1 \end{bmatrix}$$

$$C = \begin{bmatrix} 1 & 0 & 0 & 0 & 0 & 0 \\ 0 & 1 & 0 & 0 & 0 & 0 \\ 0 & 0 & 1 & 0 & 0 & 0 \\ 0 & 0 & 0 & 1 & 0 & 0 \\ 0 & 0 & 0 & 0 & 1 & 0 \\ 0 & 0 & 0 & 0 & 0 & 1 \end{bmatrix}$$

$$D = 0$$

In this model, outputs $y(t)$ coincide with states $x(t)$ (C is in fact an identity matrix), inputs $u(t)$ represent the control actions fed to the system (i.e. force provided by actuators). It will be seen later that this representation is used for the actuation of the controller model.

3.4 Dynamics and Kinematics

The correct attitude of the satellite is crucial for successful RVD manoeuvres. As regards rotational motion, it is necessary to define a set of dynamic equations describing a system from the torque $\boldsymbol{T}$ to the angular velocity $\boldsymbol{\omega}$ and a set of kinematic equations related to a system from $\boldsymbol{\omega}$ to $\boldsymbol{q}$ (attitude expressed in quaternion). The overall system results into the one with $\boldsymbol{T}$ as input torque applied to the body and $\boldsymbol{q}$ as output to control.

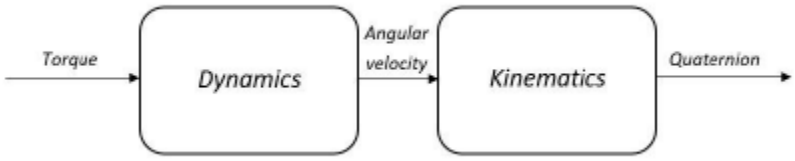

Figure 10 Dynamics and Kinematics model

Given the torque $\boldsymbol{T}$ acting on the body and the inertia matrix of the body $\boldsymbol{J}$, the Euler moment equation is:

$$T = J\dot{\omega} + \omega \times J\omega$$

The aim of rotational kinematics is to represent the time evolution of the quaternion in function of the angular velocity. At the time instant $t+\Delta t$ attitude expression is obtained from the Hamilton product between the quaternion at time t and the quaternion variation occurred from time t and time $t+\Delta t$, i.e.:

$$q(t + \Delta t) = q(t) \otimes \Delta q(t)$$

Given ω the magnitude of the angular velocity vector $\boldsymbol{\omega}$, for small time variation Δt the rotation angle can be expressed as $\omega \cdot \Delta t$. Being $\mathbf{u}$ the rotation axis, when $|\mathbf{u}| = 1$, $\omega = \omega\mathbf{u}$.

3.5 External Disturbances

The main disturbances acting on the CubeSat are, in this design phase, coming from the external environment. The causes of these disturbing elements are the gravitational and magnetic field and atmospheric drag.

3.5.1 Gravity Gradient

By making an a-priori assumption that the satellite is affected only by the Earth's gravitational field, the intensity of the latter on the Chaser can be computed by means of the Newton's law of gravitation:

$$\bar{g} = -\frac{GM}{r^2} M\hat{r}$$

In which:

- G: gravitational constant
- r: distance from the center of mass
- M: mass of the body

The parts of the vehicle, finding itself inside the gravitational field, which happen to be closer to the body generating the said field, are subject to a higher attraction force. This phenomenon generates an offset between the forces applied to different parts of the satellite, resulting in a disturbing torque trying to align the major axis of the spacecraft with the local vertical one. The expression of the disturbance torque is:

$$T_g = -3\omega^2 \hat{r} \times J \cdot \hat{r}$$

3.5.2 Magnetic Field

The second source of external disturbance is the interaction between the residual magnetic field of the satellite and the Earth's magnetic field. Along its orbit, in fact, the CubeSat is included the Earth's magnetosphere whose greatest advantage is the protection of the spacecraft from the cosmic radiation. The satellite's residual magnetic field is due to electrical currents and hysteresis noise produced by on board electronics and ferromagnetic materials. The outcome of this phenomenon is a disturbing torque expressed as follows:

$$T_m r = \bar{m_r} \times B$$

With:

- $\bar{m_r}$: the residual magnetic dipole associated to the CubeSat;
- $\bar{B}$: Earth's magnetic field-

3.5.3 Atmospheric drag

The phenomenon of atmospheric drag is due to the collision between atmospheric molecules and the CubeSat's surface, resulting into a slight perturbation in the attitude and in the height of the orbit too. The drag force is obtained as follows:

$$F_D = \frac{1}{2} C_D A \rho v^2$$

In which:

- C_D: ballistic coefficient
- A: reference area
- ρ: density of atmosphere
- v: velocity of the flow wrt the CubeSat

The resulting disturbance torque has a nonzero value only if the centre of mass and the centre of pressure of the spacecraft do not coincide; it can be expressed as:

$$T_D = \bar{r}_{cp} \times F_D$$

With:

- $\bar{r}_{cp}$: distance vector between center of mass and centre of pressure.

The product between the drag force F_D and the rotation matrix resulting from the Chaser's attitude is fed to the part of the plant modelling the translational motion: this makes the atmospheric drag a disturbance for both linear and rotational motion of the satellite.

3.6 NMPC Theory

The Nonlinear Model Predictive Control (NMPC) is based on the concept of solving an optimisation problem over finite time horizons. In particular, it is based on two fundamental concepts: at each step an approximate model of the plant is used to make predictions on the future behaviour of the system over a given time horizon; on the basis of the predicted behaviour of the system, the best command sequence to provide the system is chosen.

One considers a MIMO system, whose plant can also be described by as a non-linear dynamics and whose state is measured in real time with a sampling time Ts. At each discrete time instant t_k a prediction of the

system at future time t_k+T_p is made, where T_p is the prediction horizon. By integrating the model of the plant above over the period $[t_k, t_k+T_p]$ with initial conditions equal to those of the state at time tk. From the integration we find the predicted output that is a function of time of the initial state and of the input command u. The state of the system in the desired time interval $[t_k, t_k+T_p]$ is called predicted state. Since by varying the command the predicted state and the predicted output also vary, the algorithm consists in finding the input signal u such that the output is the desired one.

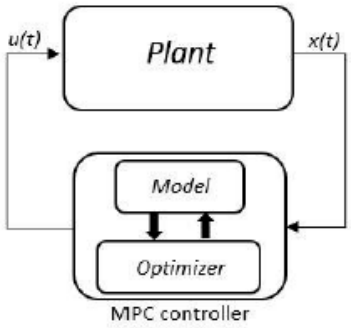

Figure 11 NMPC model

This is done by defining a cost function J, that is a function of the input signal on the interval $[t_k,t_k+T_p]$ and of the predicted tracking error, i.e. the difference between the reference signal and the predicted output. A weighted norm is made of both, based on the R matrix for the former and on the Q matrix for the latter. By minimising J over the whole time interval considered with respect to the signal u, the predicted tracking error is minimised.

$$J(u(t{:}\, t+T_P)) \doteq \int_{t}^{t+T_P} \left(\|\tilde{y}_p(\tau)\|_Q^2 + \|u(\tau)\|_R^2 \right) d\tau + \|\tilde{y}_p(\tau+T_P)\|_P^2$$

In which:

- $\tilde{y}_p(\tau)$ is the predicted tracking error at the time t;
- $u(\tau)$ is the input signal at the time t;
- $\tilde{y}_p(\tau+T_P)$ is the predicted tracking error at the time $t+T_P$.

Q and R are two matrices of weights, which, together with the matrix P, must be well set for the correct functioning of the NMPC. They are diagonal matrices with non-negative elements, whose diagonal components correspond to the weights we wish to give to the components by which they are multiplied. The algorithm minimises more the components that are given a higher weight. In particular, Q affects the weights of the states from the first discrete time instant to the one immediately prior to the prediction horizon T_p, R weights the input command and P is responsible for the weight of the state corresponding to the last time instant of the prediction horizon.

An important constraint of the NMPC to consider is that the predicted output depends on the predicted state which, in turn, depends on the command u(t). Other constraints are on the predicted output, on the predicted state or on the input u, which has limited values for a physical system.

3.6.1 Controller model

The model is based on a pre-existing function implementing the NMPC which has the following parameters as input:

- Plant model (even approximated equations);
- Function corresponding to the constraint that states must respect;
- Prediction Horizon;
- Sampling time;
- Number of states components;
- Weight Matrix;
    - Q Matrix;
    - R Matrix;
    - P Matrix;
- Maximum force level;
- Minimum force level;
- Tolerance.

3.6.2 Choice of parameters

The parameters to be chosen are T_s, T_p, the matrices Q, R, P, the range of variability of u and the tolerance. Concerning T_s, when it can be chosen it must be small enough to follow well the dynamics of the system, but not too much because, if so, numerical problems could arise and the computational velocity could not be sufficient to solve the optimisation problem. In the present case the sampling time is 0.5s and therefore T_s is equal to this value.

T_p is such that, if it is increased, the stability and robustness of the controller increases. Indeed, a high value of T_p allows longer term predictions to be made, but this can lead to reduced tracking accuracy in the short-term ones.

With regard to the choice of the Q, R and P matrices, one usually starts from an initial estimate and then proceed by trial and error. One starts by assigning 1 to the weight of a variable if it has to meet requirements, otherwise assign the zero value. They are then modified iteratively.

The work has been carried out on a pre-existing NMPC model and consisted of tuning its parameters to make the trajectory as aligned as possible with the R-bar axis and to the requirements which will be discussed later.

Q Matrix

With respect to the first controller, i.e. the one acting during the close rendezvous range from 50m to 15m, the relative weights for the second and third states, i.e. position on V-bar and H-bar, are very high because lower values lead to unwanted overshoots. A lower weight corresponds to the first state, i.e. the position along R-bar (the docking axis). Increasing the latter causes an increase in velocity which spills over to the second controller causing the relative requirement not to be met. The same has been done for the last three

states, i.e. the relative velocities. The last two states in particular have very high weights; this was done in anticipation of possible initial conditions other than the nominal one. The robustness of the controller is affected by velocity variations, especially in the lateral directions. For this reason, the controller has been set so that it can ensure robustness even for non-zero velocities along the V-bar and H-bar axes.

$$Q_1 = \begin{bmatrix} 20 & 0 & 0 & 0 & 0 & 0 \\ 0 & 900 & 0 & 0 & 0 & 0 \\ 0 & 0 & 900 & 0 & 0 & 0 \\ 0 & 0 & 0 & 80 & 0 & 0 \\ 0 & 0 & 0 & 0 & 1000 & 0 \\ 0 & 0 & 0 & 0 & 0 & 1000 \end{bmatrix}$$

In the second controller, even greater weights can be seen. This controller comes into action during mating, from 15 m to contact. Its performance is therefore crucial to the success of the docking. Increasing the weights corresponding to the states leads to a straighter trajectory, almost eliminating overshoots, and to even greater robustness to disturbances, as will be seen in chapter 2.5 .

Lower weights associated with the velocity states can be seen. This is due to the fact that the first controller does its job perfectly by decreasing the velocities and making them in the order of centimetre when the second controller is activated. Increasing these values leads to a decrease in velocities with a consequent lengthening of the overall docking duration. A trade-off has been made so that both requirements on lateral misalignment and final velocity are met.

$$Q_2 = \begin{bmatrix} 13 & 0 & 0 & 0 & 0 & 0 \\ 0 & 2000 & 0 & 0 & 0 & 0 \\ 0 & 0 & 2000 & 0 & 0 & 0 \\ 0 & 0 & 0 & 50 & 0 & 0 \\ 0 & 0 & 0 & 0 & 700 & 0 \\ 0 & 0 & 0 & 0 & 0 & 700 \end{bmatrix}$$

3.6.2.1 P and R Matrix

With regard to the P-matrix, since the Q-matrix already provides very good performance, its elements have been left unitary in both controllers, so increasing the weights would only cause an increase in computational cost.

$$P = \begin{bmatrix} 1 & 0 & 0 & 0 & 0 & 0 \\ 0 & 1 & 0 & 0 & 0 & 0 \\ 0 & 0 & 1 & 0 & 0 & 0 \\ 0 & 0 & 0 & 1 & 0 & 0 \\ 0 & 0 & 0 & 0 & 1 & 0 \\ 0 & 0 & 0 & 0 & 0 & 1 \end{bmatrix}$$

The elements of the R-matrix are chosen to be almost zero for both NMPC. They are not null because the way the NMPC is defined, they cannot be null. Thus, all the computational and actuation effort is used to control the states.

$$R = \begin{bmatrix} 1e^{-50} & 0 & 0 \\ 0 & 1e^{-50} & 0 \\ 0 & 0 & 1e^{-50} \end{bmatrix}$$

3.6.2.2 Prediction Horizon

Once the values of the matrices had been identified, an iteration was performed to determine the values of T_p for each of the two controllers. Larger T_p values make the trajectory characterised by fewer oscillations but larger amplitudes. This can cause unwanted overshoots. On the contrary, too low T_p values cause oscillations with much smaller amplitude but make the trajectory less damped (even if in the order of a thousandth of a metre). Furthermore, it has been noted that increasing the prediction horizon increases the velocity at the end of the trajectory. On the basis of these experimental considerations (i.e. from iterative tests) a lower prediction horizon was chosen for the first NMPC than for the second. In fact, the former is the one that is most responsible for decreasing velocities.

$$T_{p1} = 0.05$$

The second, on the other hand, working at lower velocities, must guarantee oscillations of the smallest possible amplitude at short distances from the Target.

$$T_{p2} = 0.12$$

Furthermore, adopting a higher T_p for the second NMPC increases its robustness and stability. This is clearly visible in the results in the section 3.2 where we notice the higher robustness of the second controller compared to the first one.

3.6.2.3 Control Input Boundary

Another parameter to define the NMPC model considered is the limits of the control force. These are derived from the propulsive model discussed in the next section. The maximum thrust that the propulsion system can provide is $F = 0.035\ N$, then one has:

$$U_{max} = \ 0.035\ N$$

$$U_{min} = -0.035\ N$$

3.6.2.4 Cone Constraint

Finally, there is the constraint that states must respect. This relates to the first three states, i.e. the components of the position. As discussed in the section 1 during the approach in the last few metres a safety zone must be defined which conventionally is a cone. In the case under consideration a cone angle of 15° has been chosen as shown in the figure. In reality, in the last few metres of the trajectory, i.e. from 2 m to contact, the constraint is more stringent. As explained in the section 1 they correspond to a circular cylinder with base on the [V-bar, H-bar] plane and height on R-bar of radius 0.02 cm. This has not been set in the controller constraint, but its parameters have been set so that it can be respected.

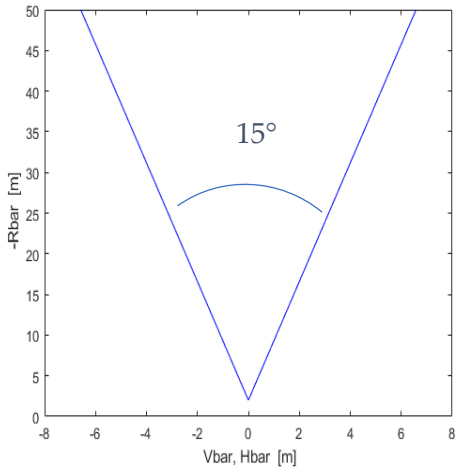

Figure 12 Cone Constraint

3.6.3 Actuation Model

The actuation model is based on the propulsion module design which is shown in the following diagram:

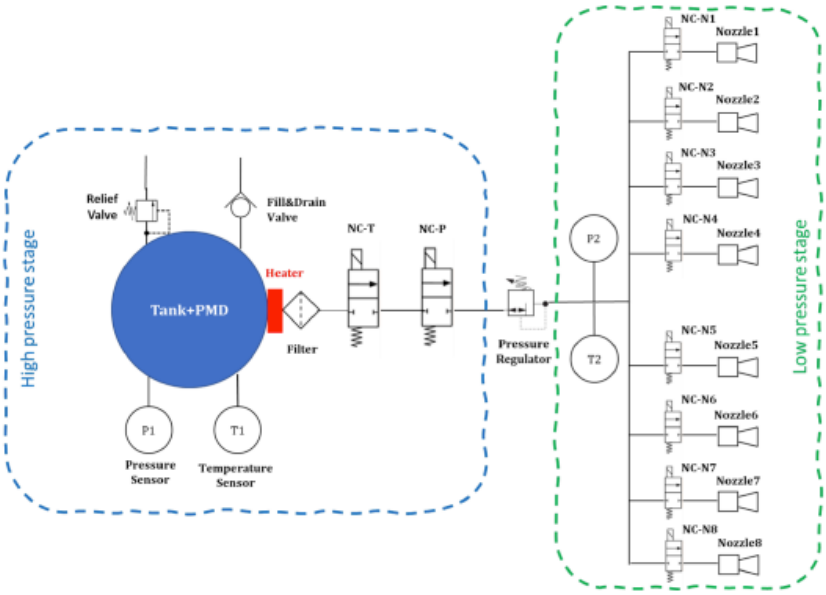

Figure 13 Propulsion Module

It is a cold gas consisting of an high pressure stage composed of the tank and a PMD (Propellant Management Device) and a vapour/liquid filter to ensure that only gas is drawn in the fluidic line. Furthermore, a heater on the tank output ensures full evaporation even in case of liquid leakage. Upon exit, the tank flows in the pipes of the high-pressure stage, through a set of 2 redundant and independent NCvalves, up to the pressure regulator, where its pressure is set to 1,5 bar. The low-pressure stage follows, composed of 8 lines each of which includes a NC-valve (independently controlled) and a nozzle.

Every nozzle is inclined with respect to the body reference frame with the origin in the CoM of the spacecraft of the angles:

- α=π4 with respect to x body axis;
- β=π6 with respect to z body axis.

The valves are on/off type so it was chosen to simulate the model through a Pulse Width Modulation (PWM) of the control signal. The overall available thrust in module is:

$$Max\ Thrust = 0.035\ N$$

Therefore, every thruster has a maximum thrust of:

$$Max\ Single\ Thruster\ Force = 8.75\ mN$$

It follows that the maximum thrust on the axes of the body reference system is:

$$f_x = f \cdot \sin(\beta)$$

$$f_y = f \cdot \sin(\alpha) \cdot \cos(\beta)$$

$$f_z = f \cdot \cos(\alpha) \cdot \cos(\beta)$$

The distribution of control force components on the eight thrusters is as follows:

Table 2Components for every thruster

Thruster components			
Thruster 1	f_x	f_y	f_z
Thruster 2	$-f_x$	f_y	f_z
Thruster 3	f_x	$-f_y$	f_z
Thruster 4	$-f_x$	$-f_y$	f_z
Thruster 5	f_x	f_y	$-f_z$
Thruster 6	$-f_x$	f_y	$-f_z$
Thruster 7	f_x	$-f_y$	$-f_z$
Thruster 8	$-f_x$	$-f_y$	$-f_z$

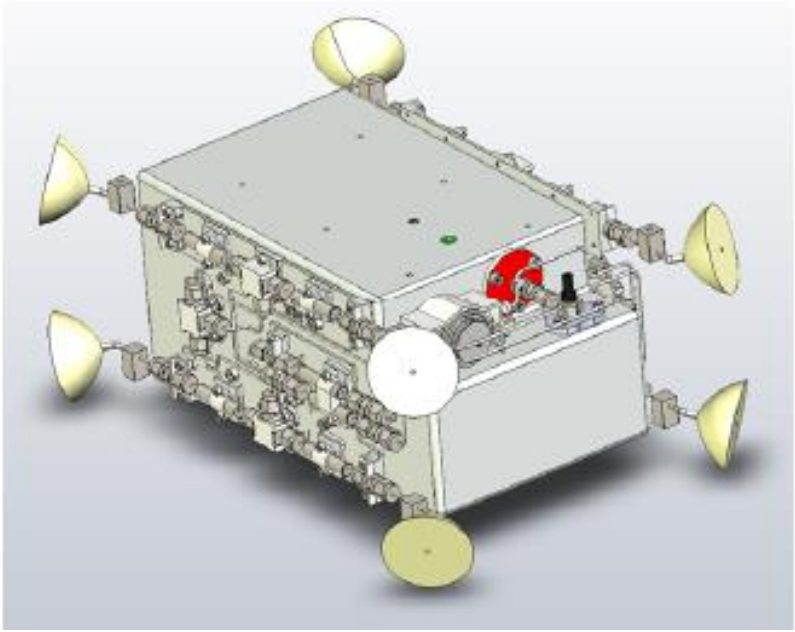

Figure 14 Thrusters disposition

This means that, depending on the control actions [Fx,Fy,Fz] provided by the controller, only the corresponding valves are activated.

Table 3 Valves activation

Control Thrust	F_x		F_y		F_z	
	$F_x > 0$	$F_x < 0$	$F_y > 0$	$F_y < 0$	$F_z > 0$	$F_z < 0$
Thruster 1	ON	OFF	ON	OFF	ON	OFF
Thruster 2	OFF	ON	ON	OFF	ON	OFF
Thruster 3	ON	OFF	OFF	ON	ON	OFF
Thruster 4	OFF	ON	OFF	ON	ON	OFF
Thruster 5	ON	OFF	ON	OFF	OFF	ON
Thruster 6	ON	OFF	OFF	ON	OFF	ON
Thruster 7	ON	OFF	ON	OFF	OFF	ON
Thruster 8	OFF	ON	OFF	ON	OFF	ON

Once these are established, the corresponding value of the control force is divided by maximum thrust to obtain the duty cycle. This procedure shall be carried out for each body axis. The value thus obtained passes into a PWM block that simulates the real behaviour of the valves and then into a quantizer discretizes the input signal. Finally, the output of the PWM referring to a certain axis and a certain thruster is multiplied by the values of the maximum force components f_x, f_y, f_z . This procedure is carried out both with respect to the three body axes of the S/C and with respect to those of each individual thruster. In addition, the torque obtained from the misalignment of the nozzles is calculated. This makes it possible to pair the translating and rotational dynamics.

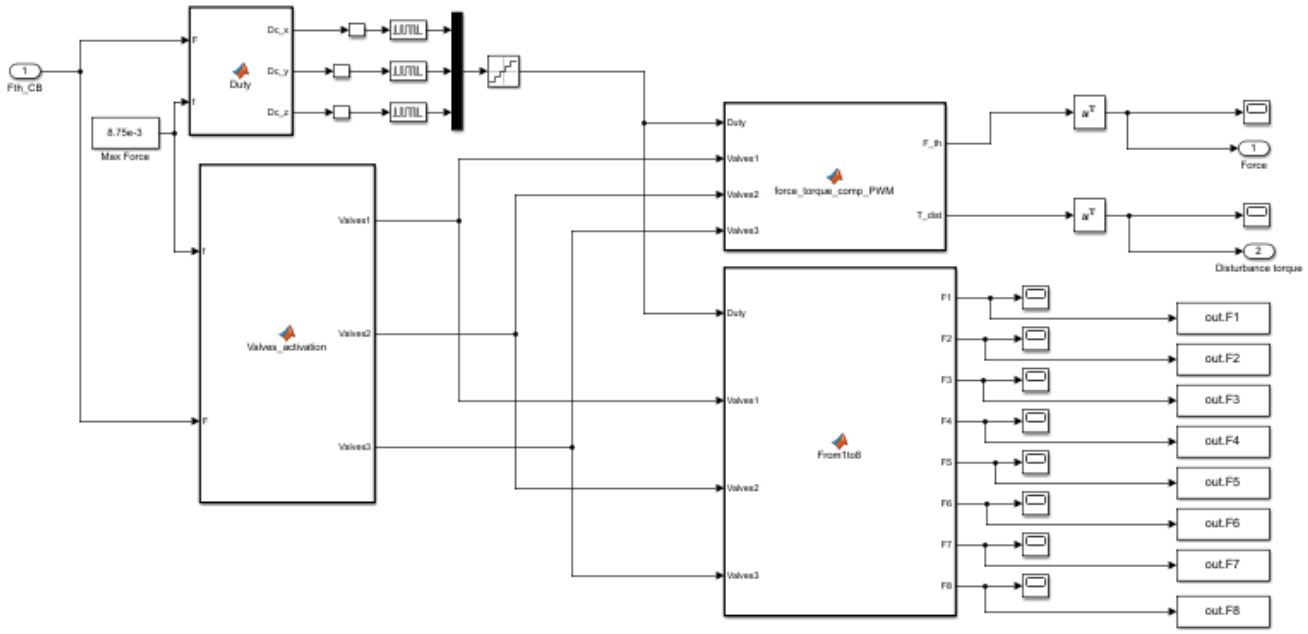

Figure 15 Actuation subsystem model

Moreover, in order to consider a more realistic architecture, a model of the sloshing of liquid propellant into the tank developed in previous studies was also included.

4 Docking maneuvers: Results and discussion

This chapter aims to show the results of the simulations regarding the docking manoeuvres carried out with the NMPC controllers designed in the previous chapter. It is divided into two parts, the first of which aims to show the results of the analyses under nominal conditions, while the second deals with the analyses under off-nominal conditions. Only results relating to the trajectory in the last 50m of the Docking and Mating Phase have been considered because the attitude controller developed previously than this thesis work already complied with the relative requirements. The purpose of this chapter is to demonstrate that the requirements are met and, if necessary, to derive others for the future continuation of the project.

4.1 Nominal conditions

The nominal conditions are those obtained considering the complete functioning of the system, therefore without failures in the GNC or in the actuation system. The nominal trajectory has been simulated considering initial position, velocity and mass as below in which x, y and z are the RIC components with the x and z axis reversed, therefore they correspond to R-bar, V-bar and H-bar.

$$x = 50\ m$$

$$y = 0\ m$$

$$z = 0\ m$$

Velocities equal to:

$$v_x = 0\ m/s;$$

$$v_y = 0\ m/s$$

$$v_z = 0\ m/s$$

And mass as following:

$$m_c = 20\ kg$$

Regarding the controller, the NMPC parameters resulting from the tuning discussed in section 2.6.2 have been used. Since in this case there are not considered failure of the propulsion module, all eight thrusters are active according to the scheme shown in the section 3.2.4.

The results obtained in terms of trajectory, position at contact, velocity along the three axes, control and effective thrust are discussed in the following.

4.1.1 Trajectory and Velocity Results

In the Figure 16, Figure 17 and Figure 18 the trajectory of the Chaser is shown in the LVLH reference centred on the Target. They are shown first in the plane [V-bar, R-bar], then in the plane [H-bar, R-bar] and finally in a 3D representation. Since the approach takes place from a distance of 50m on the negative R-bar axis, the trajectory graphs have been inverted with respect to the R-bar axis.

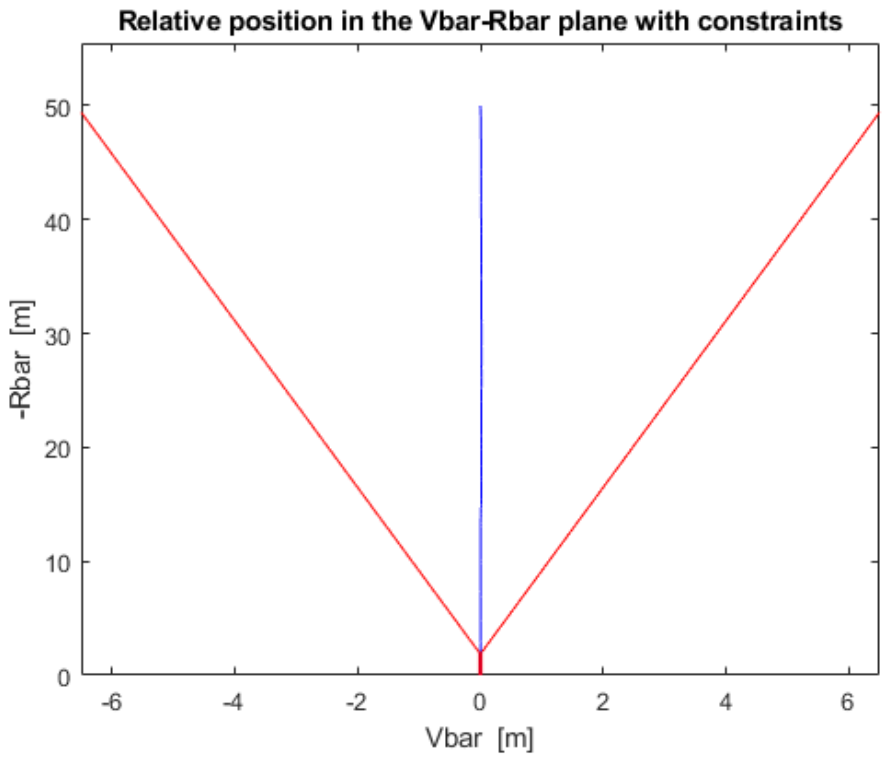

Figure 16 Relative position in [V-bar, R-bar] plane

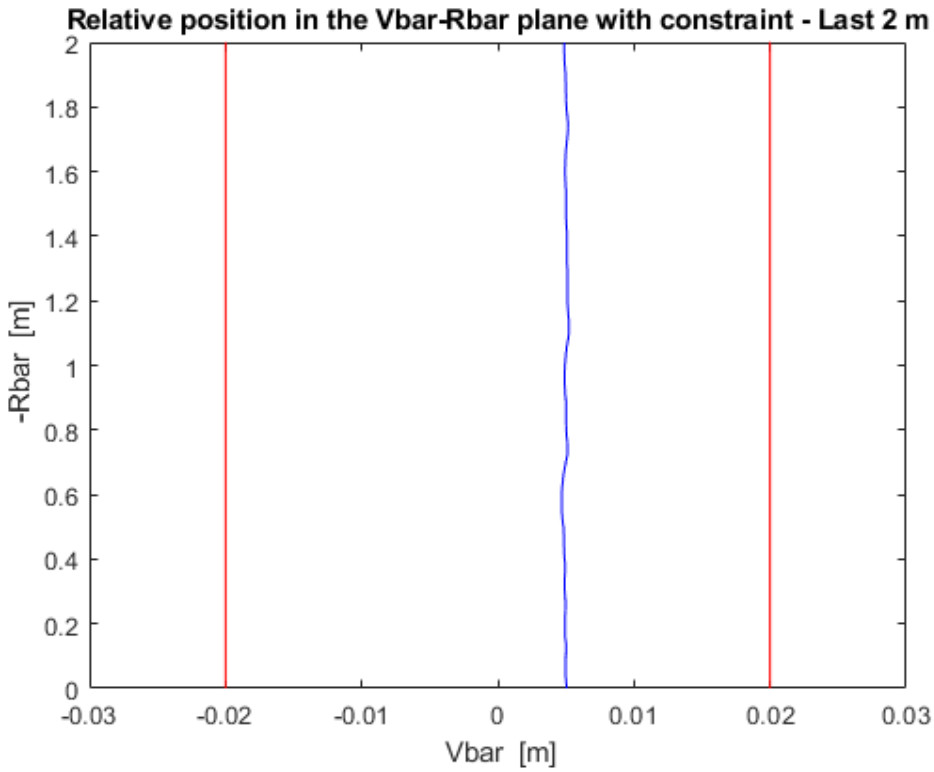

Figure 17 Zoom on relative position in [V-bar, R-bar] plane

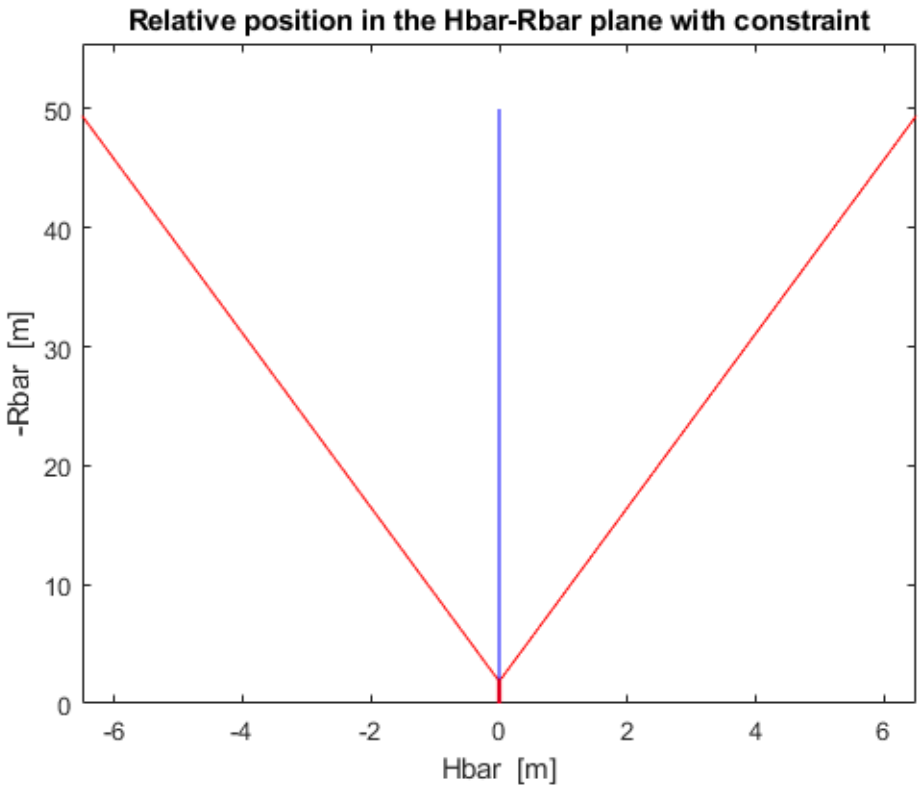

Figure 18 Relative trajectory in [H-bar, R-bar] plane

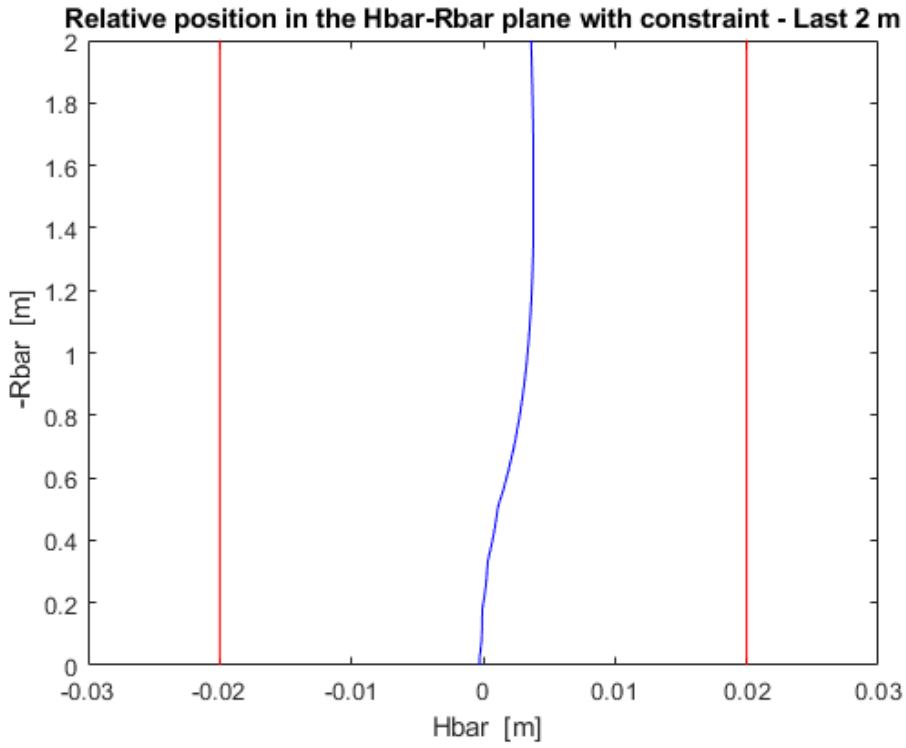

Figure 19 Zoom on relative trajectory in [H-bar, R-bar] plane

It can be seen that the trajectory is perfectly straight both in the plane [V-bar, R-bar] and in that [H-bar, R-bar]. Observing the last few meters, a small oscillation is noticed. In the [V-bar, R-bar] plane the oscillations are very small in amplitude, while in the [H-bar, R-bar] plane they are greater in amplitude but more damped. In both cases, the requirement of lateral misalignment is met, in the first the trajectory in the last meter verifies a lateral misalignment of only one centimetre, in the second it reaches almost exactly the zero value.

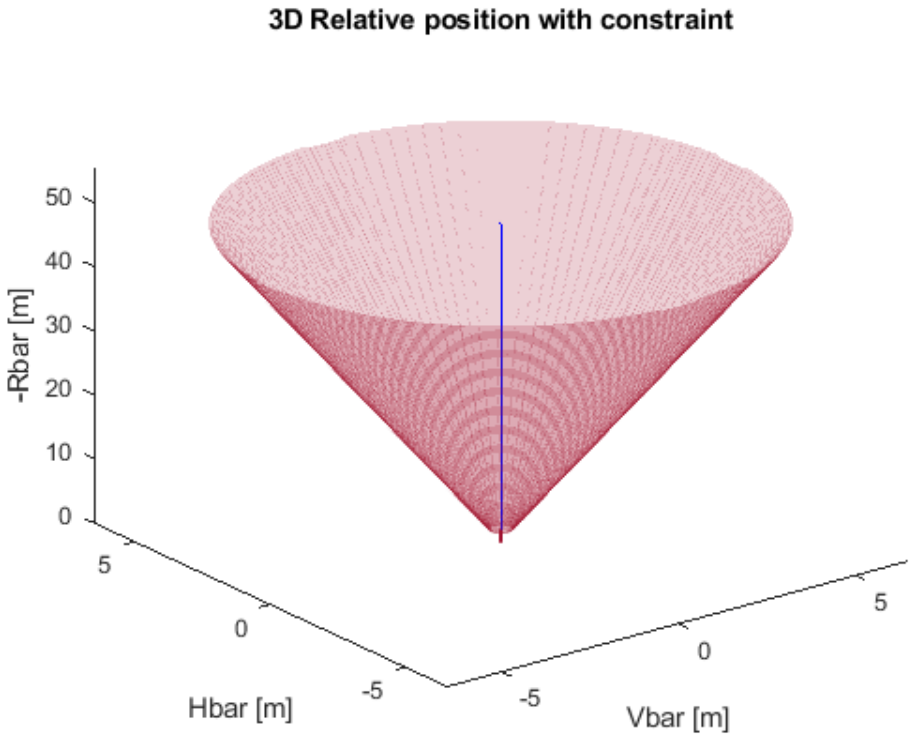

Figure 20 3D trajectory during last 50m of docking

The Figure 20 and Figure 21 show the 3D trajectories. This is useful for having an overall view of the spacecraft motion. In the Figure 21 it can be noted the deviation of the trajectory from the R-bar axis which corresponds to that seen in Figure 17 relating to the plane [V-bar, R-bar] and which is in the order of 1cm.

From these graphs it can be said that the controller developed in the Section 3.6 works perfectly, allowing a straight trajectory that falls within the required tolerances.

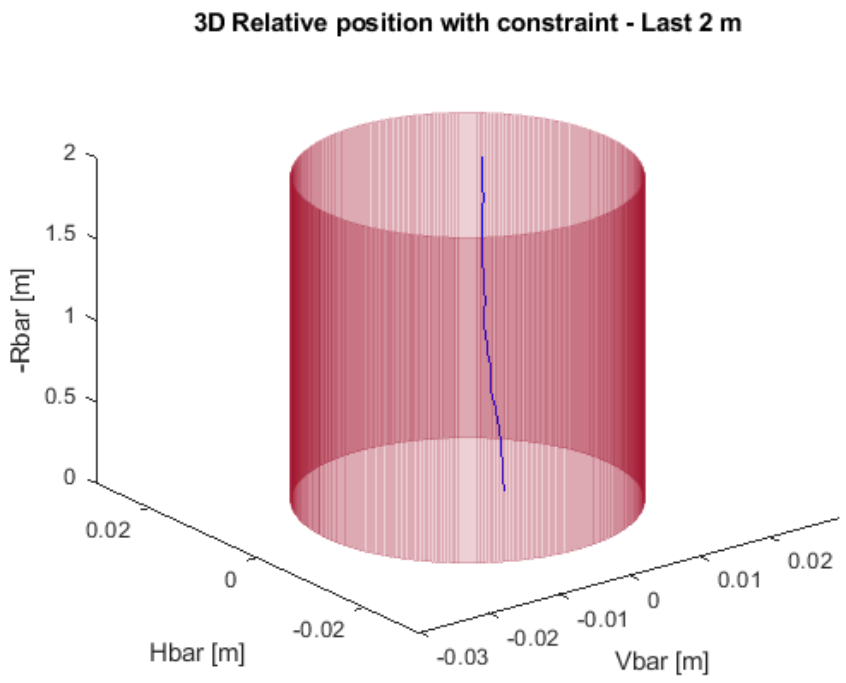

Figure 21 3D zoom on last meters of docking trajectory

Figure 22 shows the contact point at the mating. In fact, the position of the Chaser at a distance of 0m and therefore at the start of the coupling is shown on the [V-bar, H-bar] plane. It is noted that it is below 5mm on the H-bar and just above 5mm on the V-bar, which is well below the 2cm required.

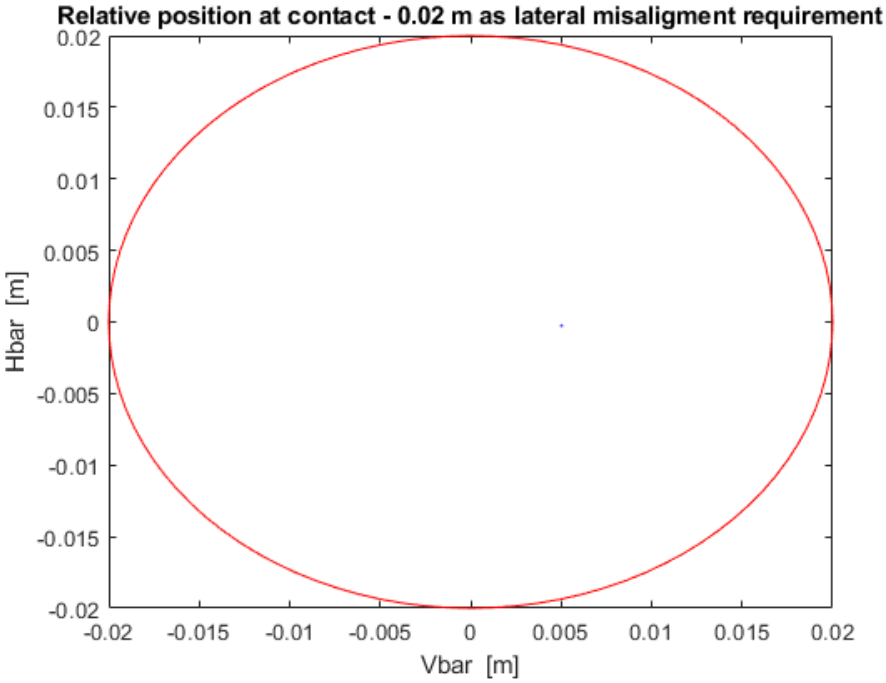

Figure 22 Position at contact in [V-bar, H-bar] plane

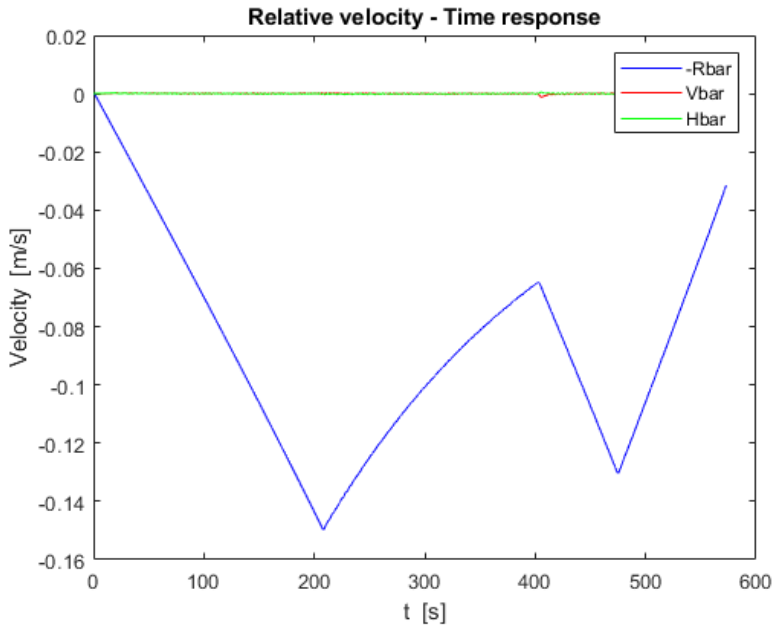

Figure 23 Velocity profiles during docking

Figure 23 shows the velocity profile along the three axes during the last 50m of the docking and mating phase. It can be seen that, the velocities along V-bar and H-bar are always close to zero, in particular they are in the order of millimetres. The velocity along the R-bar is instead always higher ending with a value equal to 0.04m, which is within the required limits (i.e. < 0.05m). It is noted that, around 200s from the start of docking, the velocity along R-bar increases and then decreases again. The corresponding distances as shown in Figure 24 are around 15m and 5m. In the Chapter 5 it will be seen that it will influence the execution of collision avoidance manoeuvres.

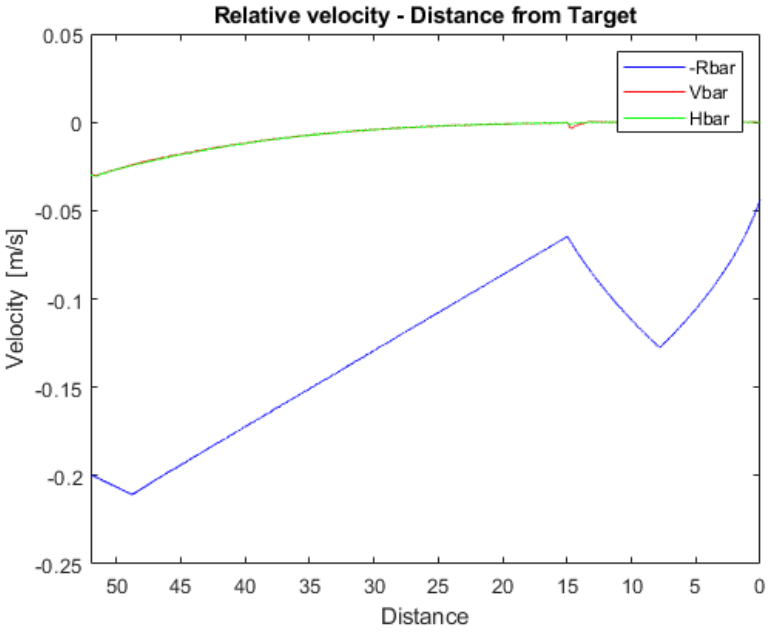

Figure 24 Velocity profiles during docking for the axial distances

4.1.2 Control and Effective Thrust Results

Figure 25 and Figure 26 show her the output of control and the force of enforcement. It is noted that the control force has lower values along V-bar and H-bar than along R-bar because it is along this last component that the greatest deceleration occurs due to the higher velocities reached during the trajectory. The force along the V-bar and H-bar is used to make the velocities along these axes millimetric, which in any case remain small throughout the docking as it can be seen and to keep the trajectory as close to the axis as possible. It is noted that the actuating force is in line with the PWM modulation discussed in Section 3.2.4. The duty cycle was calculated from the control force and then served to modulate the pulses by the right amplitude.

Regarding the control thrust, with the reference to [12] is considered the metric J_2 that represents a quadratic penalty on the control effort and is closely related to the control cost in the MPC cost function. It is calculated as:

$$J_2 = \sum_{k=0}^{T_d} (u_x(k))^2 + \left(u_y(k)\right)^2$$

where $T_d = ceil(\frac{t_d}{T_s})$, ceil is the rounding to the closest larger integer, and t_d is the 'time-to-dock' in seconds, that is, the time the Chaser takes from the initial condition to achieve docking. In this case it is equal to:

$$J_2 = 1.18$$

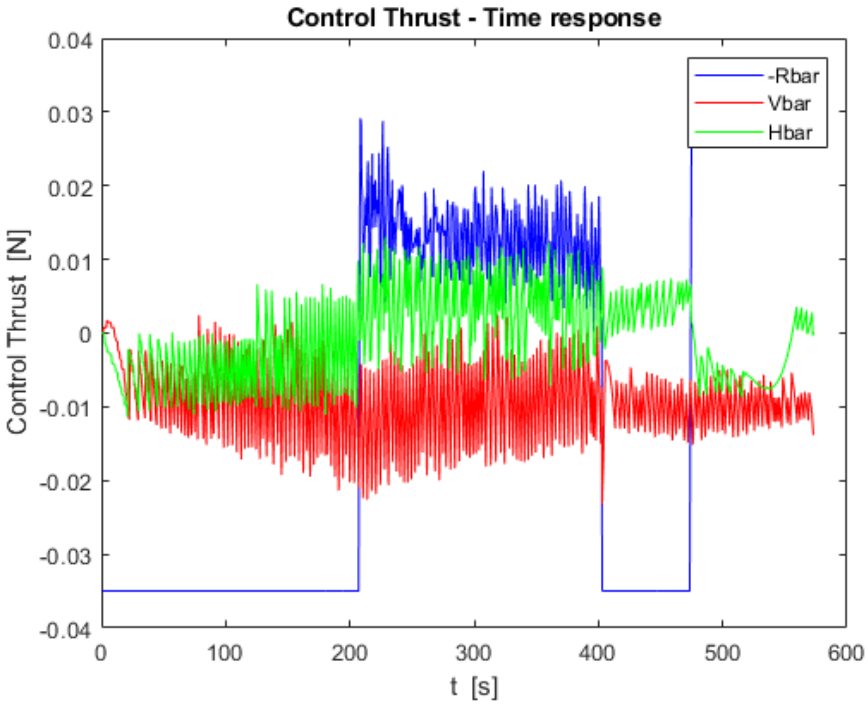

Figure 25 Control thrust under nominal conditions

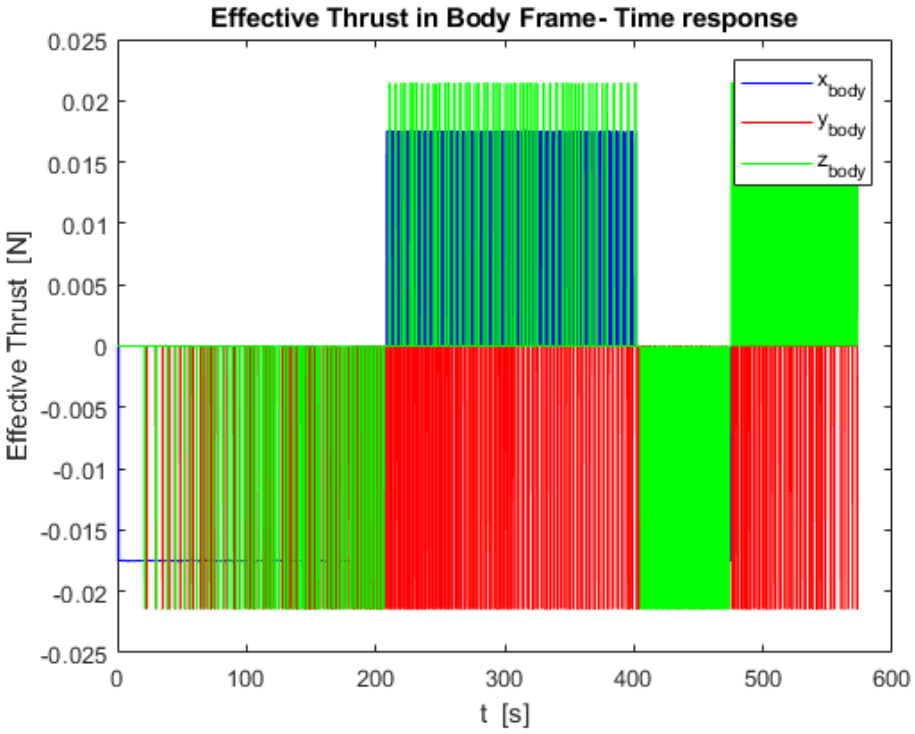

Figure 26 Effective thrust under nominal conditions

Table 4 Effective thrust along every single thruster

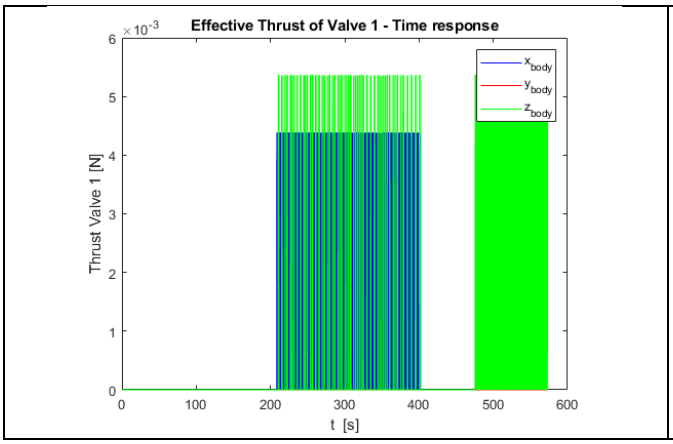

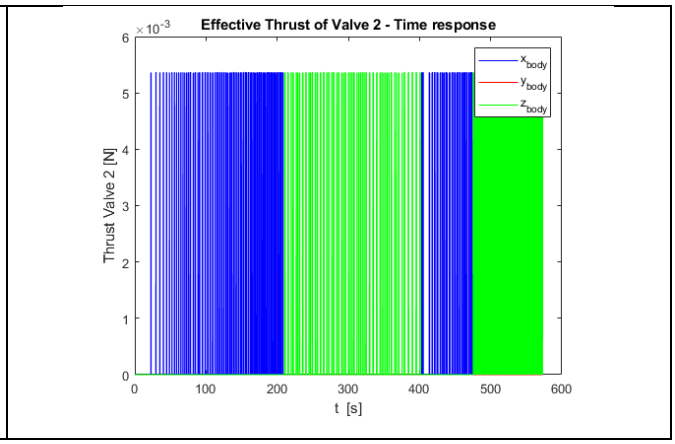

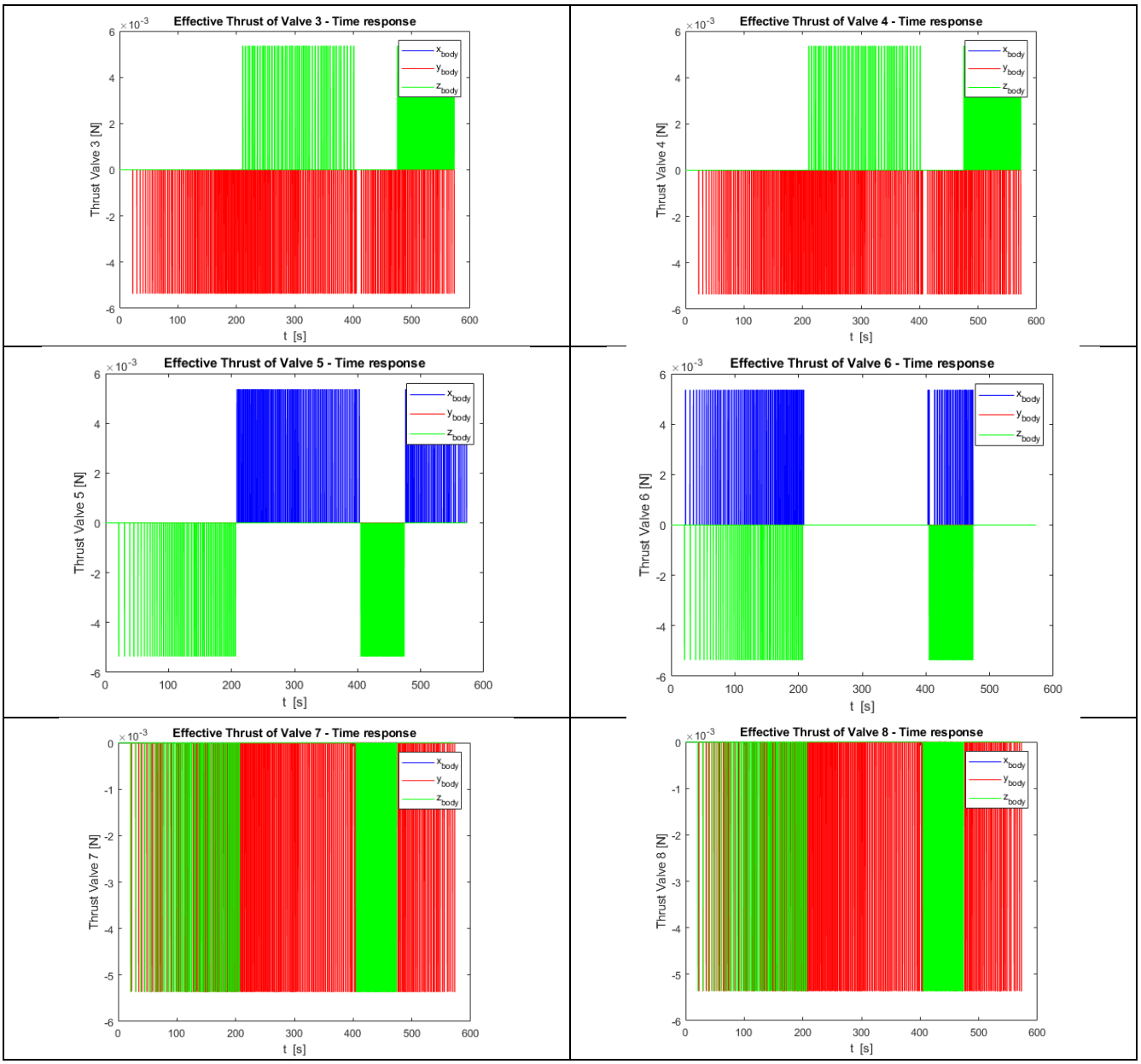

The effective forces for each individual thruster are shown in Table 4. In fact, as mentioned in the Section, the propulsion module is formed by eight thrusters such that for each control thrust direction 4 are activated.

Finally, it can be seen from the results that, under nominal conditions, the trajectory follows the negative R-bar axis Moreover, the duration of the docking is less than the ten minutes, so even this requirement is met.

$$T_{docking} = 9.63\ min$$

Moreover, the Delta-V (Δv) is estimated to be:

$$\Delta v = 0.52\ m/s$$

4.2 Worst-Case Scenario

The worst-case nominal scenario corresponds to the worst possible conditions but in a nominal operation. In this discussion the following conditions in terms of position, velocity and mass have been assumed, in which x, y and z are the RIC components with the x and z axis reversed, therefore they correspond to R-bar, V-bar and H-bar.

Position has been assumed:

$$x = 50\ m$$

$$y = 7\ m$$

$$z = 7\ m$$

It has been considered the following velocities:

$$v_x = \ \ 0.1\ m/s$$

$$v_y = -0.1\ \ m/s$$

$$v_z = -0.1\ m/s$$

While the mass is set equal to:

$$m_c = 20\ kg$$

Regarding the controller, the NMPC parameters resulting from the tuning discussed in section 2.6.2 have been used. Since in this case there are not considered failure of the propulsion module, all eight thrusters are active according to the scheme shown in the section 3.2.4.

Even in this case, the results obtained in terms of trajectory, position at contact, velocity along the three axes, control and effective thrust are given below.

4.2.1 Worst-Case Trajectory and Velocity Results

Figure 27 and Figure 28 show the trajectory in the [H-bar, R-bar] plane while Figure 29 and Figure 30 show the trajectory in the [V-bar, R-bar] plane. Figure 31 and Figure 32 give a 3D representation.

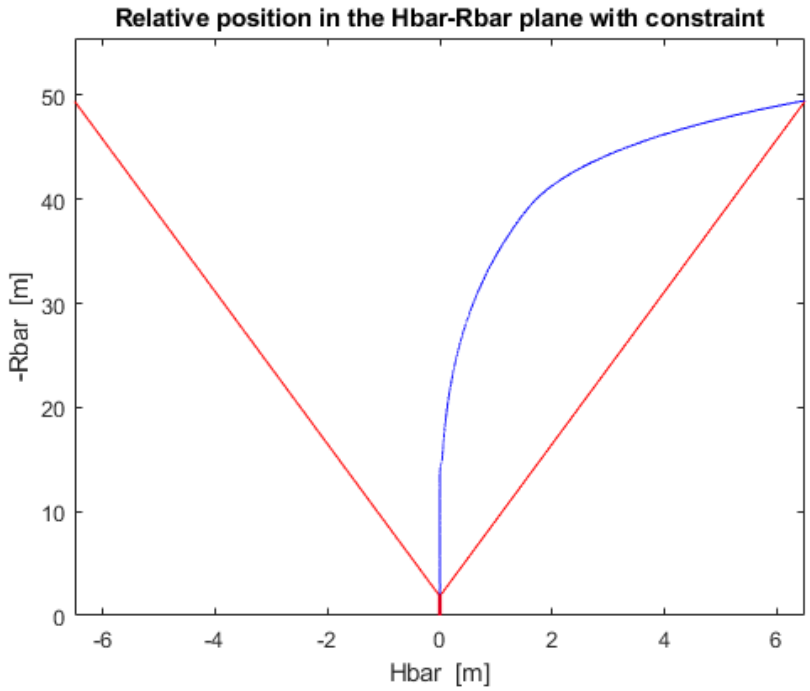

Figure 27 Trajectory in worst-case scenario in [H-bar, R-bar] plane

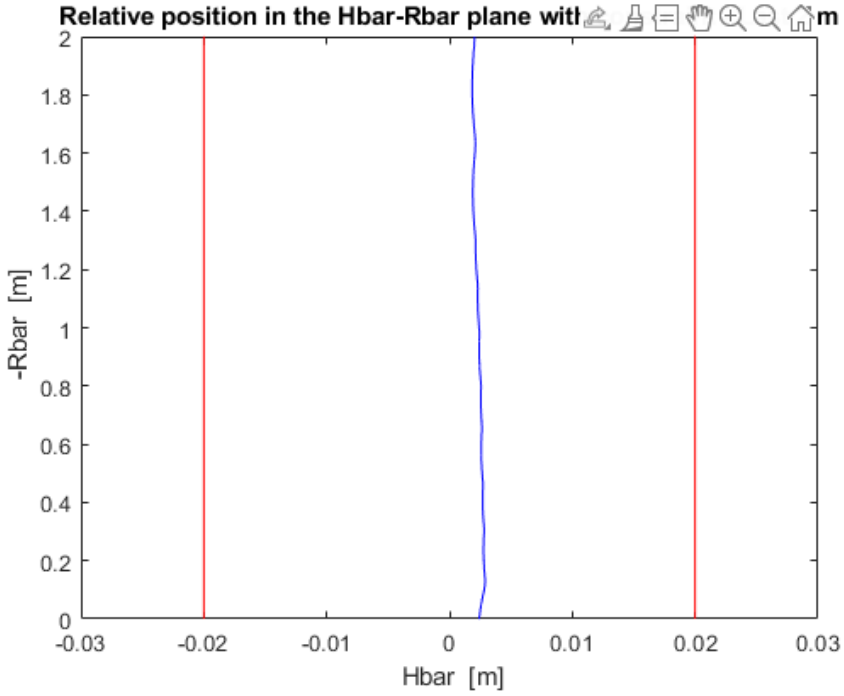

Figure 28 Zoom on trajectory in worst-case scenario in [H-bar, R-bar] plane

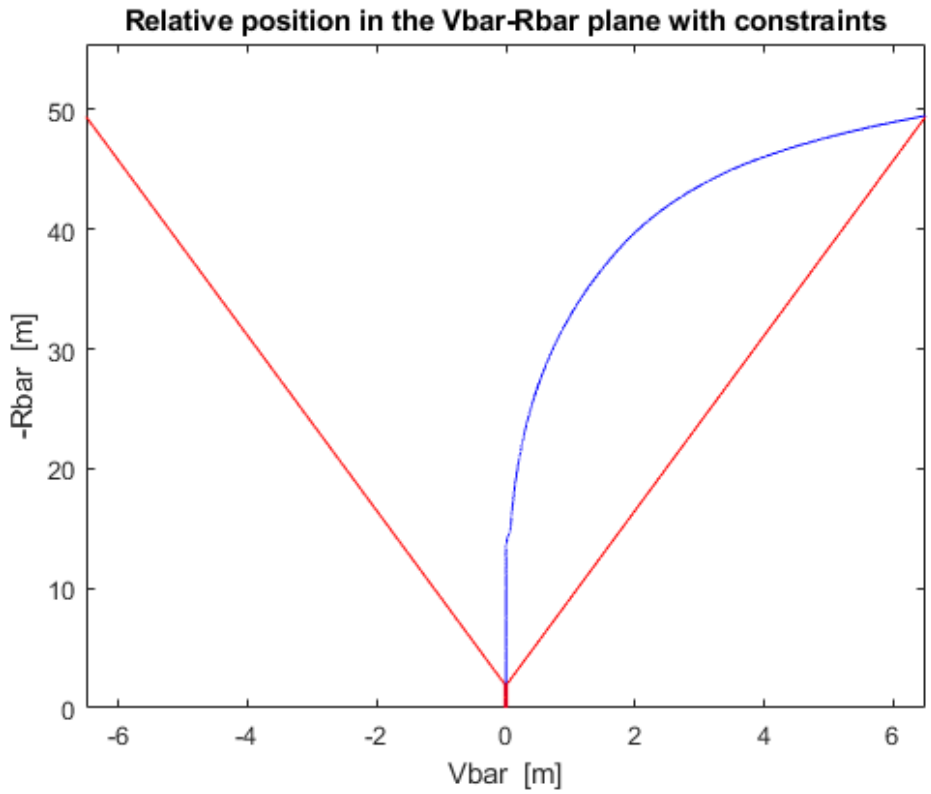

Figure 29 Trajectory in worst-case scenario in [V-bar, R-bar] plane

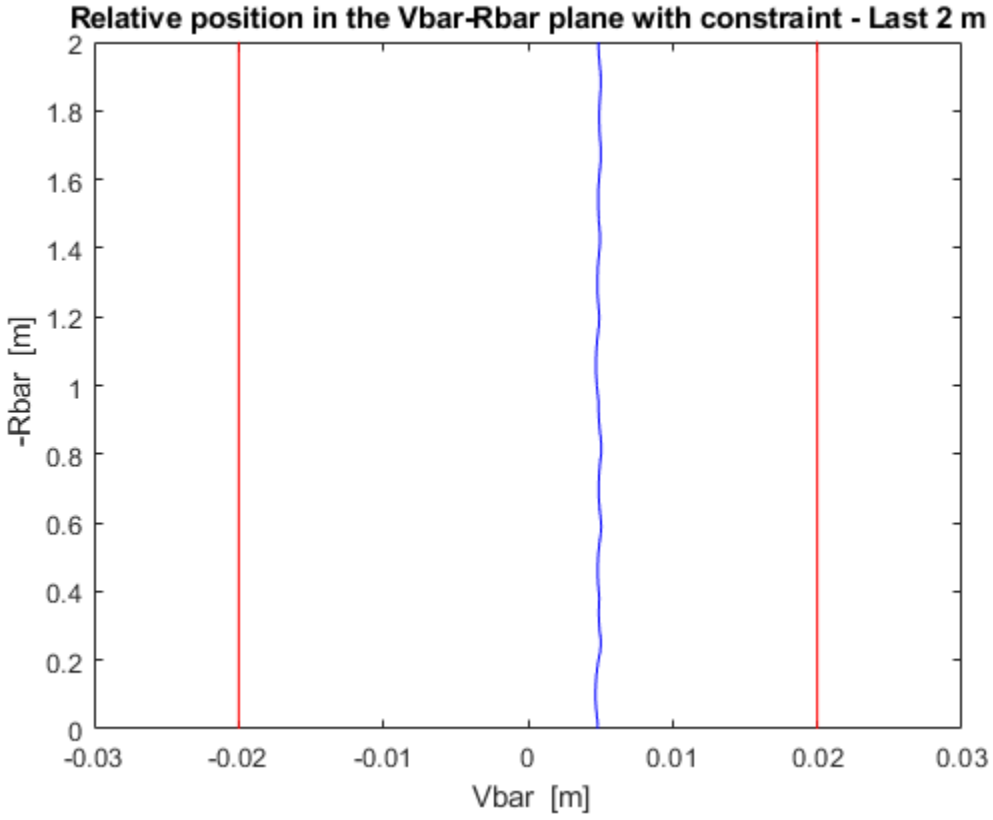

Figure 30 Zoom on trajectory in worst-case scenario in [V-bar, R-bar] plane

From Figure 27, Figure 28, Figure 29 and Figure 30 it can be seen that the trajectory no longer follows the straight line as before, especially along the first few meters. This is due more to the high velocity values than to the position ones. The axial velocity in fact lowers the trajectory, giving it this humped appearance. While it is noted that the controller is also able to work with lateral velocity values comparable to the axial ones. The work done by the second NMPC controller is also noted. When this is activated, at 15m, the trajectory becomes much straighter since the controller parameters relating to the position (i.e. the first 3 diagonal values of the Q matrix) are of an order of size greater than those of the controller which acts from 50m to 15m. This ensures that even in this case the final position is within the desired tolerances.

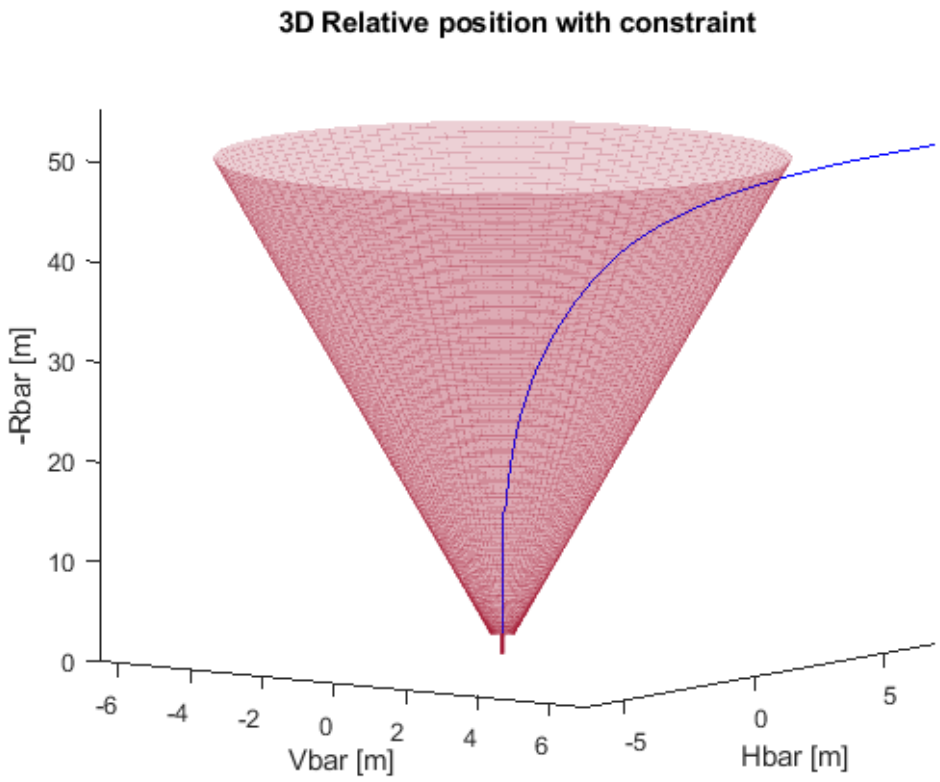

Figure 31 3D Trajectory in worst-case scenario

Figure 31 and Figure 32 show the 3D trajectory to give a more complete view. From these it can better see the initial lowering of the trajectory and the variation it undergoes when the controller at 15m comes into action. In addition, it can be seen that the performances in the last 2m are comparable with those of the nominal case.

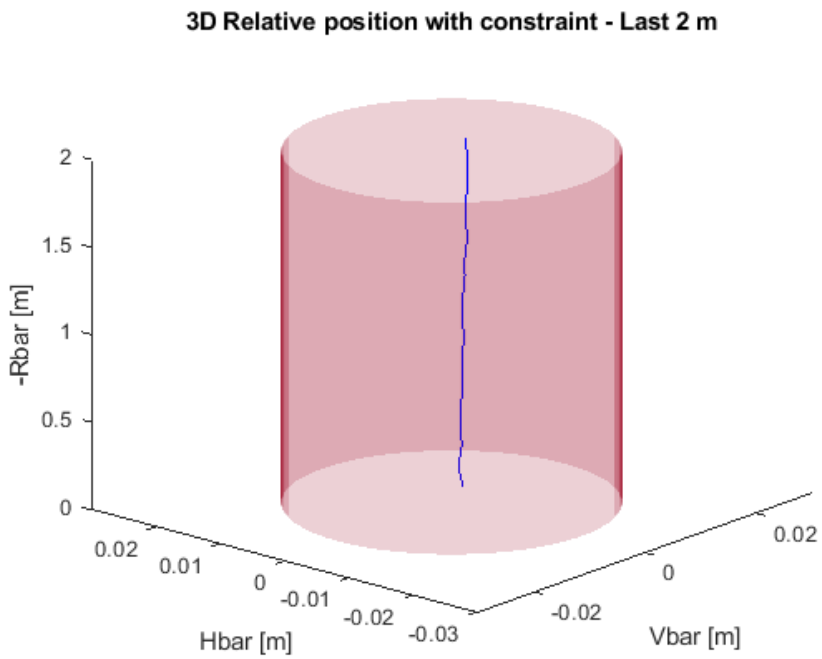

Figure 32 Zoom of 3D trajectory in worst-case scenario

Figure 33 shows the last position of the Chaser during the analysed phase in the [V-bar, H-bar] plane. It can be seen that, as in the previous case, the point found is around 5mm both along V-bar and along H-bar. This is due to the performance of the second controller, which as seen ensure a straight trajectory in the last meters even in worst-case scenario conditions. The requirement for lateral misalignment (<2cm) is largely satisfied.

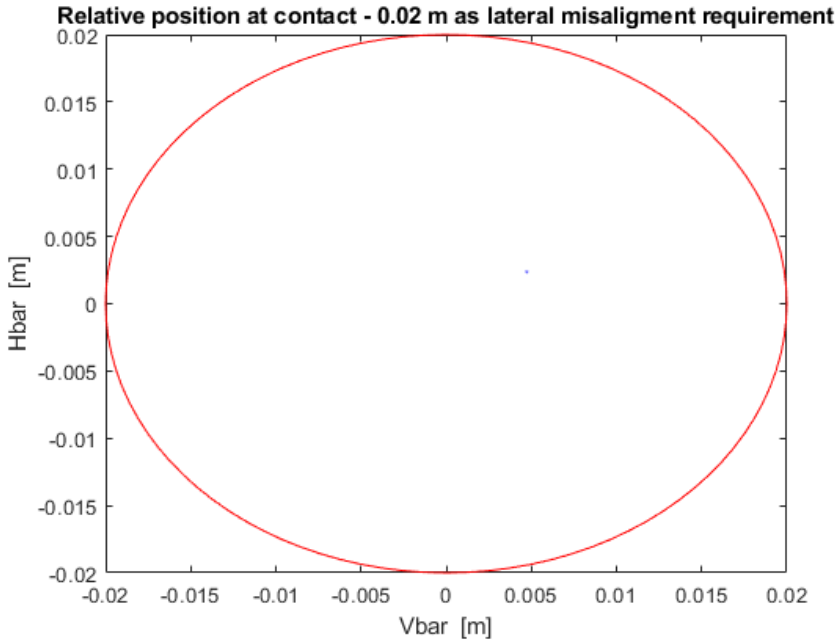

Figure 33 Position at contact for worst-case scenario

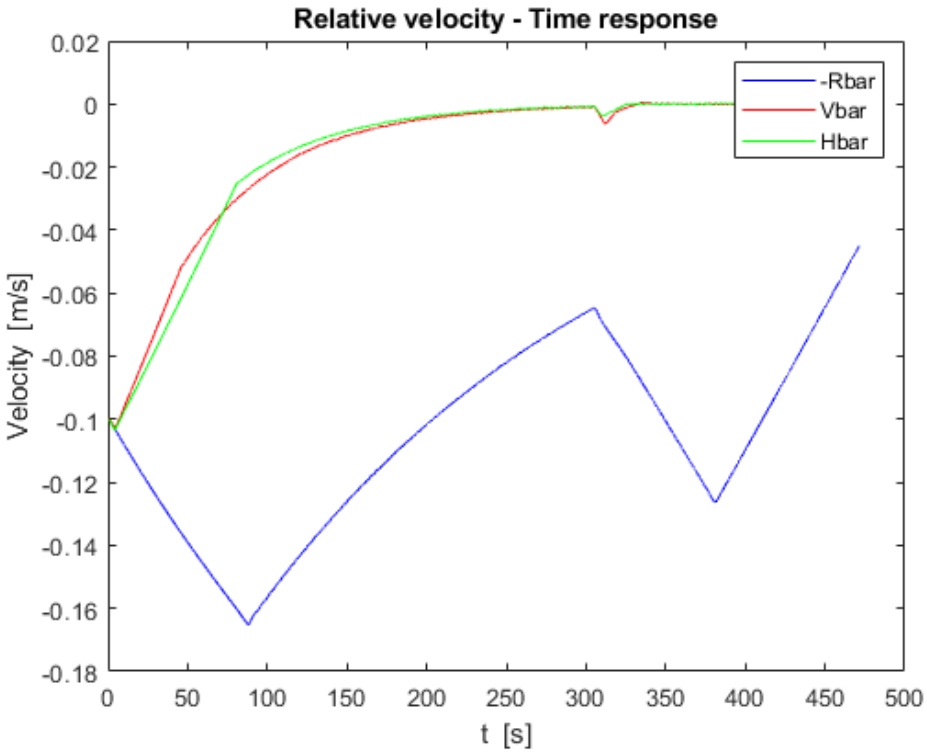

Figure 34 Velocity profiles in worst-case scenario

Figure 34 shows the velocity profiles along axes. The behaviour is the same as in the nominal case, but it should be noted that docking takes less time in this case. This is due to the higher initial velocities, especially the axial velocity, which accelerate the manoeuvre. In fact, it is noted that the velocities in the final point are greater than the nominal ones, but still below 0.05m. Higher initial velocities would lead to an increase in contact velocity which in turn would lead to modifications of the capture mechanism to be resistant to higher energy shocks.

4.2.2 Control and Effective Thrust Results

Figure 35 and Figure 36 show the control thrust output from the control system and the actual thrust output from the actuators. It is noted that both are greater than in the previous case and this is due to the higher velocities. the increase in control forces along the V-bar and H-bar axes is particularly noticeable. Also in this case it can be noted the parallelism between the control forces and the actuating ones that have been obtained through the technique of PWM modulation the duty cycle obtained by the control forces divided by the maximum value the propulsion system can give and sorting the force along the eight thrusters of the propulsion system

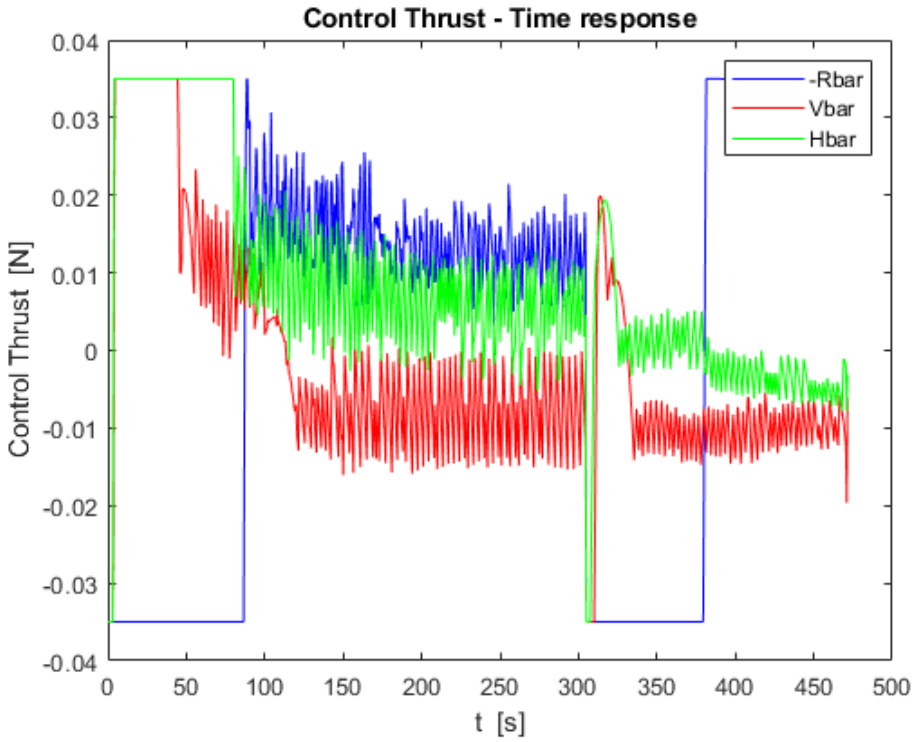

Figure 35 Control thrust in worst-case scenario

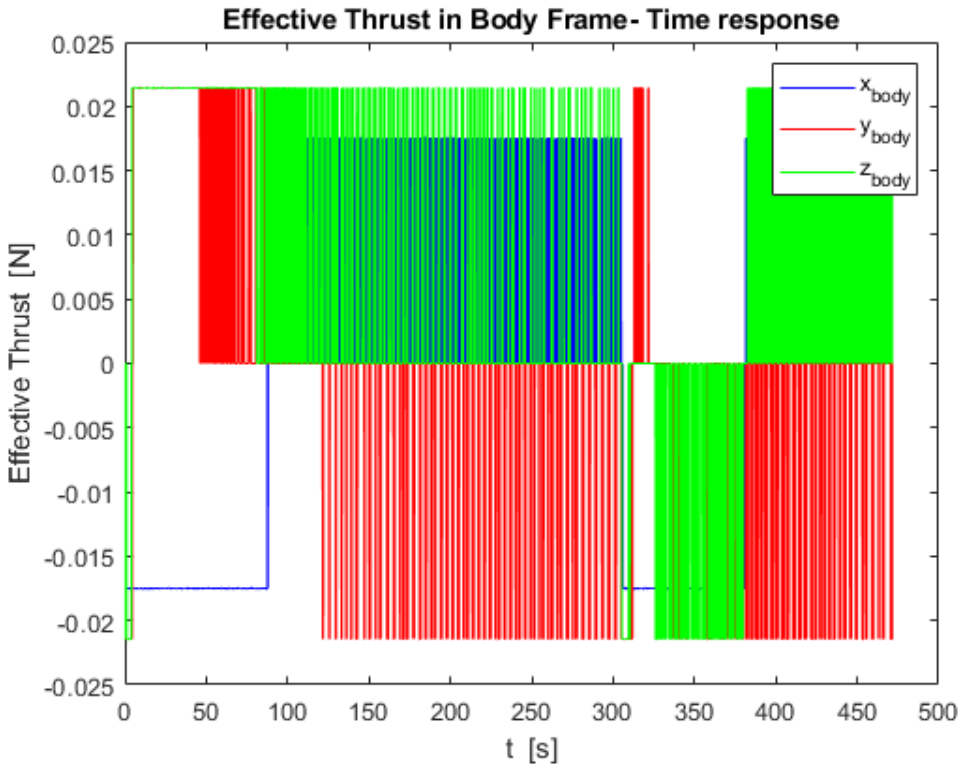

Figure 36 effective thrust in worst-case scenario

Table 5 Effective thrust for every single thruster

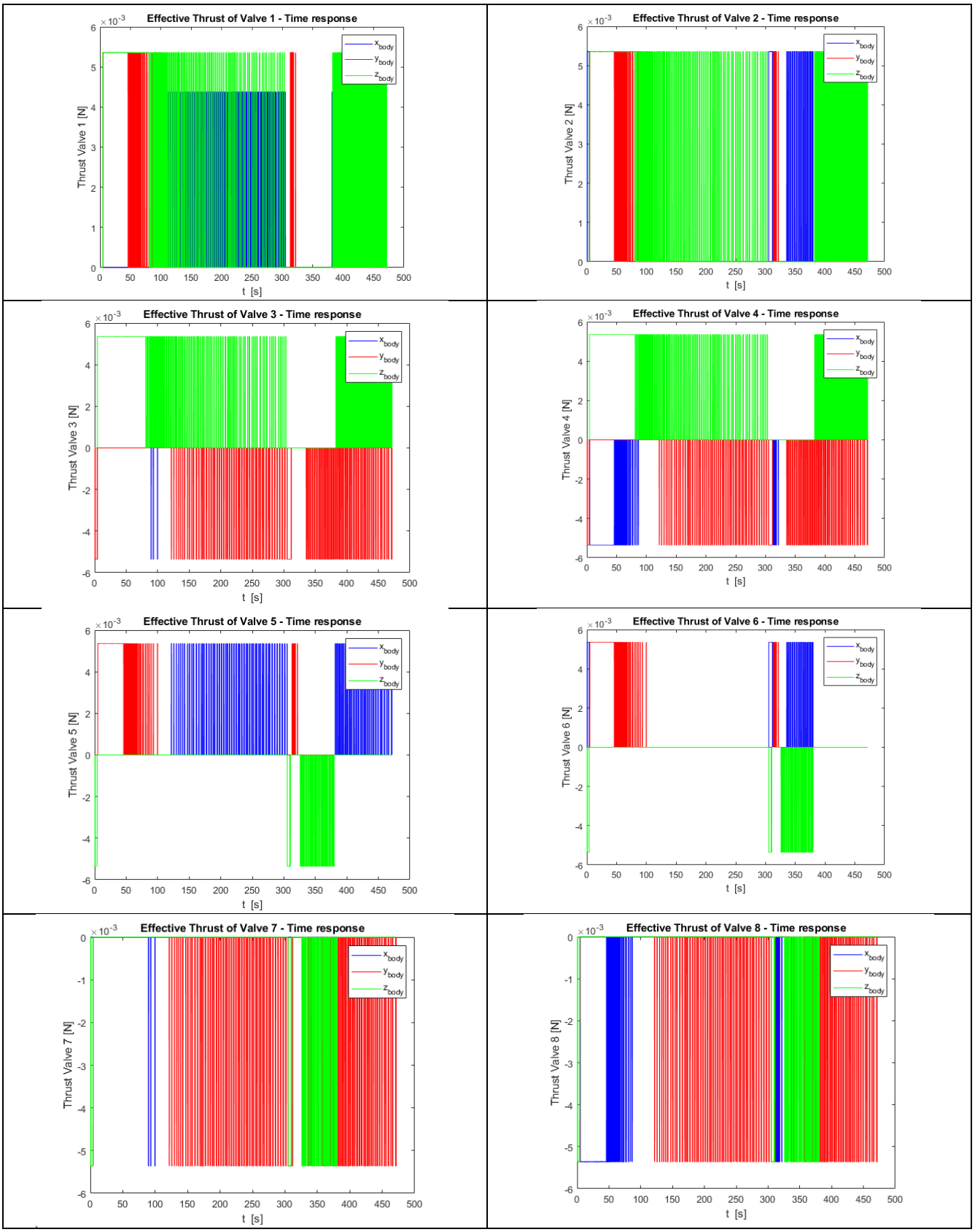

It can be seen from the results that, under worst-case scenario conditions but nominal operation, the trajectory does not follow the same straight line as in the case of better initial conditions, but still does not exit the cone maintaining a straight line in the last few metres as in the nominal case. The lateral misalignment is respected in both directions and the contact velocity is within the requirement even if with little margin. The graphs also show, on the abscissa axis, the manoeuvre duration, which in this case is:

$$T_{docking} = 7.93\ min$$

Decreased due to velocity increase. The controller effort metric, computes as in 4.1.2 is instead:

$$J_2 = 1.09$$

While the total Delta-V (Δv) is less than the previous case, equal to:

$$\Delta v = 0.43\ m/s$$

Examining these worst-case results shows that both the docking duration, the controller effort indicator parameter and Delta-V have decreased. In this case, the initial velocities are not zero. This leads to a decrease in the duration of docking and therefore a decrease in the other two parameters.

4.3 Robustness Analysis

To verify the robustness of the controller, it was subjected to 300 Monte Carlo analyses. Monte Carlo analysis is a statistical analysis technique that provides a range of possible estimates for the analysed value and is usually performed in situations where there is uncertainty about the design values.

In this case, the uncertainty concerns the initial conditions in terms of mass, position, velocity, attitude and angular velocities. Analyses are performed by varying each of these values within a certain range in order to verify the performance of the controller when subjected to changes in initial conditions. The ranges of variability of each of the variables considered are listed.

4.3.1 Mass Uncertainty

Mass is considered uncertain due to the decrease in propellant consumption. As the nominal mass is 20 kg, it is varied by +/- 2 kg:

$$18\ kg < m_c < 22\ kg$$

using the following mathematical model:

$$m_c = (4 \cdot rand) - 2$$

4.3.2 Position Uncertainty

The initial position is uncertain because its accuracy will depend on the performance of the controller relative to the previous phase of the analysis. It has been chosen to vary the position by +/- 2 metres from the nominal position of $x = 50, y = 0,\ z = 0$. In which x, y and z are the RIC components with the x and z axis reversed, therefore they correspond to R-bar, V-bar and H-bar

obtaining the range of variability :

$$48\ m < x < 52\ m$$

$$-2\ m < y < 2\ m$$

$$-2\ m < z < 2\ m$$

given by the following variational ranges:

$$x = 50 + (4 \cdot rand - 2)$$

$$y = (4 \cdot rand - 2)$$

$$z = (4 \cdot rand - 2)$$

4.3.3 Velocities Uncertainty

Initial velocities are assumed to be zero in the ideal case but will not be exactly zero in the real one. The following ranges have been considered:

$$-0.2\ \frac{m}{s} < v_x < 0\ \frac{m}{s}$$

$$-0.03\ \frac{m}{s} < v_y < 0.03\ \frac{m}{s}$$

$$-0.03\ \frac{m}{s} < v_z < 0.03\ \frac{m}{s}$$

given by the equations:

$$v_x = (4 \cdot rand - 2) \cdot 10^{-1}$$

$$v_y = (6 \cdot rand - 3) \cdot 10^{-2}$$

$$v_z = (6 \cdot rand - 3) \cdot 10^{-2}$$

Regarding the controller, the NMPC parameters resulting from the tuning discussed in section 2.6.2 have been used. Since in this case there are not considered failure of the propulsion module, all eight thrusters are active according to the scheme shown in the section 3.2.4.

Even in this case, the results obtained in terms of trajectory, position at contact, velocity along the three axes, control and effective thrust are given below.

4.3.4 Monte Carlo Analysis Results

Figure 37 and Figure 38 show the trajectory results in the [H-bar, R-bar] plane while Figure 39 and Figure 40 show those in [H-bar, R-bar] plane. One sees that the results are very satisfying. The trajectories not only never leave the cone but are almost always straight, except for the first few meters due to the non-zero position components on the V-bar and H-bar axes. It can be seen that, all cases present the behaviour already seen in the nominal case, namely that the trajectories after the switch to the second controller at 15m become even more aligned with the docking axis.

In both planes the lateral misalignment is well below that required and in this regard, it can be seen that in the plane [H-bar, R-bar] in the last meters the trajectories are more accurate (i.e. more dispersed around the zero value) than to those on the plane [V-bar, R-bar] which are less accurate and more precise.

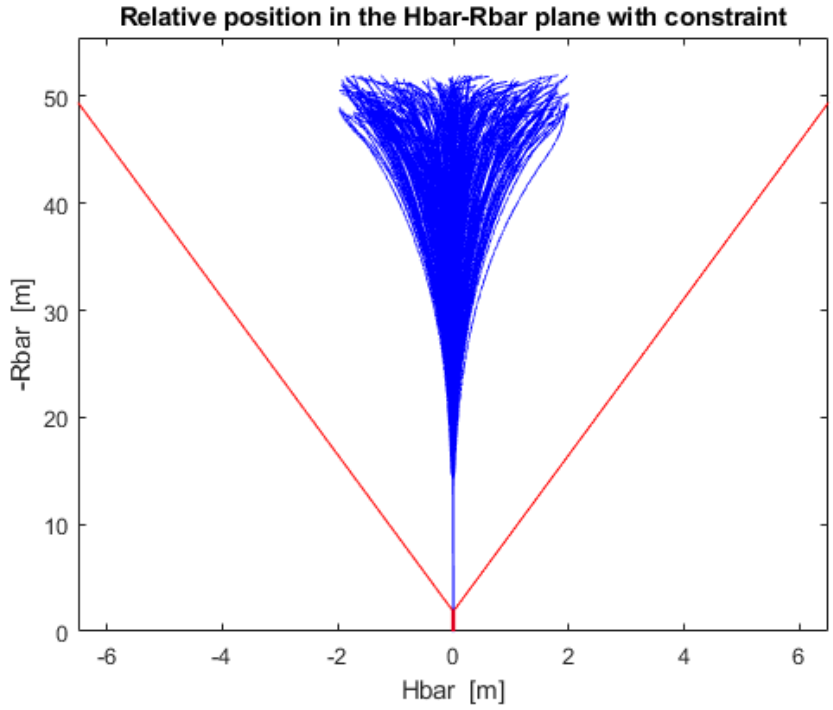

Figure 37 Trajectory in [H-bar, R-bar] plane during 300 Monte Carlo analysis

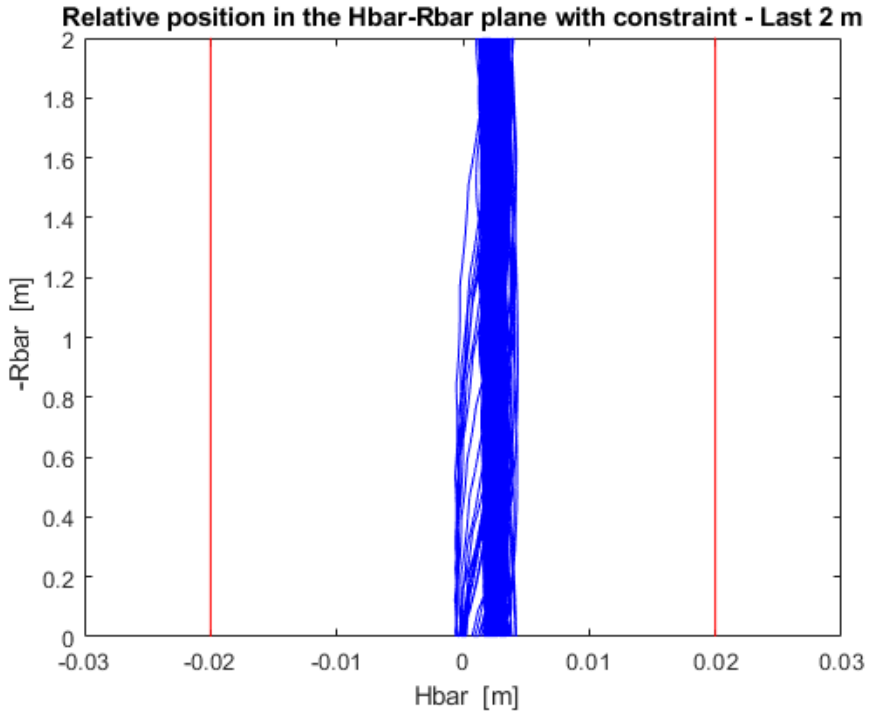

Figure 38 Zoom on trajectory in [H-bar, R-bar] plane during 300 Monte Carlo analysis

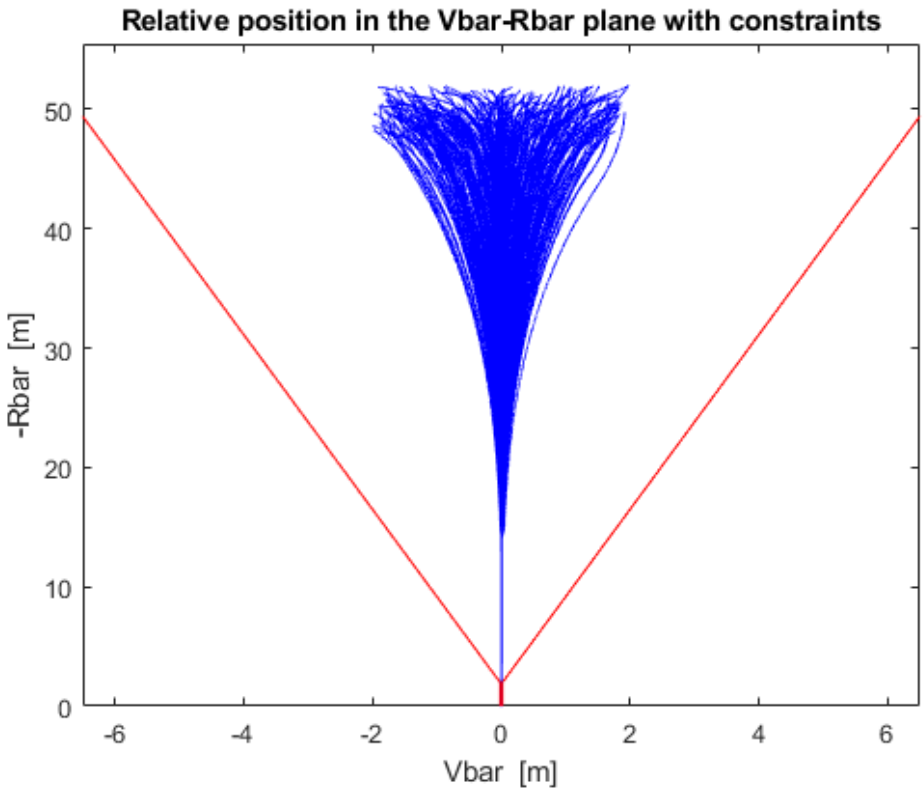

Figure 39 Trajectory in [V-bar, R-bar] plane during 300 Monte Carlo analysis

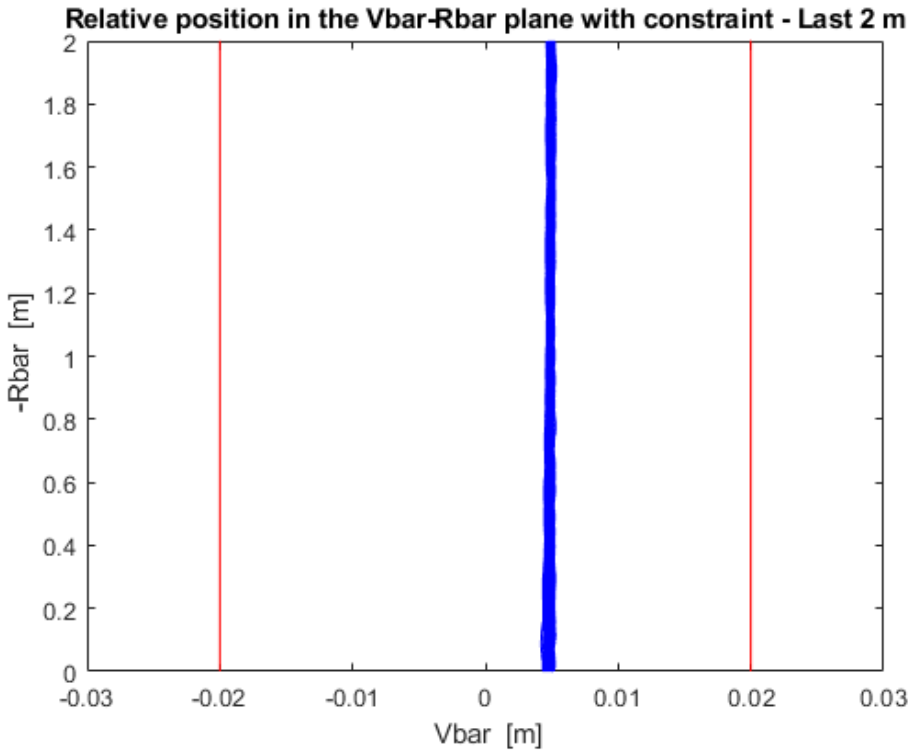

Figure 40 Zoom on trajectory in [V-bar, R-bar] plane during 300 Monte Carlo analysis

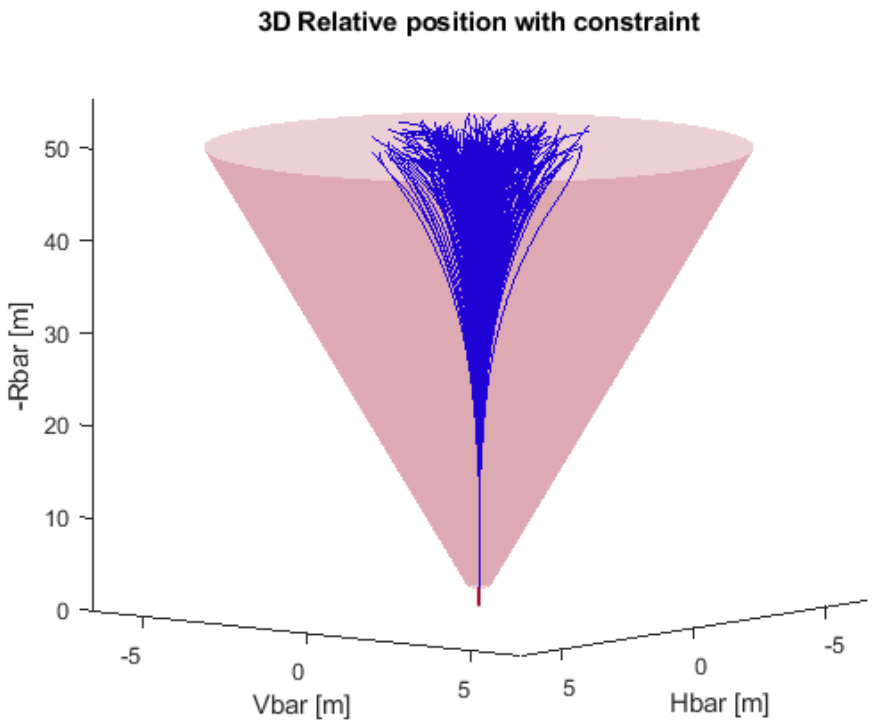

Figure 41 3D Trajectory during 300 Monte Carlo analysis

The 3D trajectories of Figure 42 and Figure 41 can better visualize the figure. It can be seen how the cone constraint is always respected and how the behaviour on the [V-bar, R-bar] and [H-bar, R-bar] planes are so similar that they appear the same in the 3D view.

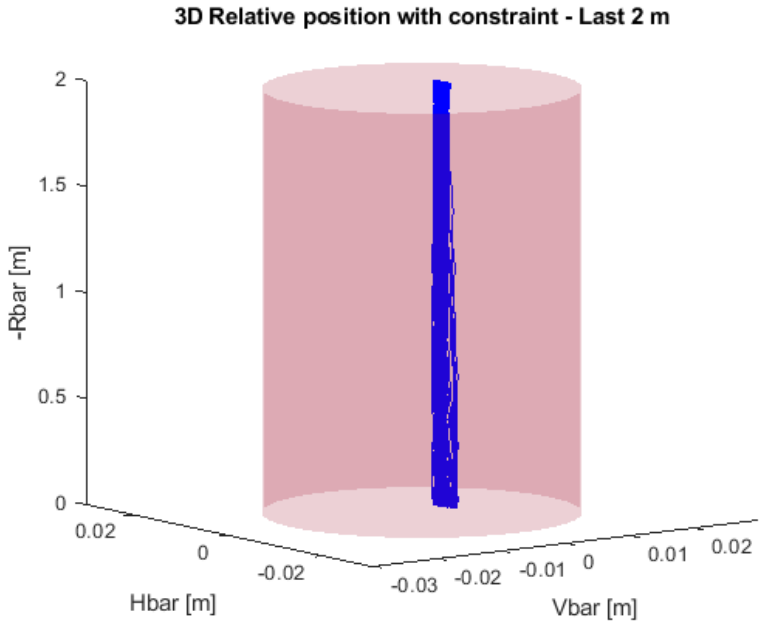

Figure 42 Zoom of 3D trajectory during 300 Monte Carlo analysis

Figure 43 shows the last point of trajectory on the [V-bar, H-bar] plane. Also in this case all the trajectories verify the tolerances of the previous cases, i.e. below or equal to the order of 5mm. However, it can be seen that the contact points of all the trajectories fall in the same area, around 5mm along both V-bar and H-bar. This indicates precision, but not accuracy. Despite this and given the small distances, the lateral misalignment requirement is largely met for all 300 Monte Carlo analysis.

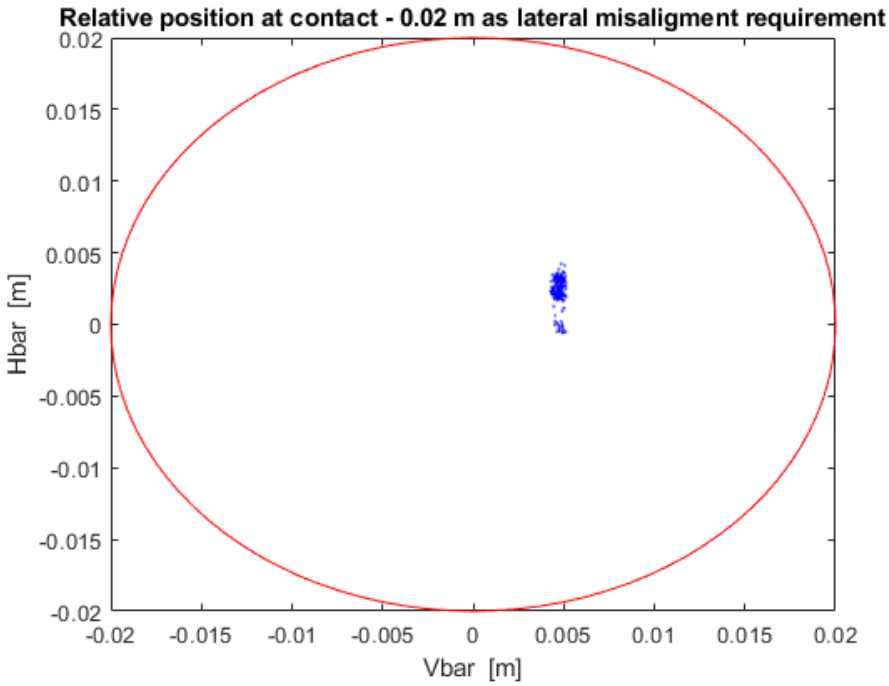

Figure 43 Position at contact during 300 Monte Carlo analysis

In Figure 44 there are the velocity profiles of all 300 Monte Carlo analysis. It can be noted that the trend common to all trajectories is the same as in the nominal case. It presents a first deceleration and then an acceleration starting from 15m on negative R-bar followed by a second deceleration which leads to obtaining the final velocities. These, also in this case, are always below 0.05m, but in some cases the margin is zero. This could lead to an re-iteration of the controller parameters to cause this margin to increase. Furthermore, due to the multiple overlapping profiles, the behaviour of the velocities along the lateral directions is seen in a more pronounced way. In particular, it can be seen an oscillation around the time corresponding to a distance of 15m and therefore when the switch between the first and second controller occurs. At this point, therefore, the lateral velocity components increase to straighten the trajectory and make it even more axial.

On the abscissa axis of Figure 44 is the time taken by the simulation i.e. the duration of the docking manoeuvre. In Figure 45 this has been represented for each simulation. It can be seen that, the average value is around 450s or 7 minutes, and never exceeds ten minutes thus respecting the relative requirement.

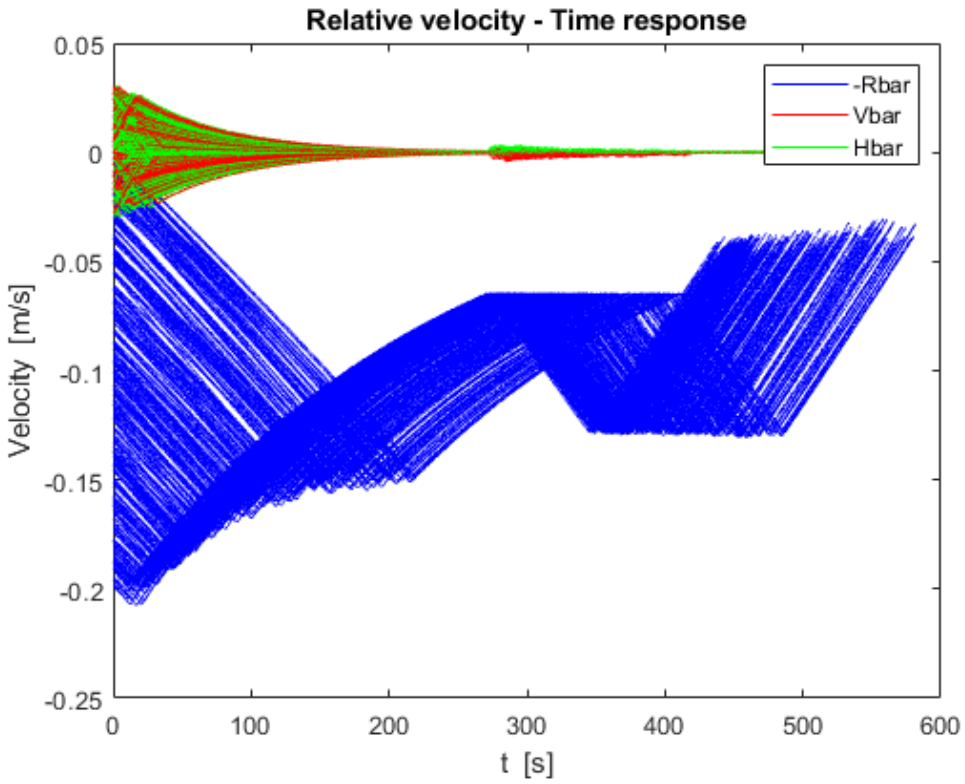

Figure 44 Velocity profiles during 300 Monte Carlo analysis

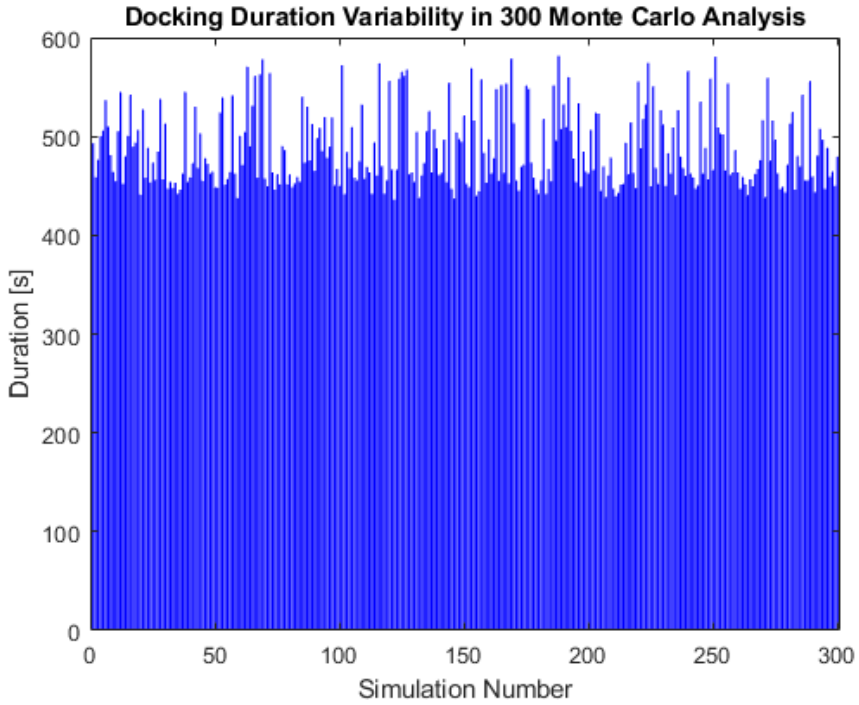

Figure 45 Docking duration for 300 Monte Carlo analysis

Thus, it was observed that the controller holds up well to robustness analyses by maintaining a straight trajectory The trajectory never exceeds the cone constraint, the contact velocities and lateral misalignment meet the requirements and the overall time for docking is always less than 10 minutes.

4.4 Off-nominal conditions

Given the state of the art of the simulative system being considered, the details of which are in section 2.3 and 3.2 , this study has focused on the failures that can occur to the actuation part relating to trajectory control and hence the propulsion system.

Regarding the existing model, the most important failures that can be simulated are those concerning the valves that regulate propellant delivery to the nozzles. These can be:

- Open valve failure, which occur when the valve through which the propellant is emitted from the thruster fails to close again;
- Close valve failure, which occur when the valve that injects the propellant into the thruster fails to open.

The system model described in section 3.2.4 simulates the behaviour of the 8 individual and independent thrusters seen as a combination of valve and nozzle and modelled by pulse width modulation (PWM) of the input signal as described in section 3.2.4 .

4.4.1 Close Valves Failure

The failure situation caused by a valve not opening, known as close valve failure, is simulated by nullifying the components of the thruster under consideration and redistributing the control force to the remaining ones.

In this example and in the following the thruster 4 was examined, whose components are:

$$Thruster\ 4\ force\ components: [-f_x \quad -f_y \quad f_z]$$

As a first attempt, the case where no action is taken to compensate for the valve failure was considered. To do this, a set of 60 Monte Carlo analyses was analysed in which the values varied in the ranges below, in which x, y and z are the RIC components with the x and z axis reversed, therefore they correspond to R-bar, V-bar and H-bar.

$$48\ m < x < 52\ m$$

$$-2\ m < y < 2\ m$$

$$-2\ m < z < 2\ m$$

$$-0.2\ \frac{m}{s} < v_x < 0\ \frac{m}{s}$$

$$-0.03\ \frac{m}{s} < v_y < 0.03\ \frac{m}{s}$$

$$-0.03\ \frac{m}{s} < v_z < 0.03\ \frac{m}{s}$$

$$18\ kg < m_c < 22\ kg$$

The results of Monte Carlo simulations presenting a failure close valve in terms of trajectory are shown in Figure 46, Figure 47, Figure 48, Figure 49 the first two in the [H-bar, R-bar] plane and the last ones in the [V-bar, R-bar] plane. It is noted that several situations occur along both planes where the limits of the safety cone are violated. In the [H-bar, R-bar] plane, this only happens in the last few meters and the controller is able to adjust the trajectory in the last meter before capture. While in the [V-bar, R-bar] plane several times and for different distances from the Target the cone is violated. This would lead to immediate execution of escape manoeuvres compromising the mission.

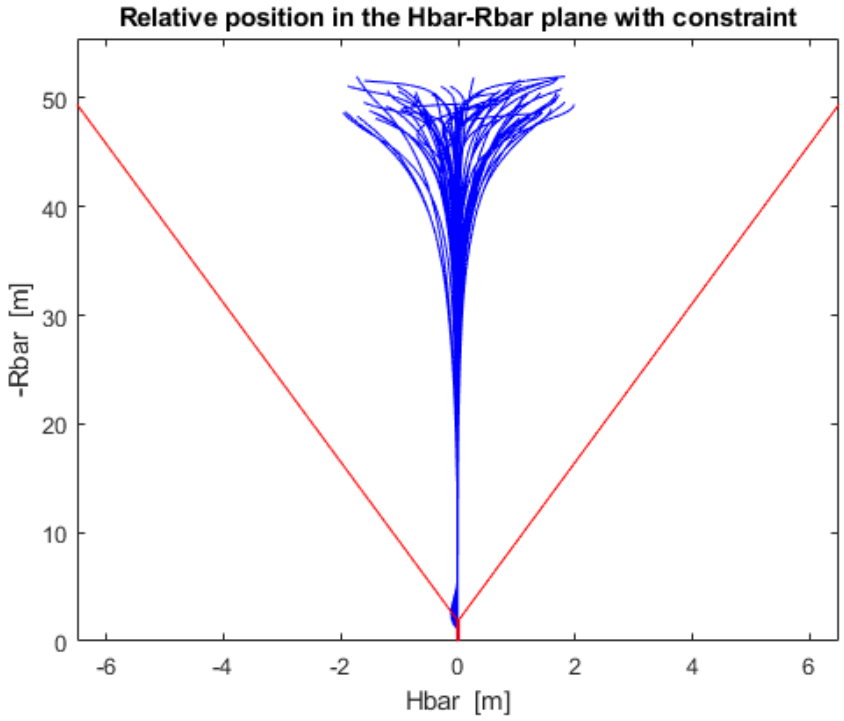

Figure 46 Trajectory in [H-bar, R-bar] plane during 10 Monte Carlo analysis

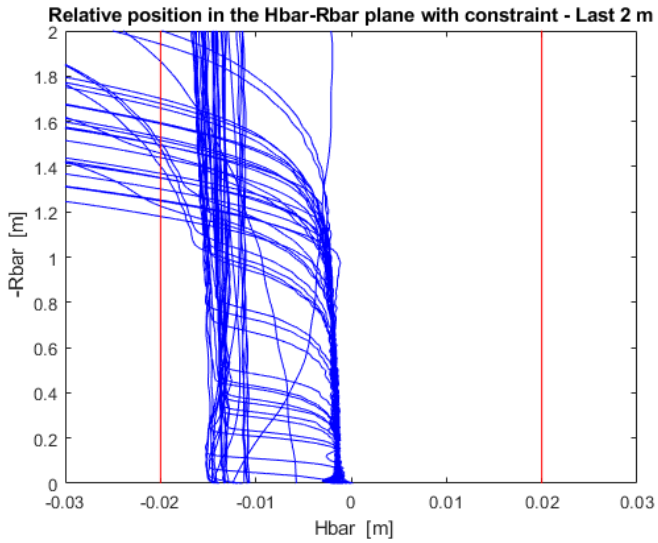

Figure 47 Zoom on trajectory in [H-bar, R-bar] plane during 10 Monte Carlo analysis

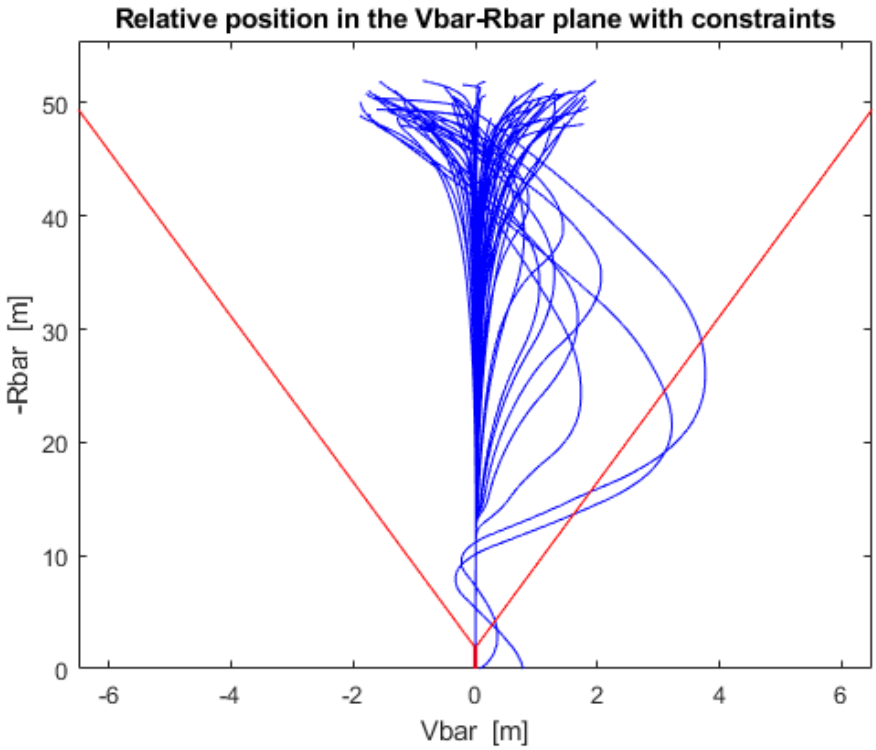

Figure 48 Trajectory in [V-bar, R-bar] plane during 10 Monte Carlo analysis

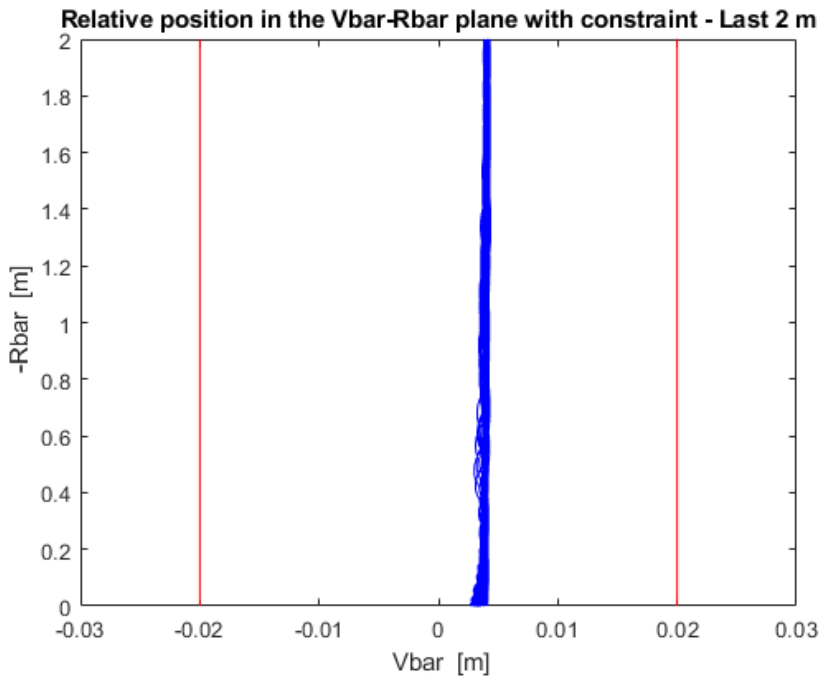

Figure 49 Zoom on trajectory in [V-bar, R-bar] plane during 10 Monte Carlo analysis

Especially in this case, the 3D trajectory helps to visualize the points where constraint violation occurs and the shape of the trajectory. It is also noted that the deviations suffered in the last few metres from the trajectory along [H-bar, R-bar] are given by the same trajectories that violate the trajectory in the [V-bar, R-bar] plane.

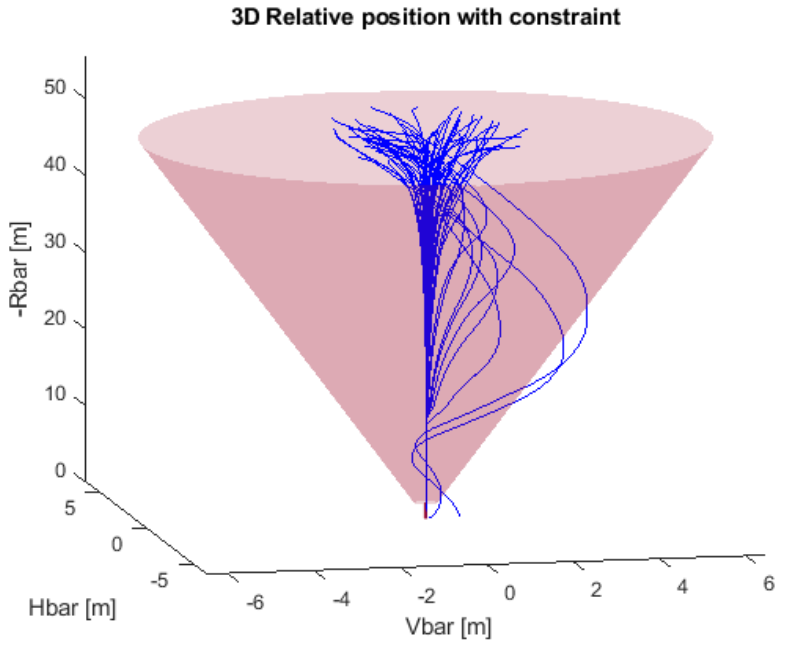

Figure 50 3D trajectory for 10 Monte Carlo analysis

The results showed that the controller cannot guarantee satisfactory performance if no compensatory action is taken. It can be seen from the Figure 51 the anomaly of some velocity trends, especially along V-bar. These increase from small values, remain constant at the maximum and then decrease to a minimum. These velocity profiles are associated with trajectories that do not respect the cone safety constraint. All these velocities are small at the beginning of the trajectory, it is possible that they are caused by a combination of values of the velocity components such that along R-bar and V-bar there are small R-bar value and comparable or higher values along V-bar. In this case the motion would be dragged more towards V-bar and, as the controller is not supported by the maximum capabilities of the actuating system, would cause the above trajectories.

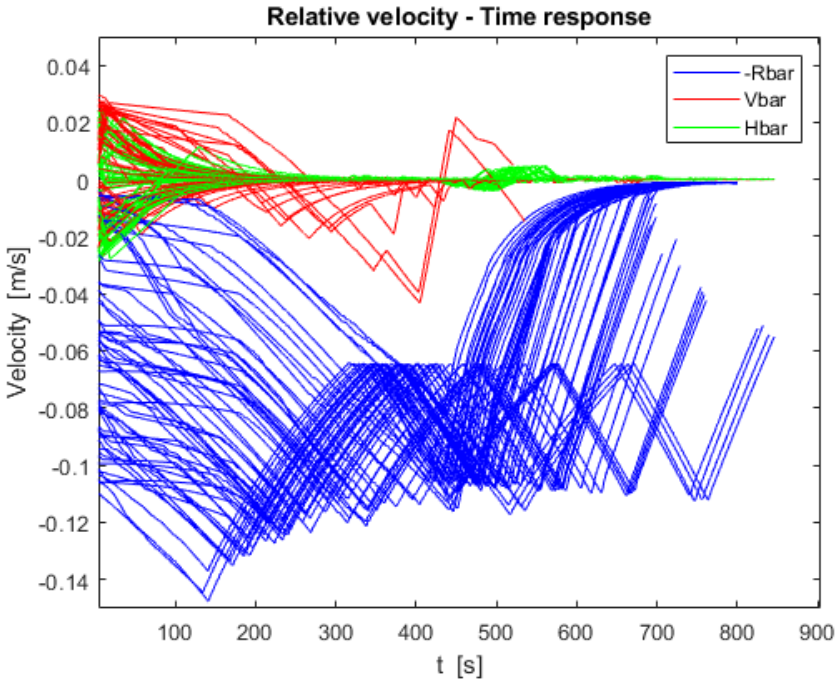

Figure 51 Velocity profiles in close valve failure

In addition, the system must work with a constant disturbance moment applied because the moment generated by the valve of opposite components is not compensated. This results in a disturbance torque, so that the attitude is different from the nominal one and the direction of firing of the thrusters is deviated.

4.4.1.1 Close Valve Failure with Compensatory Action

In order to be able to perform mating even with a close valve failure, the strategy of closing the valve of opposite components was adopted. In this way, the disturbance torque is made zero.

$$Thruster\ 5\ force\ components: [f_x \quad f_y \quad -\ f_z]$$

With this configuration, 60 Monte Carlo analysis have been run with the with the same values as before.

As can be seen from Figure 52, Figure 53, Figure 54 and Figure 55 by implementing a compensatory action the situation improves. In the [H-bar, R-bar] plane it follows the nominal trajectory and there are no longer the oscillations given in the last few metres. This is due to the improvement of the trajectory in the [V-bar, R-bar] plane as well. Here it can be noted that the cone constraint is still violated but the intersection occurs only once during a single trajectory and the violation occurs for a single trajectory. This one remains very similar to the previous case. This confirms that the cause of this phenomenon is not so much the moment of disturbance as the values of the lateral velocities, which, having decreased, drag the Chaser less towards their respective directions.

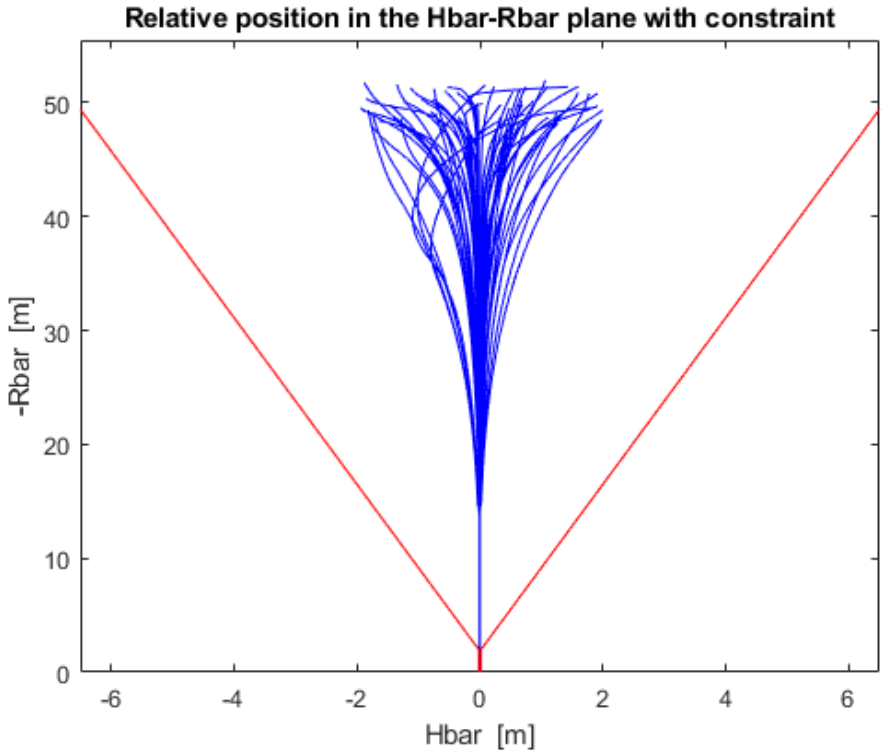

Figure 52 Trajectory in [H-bar, R-bar] plane during 60 Monte Carlo analysis

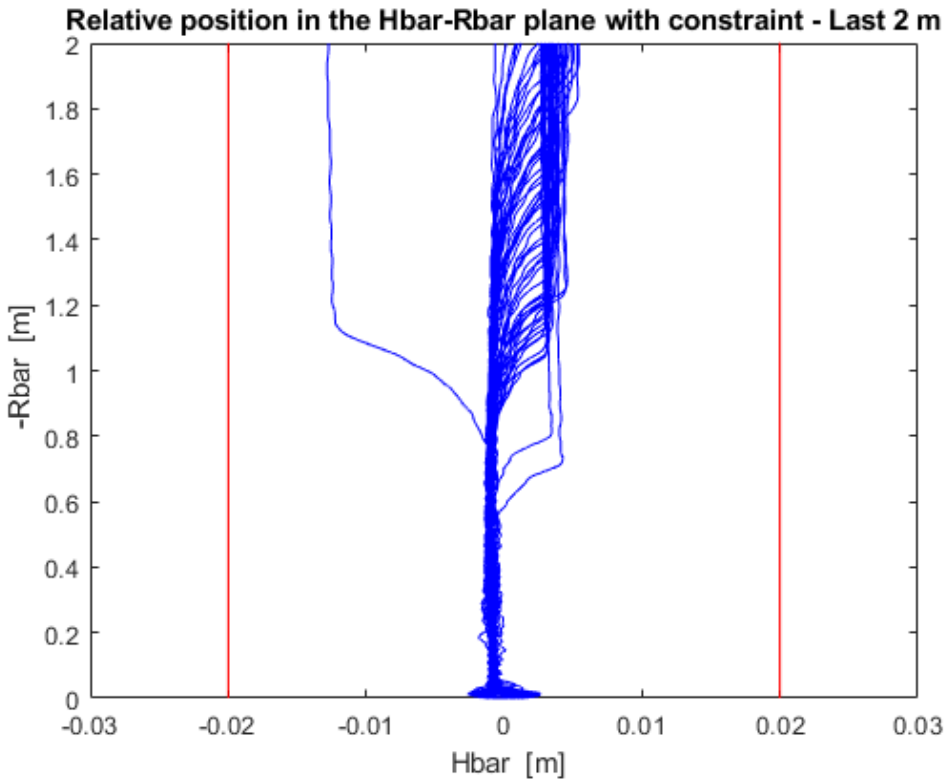

Figure 53 Zoom on trajectory in [H-bar, R-bar] plane during 60 Monte Carlo analysis

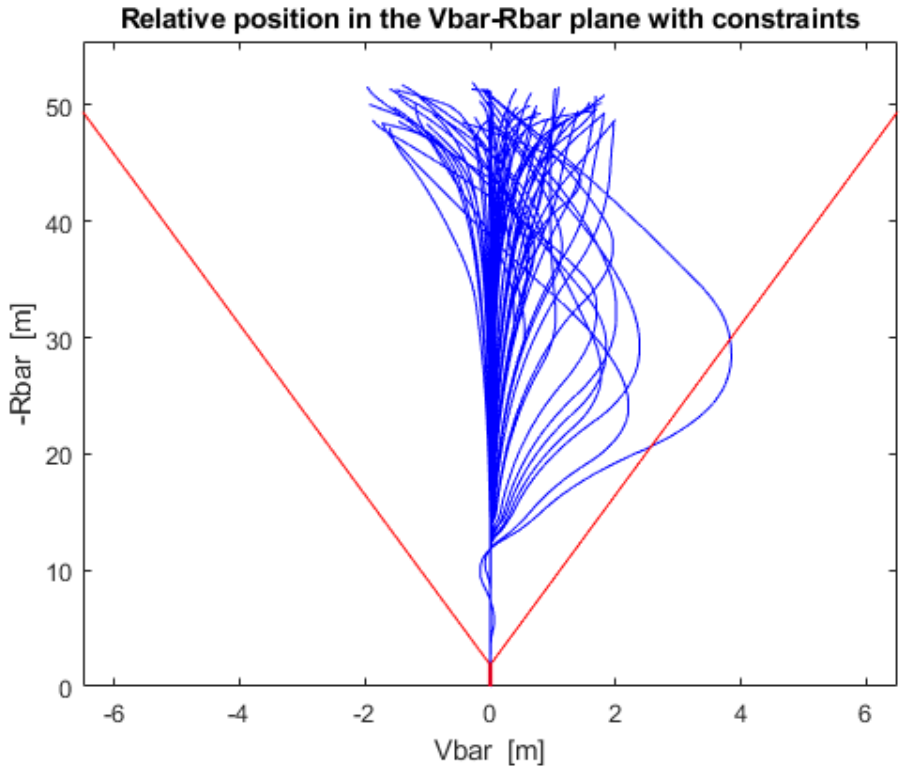

Figure 54 Trajectory in [V-bar, R-bar] plane during 60 Monte Carlo analysis

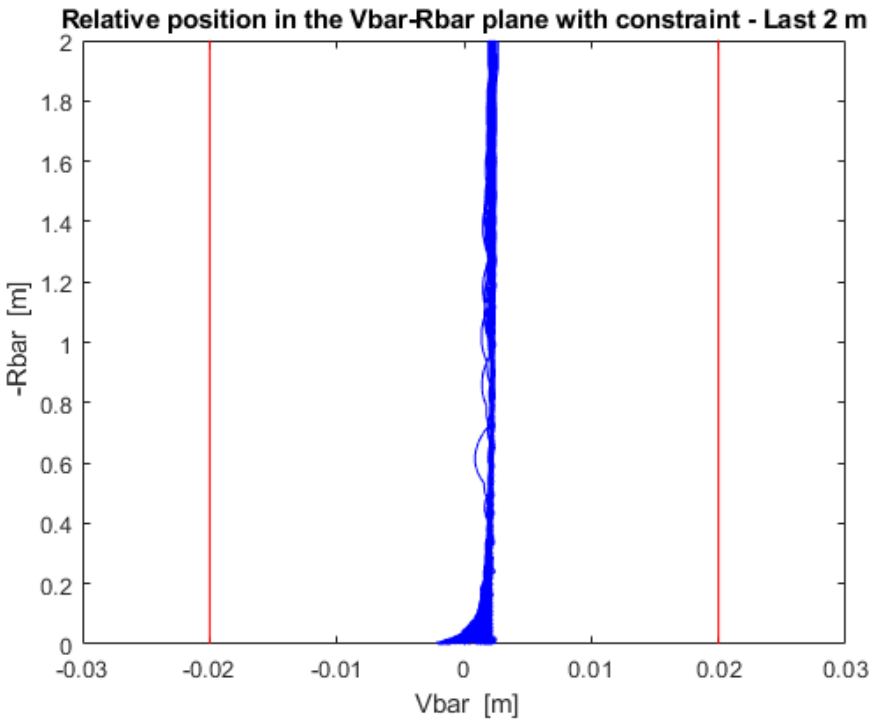

Figure 55 Zoom on trajectory in [V-bar, R-bar] plane during 60 Monte Carlo analysis

The 3D visualisation helps better visualise the trajectory. It can be seen that, the cone constraint is only violated once and that the trajectory in the last few metres looks more like the nominal case than the case in the previous paragraph. It can also be seen that the trajectory is within tolerance in the last metres.

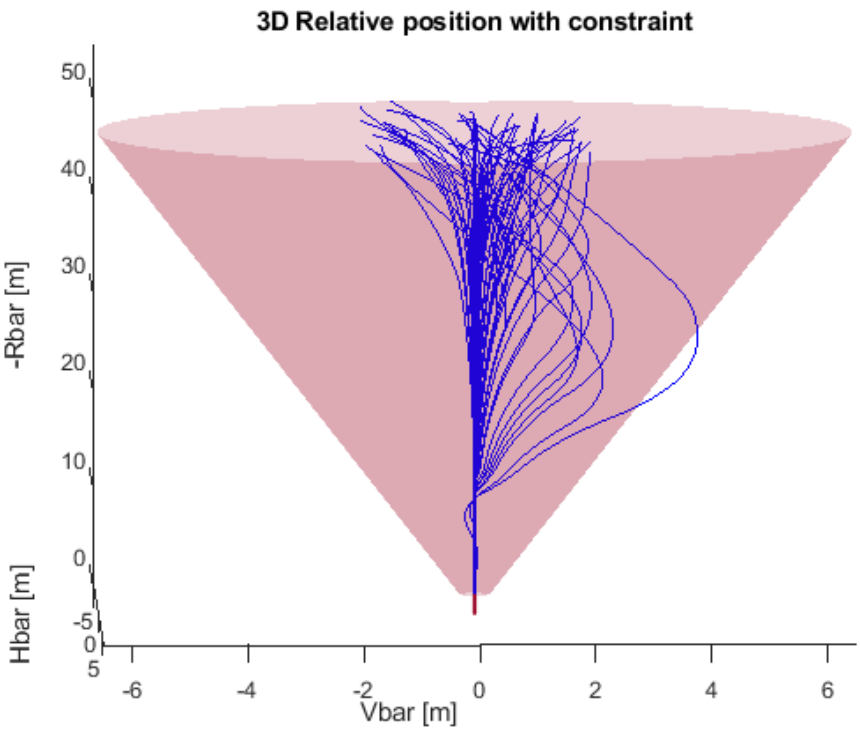

Figure 56 3D trajectory during 60 Monte Carlo analysis

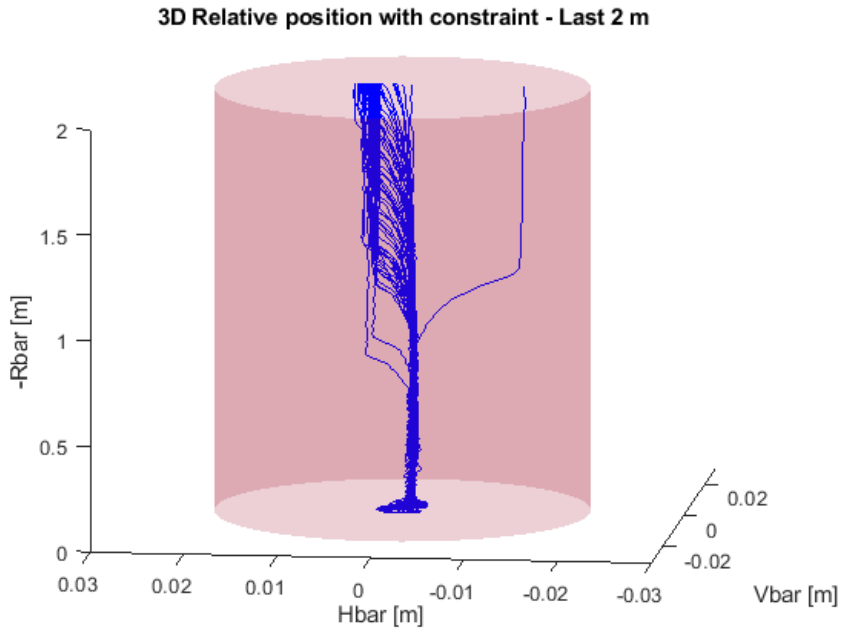

Figure 57 Zoon on 3D trajectory during 60 Monte Carlo analysis

On all simulations only once the cone was violated. However, this is not satisfactory for the safety of the manoeuvre. This occurs for high initial velocities and this leads to define a requirement on the velocity value at the beginning of the close approach to be respected. To define this, the initial velocity values have been decreased by checking what is the maximum value for which the controller can keep the trajectory within the cone. The following variational ranges have been obtained:

$$48\ m < x < 52\ m$$

$$-2\ m < y < 2\ m$$

$$-2\ m < z < 2\ m$$

$$-0.1\ \frac{m}{s} < v_x < 0\ \frac{m}{s}$$

$$-0.01\ \frac{m}{s} < v_y < 0.01\ \frac{m}{s}$$

$$-0.01\ \frac{m}{s} < v_z < 0.01\ \frac{m}{s}$$

$$18\ kg < m_c < 22\ kg$$

As can be seen from the Figure 58 and Figure 59 that, under these assumptions, the trajectory in [H-bar, R-bar] plane is in line with the nominal case. There is no violation of the constraints in the last meters and this suggests that the trajectories in the [V-bar, R-bar] plane have also improved.

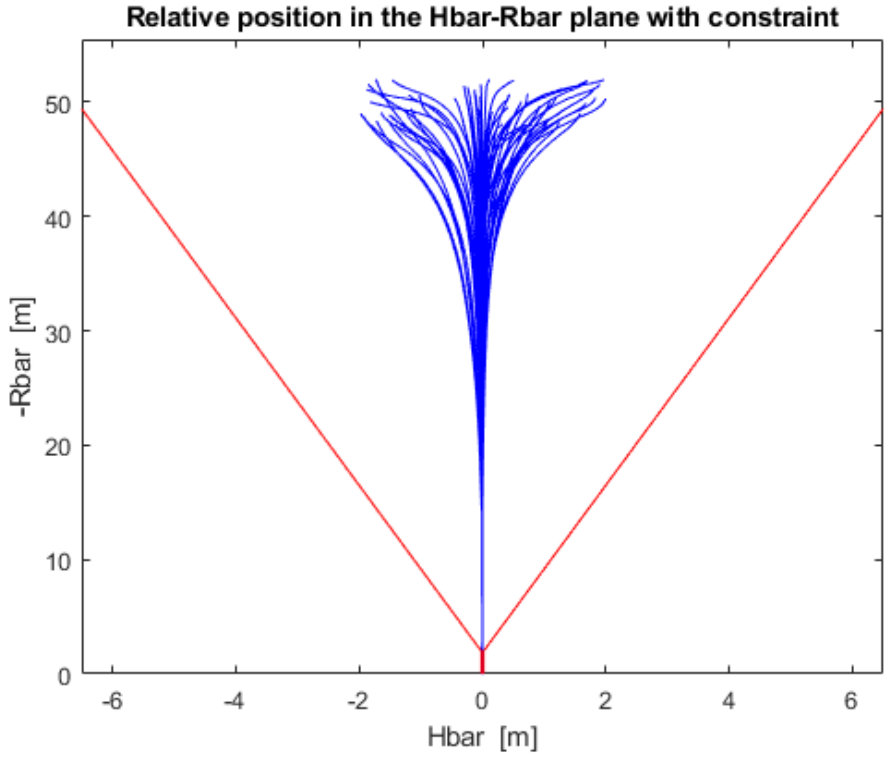

Figure 58 Trajectory in [H-bar, R-bar] plane during 60 Monte Carlo analysis

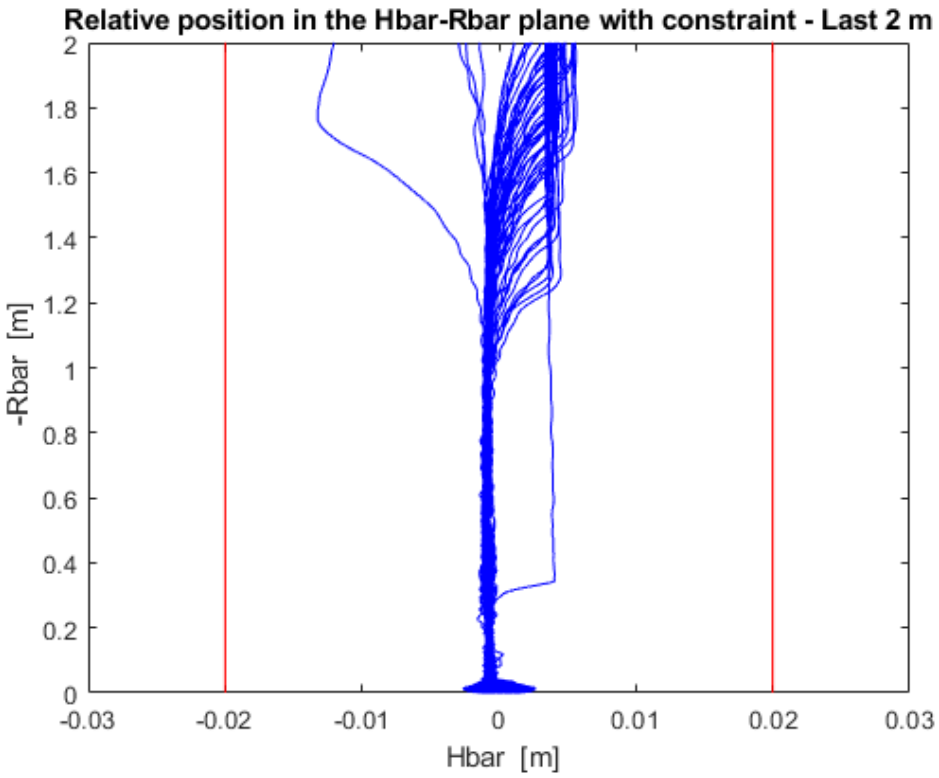

Figure 59 Zoom of trajectory in [H-bar, R-bar] plane during 60 Monte Carlo analysis

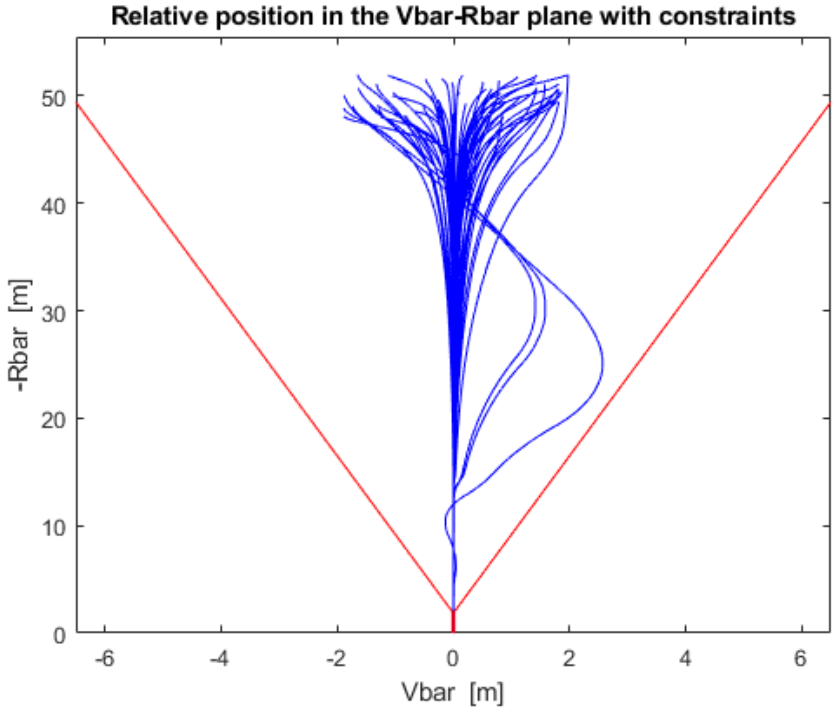

Figure 60 Trajectory in [V-bar, R-bar] plane during 60 Monte Carlo analysis

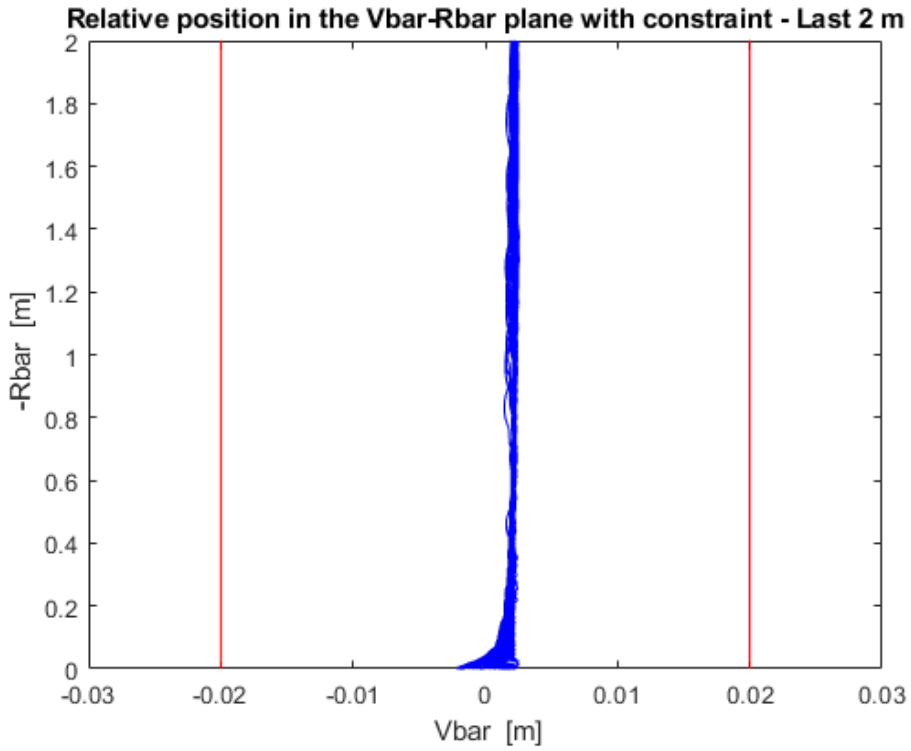

Figure 61 Zoom of trajectory in [V-bar, R-bar] plane during 60 Monte Carlo analysis

It can be seen that in the [V-bar, R-bar] plane all trajectories respect the cone constraint, but still come dangerously close to it. This is because the lateral velocity is decreased, which allows for greater controllability on the part of the system, which works with a lower than nominal actuating capacity. To prevent this situation from happening, there are two ways to act: try to re-tune the controller; set lower limits for the velocity along R-bar that the Chaser must have at the start of the trajectory. This would prevent the Chaser from being dragged along the lateral directions by obtaining more axial trajectories than these.

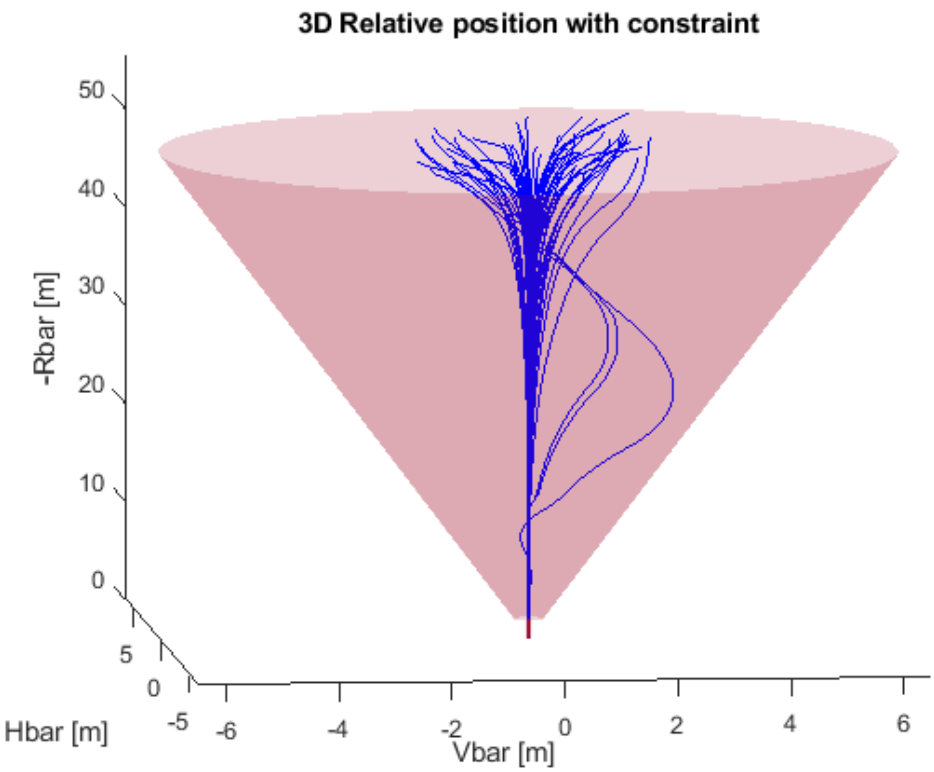

Figure 62 3D Trajectory during 60 Monte Carlo analysis

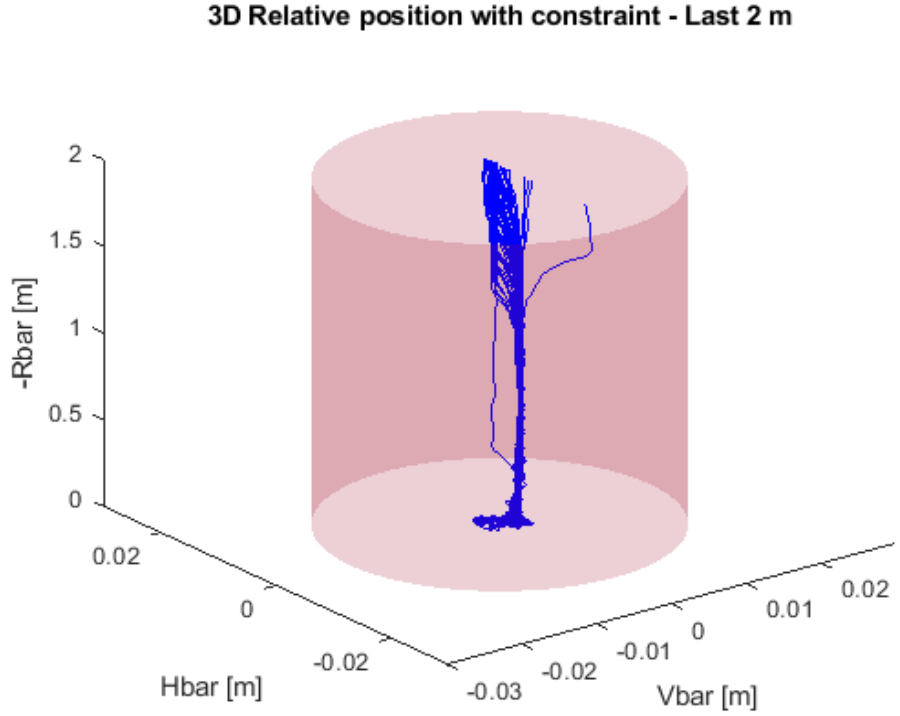

Figure 63 3D Trajectory during 60 Monte Carlo analysis

The Figure 64 shows the position at the beginning of the capture in the [V-bar, H-bar] plane. It can be seen that, as seen in the previous figures for the last few metres of the trajectory, the lateral misalignment requirement is always satisfied. In addition, high accuracy is noted and all positions are at distances on both the V-bar and H-bar axis of less than 5mm.

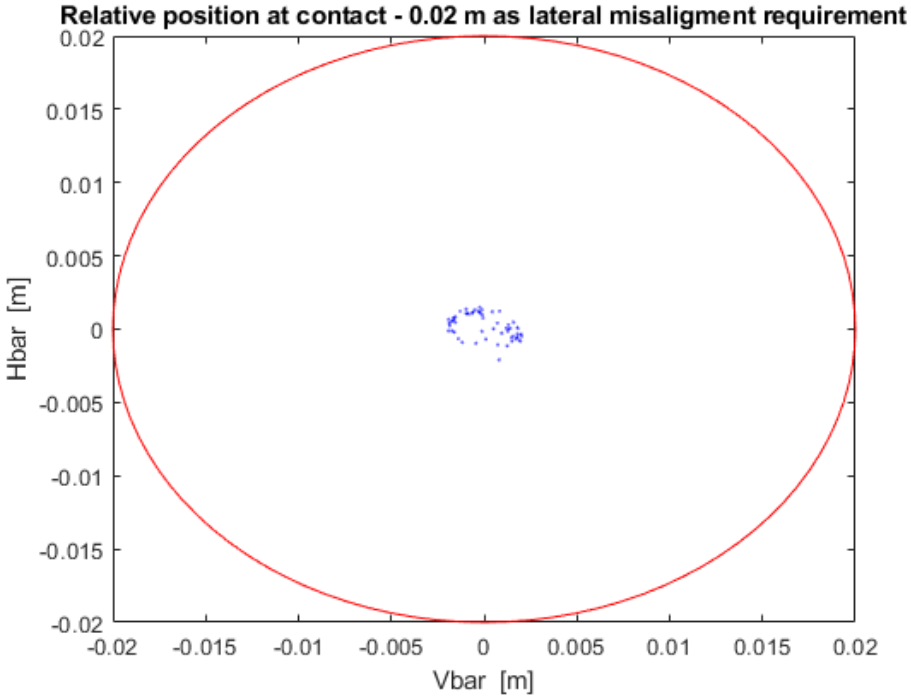

Figure 64 Position at contact during 60 Monte Carlo analysis

The disadvantage of this approach as from the x-axis of the Figure 65 is the longer docking time. As a requirement this must be no more than 10 minutes. However, some SROC scenarios include orbits where the lighting period in this phase can be up to 15 minutes. Whether this condition is acceptable can only be determined when the final scenario is identified. If it is not possible to extend the manoeuvre for longer than required (e.g. due to lighting conditions or ground station coverage) an escape manoeuvre may be performed.

This figure shows the same behaviour as before with regard to velocities, but it can be seen that in this case the negative values on the V-bar axis do not fall below 0.02 m/s whereas previously the minimum was 0.04 m/s. This is further confirmation of the fact that it is the value of the velocity along the V-bar axis that determines this undesirable shape in the trajectories. As mentioned above, this could be solved by either setting a lower limit to the velocity along R-bar or decreasing the velocity along V-bar. This last case could be difficult to implement and will have to be studied in the future implementation of the control system acting on the phase preceding the one studied, i.e. the fly around.

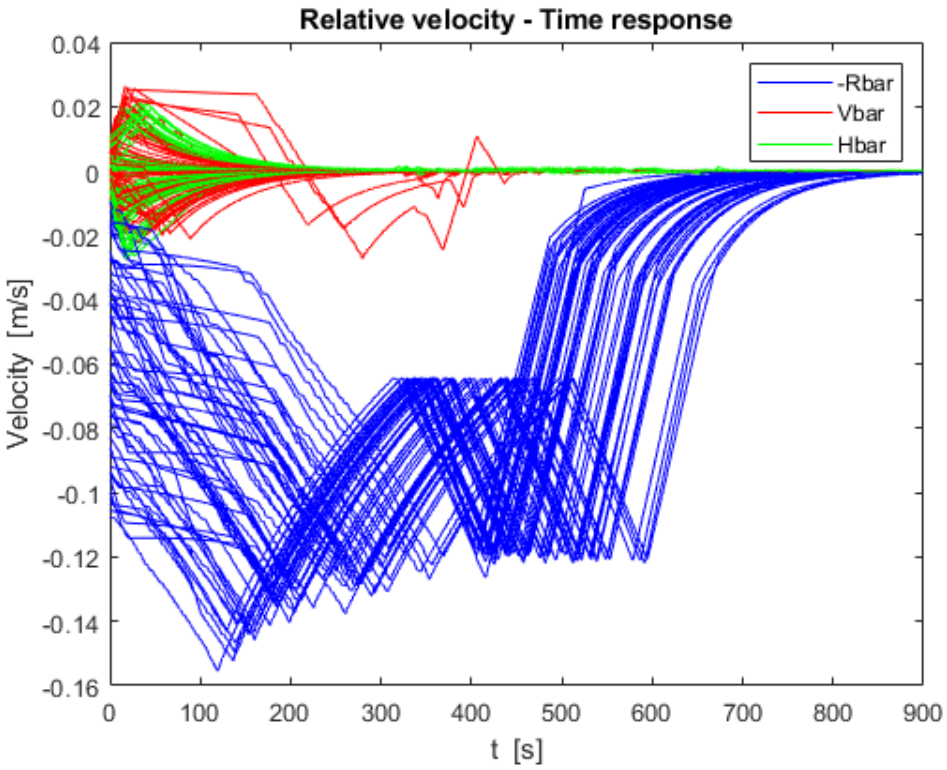

Figure 65 Velocity during 60 Monte Carlo analysis

It is noted that with these velocity values the lateral misalignment requirements are met. The requirement on the maximum velocity at the contact is also respected, but it can be seen from the velocity graph that the duration of the docking (on the abscissa axis) has increased by exceeding the 10-minute requirement. This is due to the fact that, working with only two thrusters for each force component, there are only two other thrusters available for each one.

As a function of this, a requirement can be defined considering the following values as a requirement for the docking initial velocity and therefore for the final velocities of the previous manoeuvre.

$$v_x \leq 0.1 \frac{m}{s}$$

$$v_y \leq \pm 0.01 \frac{m}{s}$$

$$v_z \leq \pm 0.01 \frac{m}{s}$$

The analyses show robustness and accuracy under the assumptions considered. It can also be seen that the behaviour is different in the case of H-bar and V-bar. In fact, aerodynamic resistance also acts along V-bar since V-bar is the direction of motion of the orbit. In addition, in the last 10m of the mating, the aerodynamic force was increased by a factor of 100 to simulate the difference between the aerodynamic resistances acting on the two S/Cs, this because the ballistic coefficients of the two S/Cs differ by two orders of magnitude. This force causes a tendency to push towards positive V-bar. This accentuates as the lateral component of the initial velocity increases.

4.4.2 Open Valves Failure

In the case of open-valve failure, the procedure was the same as for close-valve failure. Initially it has been analysed whether it is possible to end the trajectory without compensating for the failure but leaving the operating system with 7 other functioning thrusters. As before it is assumed that the failed thruster is the fourth:

$$Thruster\ 4\ force\ components: [-f_x \quad -f_y \quad f_z]$$

A total of 60 Monte Carlo analyses have been carried out considering the velocities limits identified in the previous paragraph. The variational ranges are the following, in which x, y and z are the RIC components with the x and z axis reversed, therefore they correspond to R-bar, V-bar and H-bar.

$$48\ m < x < 52\ m$$

$$-2\ m < y < 2\ m$$

$$-2\ m < z < 2\ m$$

$$-0.1\ \frac{m}{s} < v_x < 0\ \frac{m}{s}$$

$$-0.01\ \frac{m}{s} < v_y < 0.01\ \frac{m}{s}$$

$$-0.01\ \frac{m}{s} < \ v_z < 0.01\ \frac{m}{s}$$

$$18\ kg < m_c < 22\ kg$$

The results of 60 Monte Carlo analysis made with the same ranges of variation as before are as follows, it has been chosen to simulate the failure on thruster 4 and to consider the occurrence of failure at the beginning of the trajectory so as to observe the resulting behaviour up to the first to the last metres.

It can see in Figure 66 relating to the [H-bar, r-bar] plane and Figure 68 concerning the trajectory in the [V-bar, R-bar] plane that the trajectory is axial except for the first few metres because of the non-zero velocity values. The trajectory is the same as the nominal trajectory with no oscillations or cone violations and, as for the nominal trajectory, it can be seen the switch of the second controller at 15m which makes the trajectory even straighter.. Particularly Figure 67 and Figure 69 show that while in the [V-bar, R-bar] plane the trajectory in the last few metres is not only within the required tolerances but there is also a sufficiently high margin, in the [H-bar, R-bar] plane this decreases and the final positions are just below the 0.02m requirement.

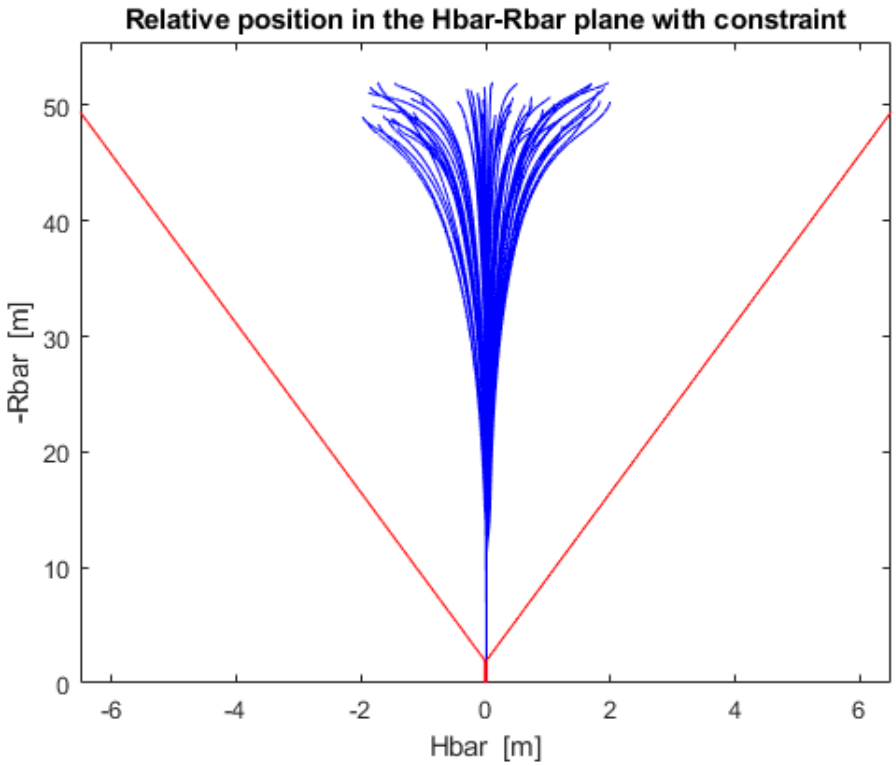

Figure 66 Trajectory in [H-bar, R-bar] plane during 60 Monte Carlo analysis

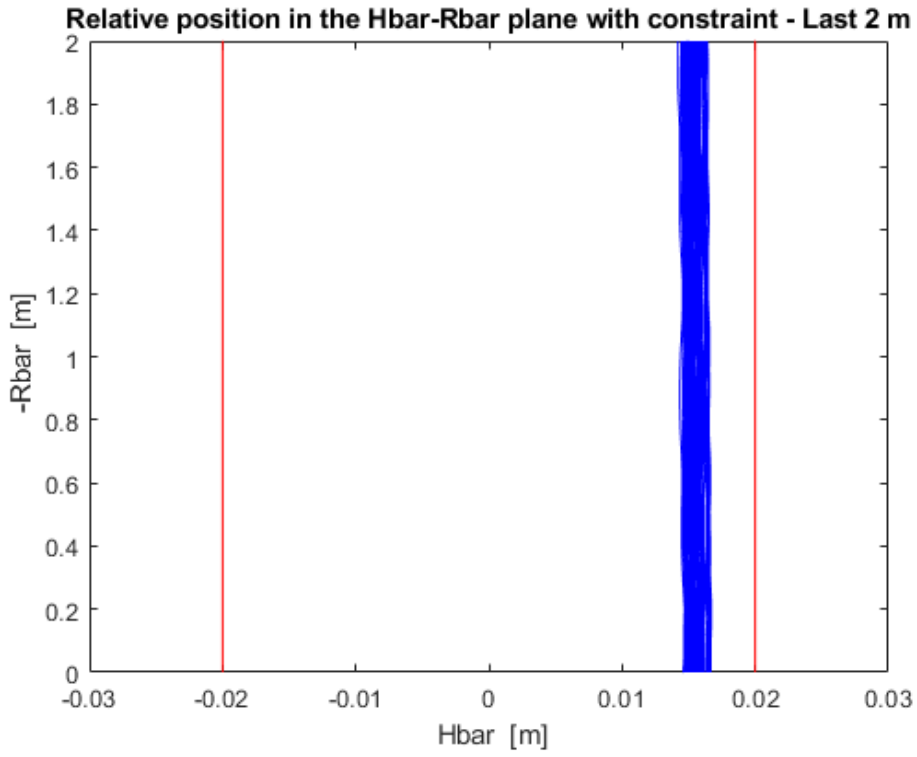

Figure 67 Zoom of trajectory in [H-bar, R-bar] plane during 60 Monte Carlo analysis

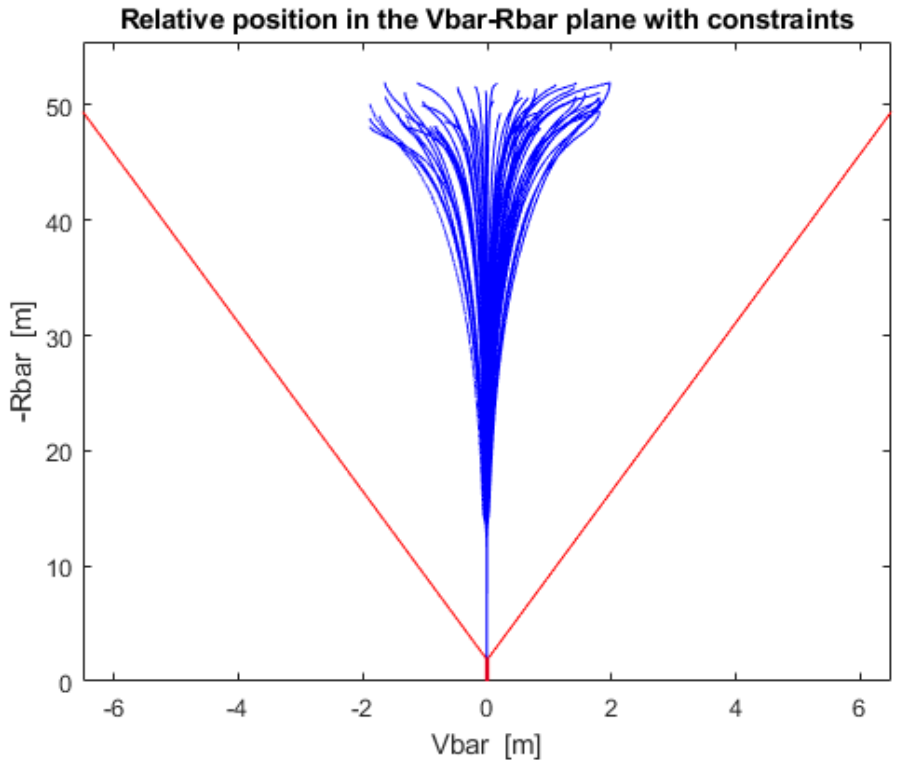

Figure 68 Trajectory in [V-bar, R-bar] plane during 60 Monte Carlo analysis

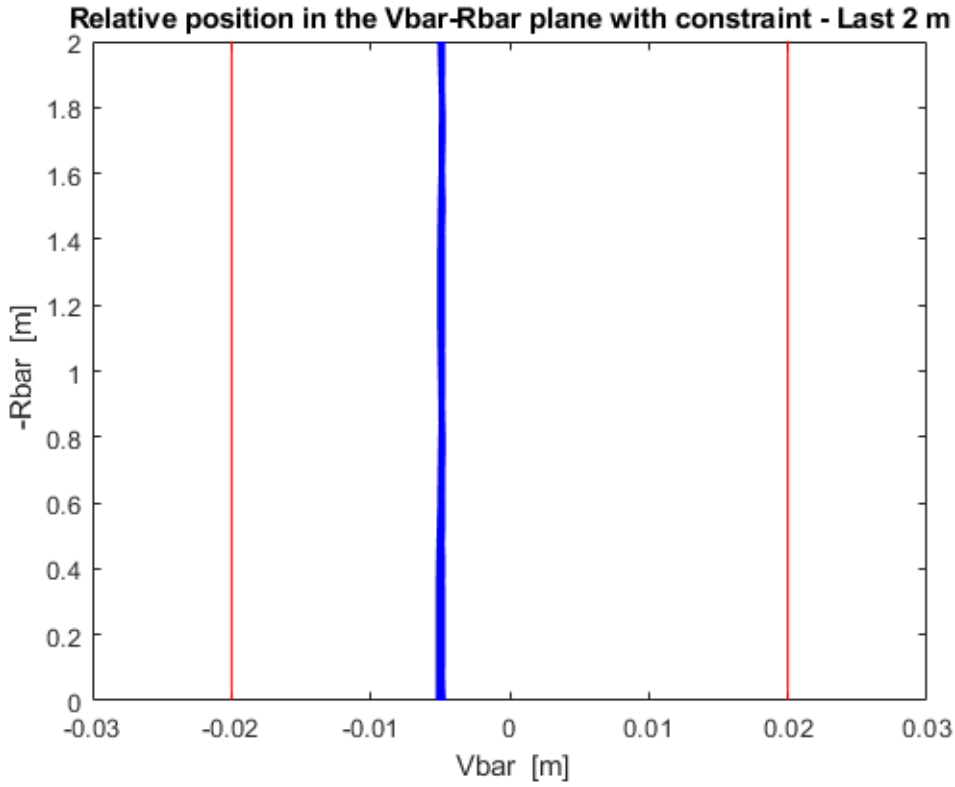

Figure 69 Zoom of trajectory in [V-bar, R-bar] plane during 60 Monte Carlo analysis

From the 3D in Figure 70 and Figure 71 trajectory it can be seen that along the 50m the trajectory is very similar to the nominal one, but in the last two the trajectory is at the limit of the tolerance region of 0.02m.

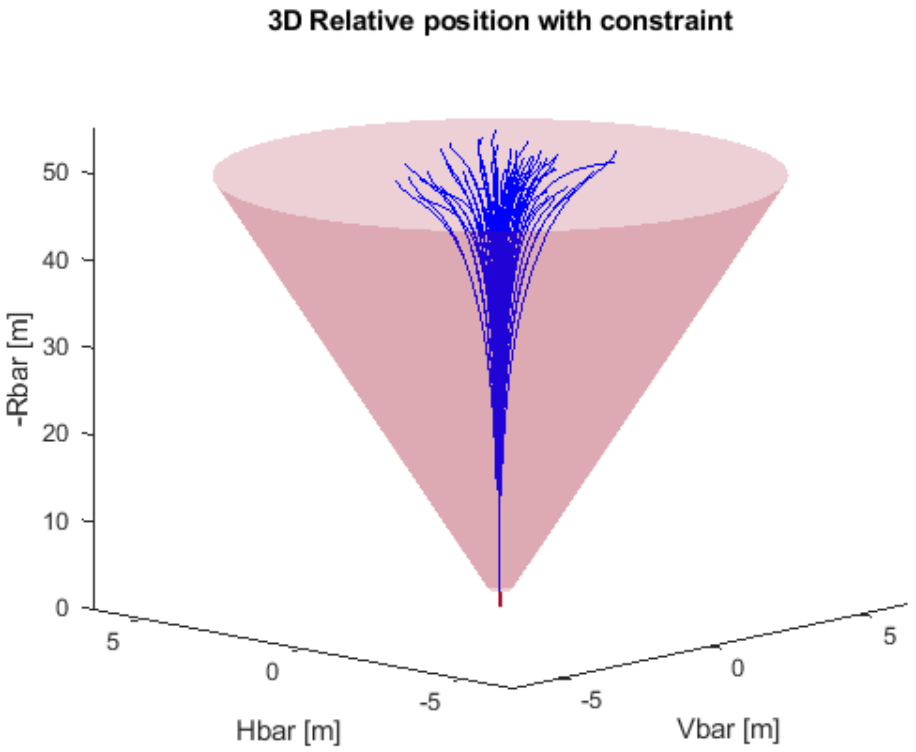

Figure 70 3D trajectory during 60 Monte Carlo analysis

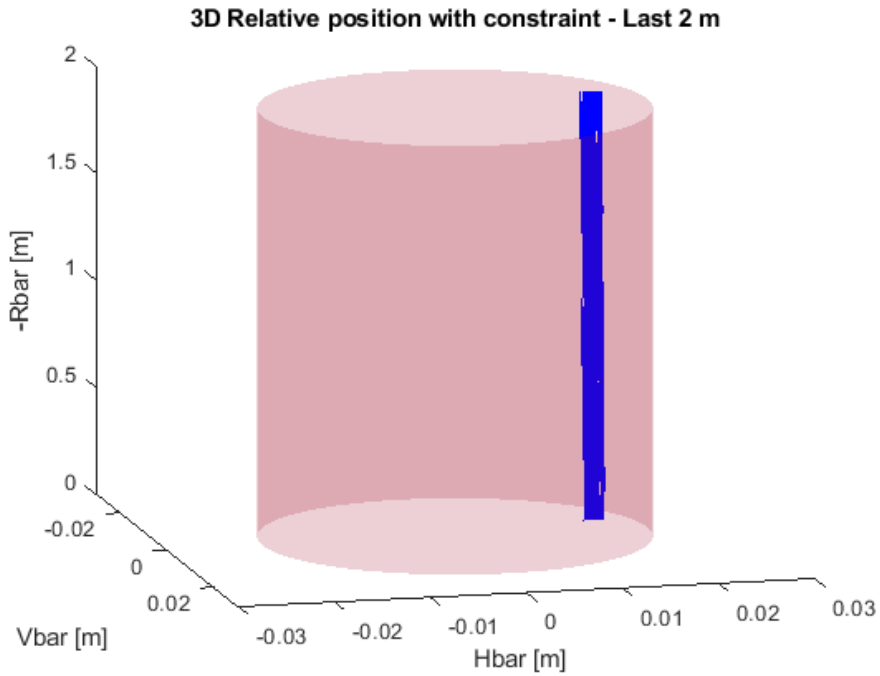

Figure 71 Zoom on 3D trajectory

Figure 72 shows that, for all the simulations carried out, the mating point at which the coupling should occur is at the limit of the tolerance region. This behaviour is accentuated, as seen above, on the H-bar axis where it is just below the requirement value while on the V-bar axis the points are all around 5mm. Moreover, in this case, the controller shows precision since all the points are close to each other, but little accuracy since they are all far from zero.

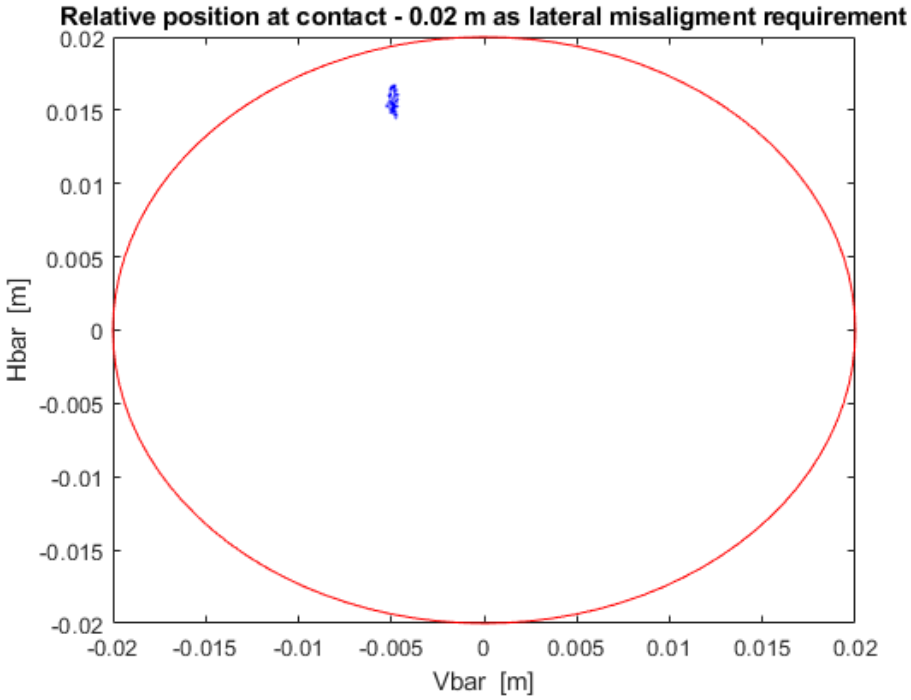

Figure 72 Position at contact for open valve failure during Monte Carlo analysis

The Figure 73 gives important information. It shows the velocity profiles along the three axes. First of all, one can notice the high values of the velocity component along the R-bar axis, which has a minimum value of around 0.15 m/s (in modulus). This velocity is outside the requirement for coupling (<0.05 m/s). This occurs because the permanently open valve causes an increase in velocity that the controller cannot handle. It can be seen, on the x-axis, that the duration of the docking is shorter than in the previous cases, ending 400s after its start, i.e. 7 minutes after its start.

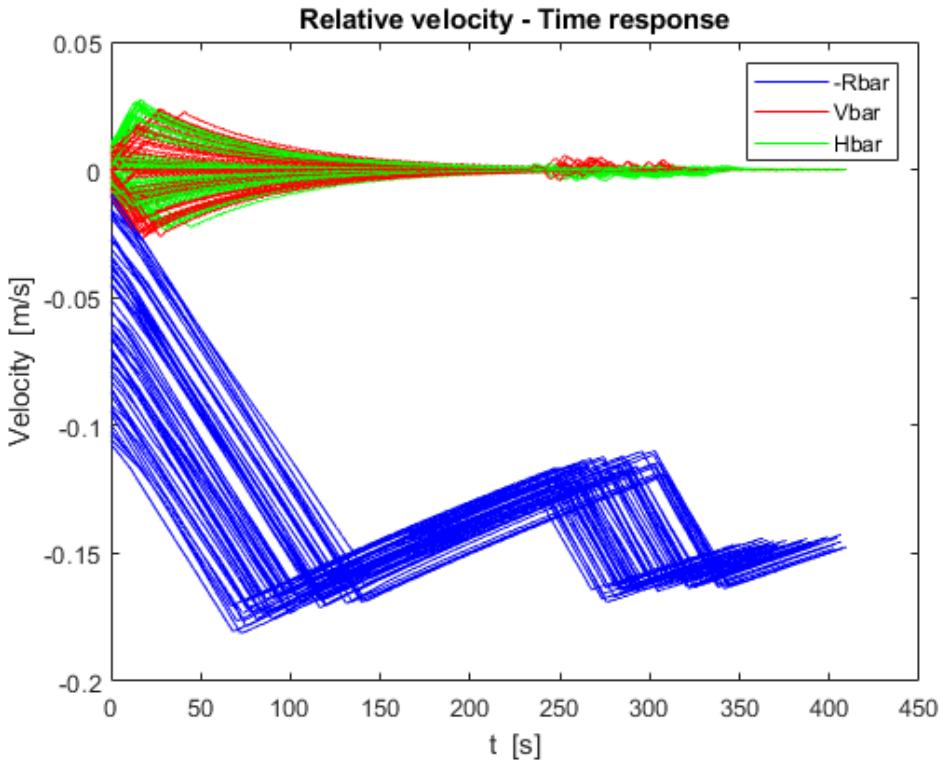

Figure 73 Velocity for open valve failure during Monte Carlo analysis

Even in the event of an open valve failure, the performance obtained by not compensating for the loss of a thruster is not always such as to allow the mission to continue.

The main question that emerges from the simulations in case of open valve failure without compensating actions is the high contact velocity along the negative axis R-bar. This velocity component should be less than 0.05m, but instead it is up to a decimetre. It follows that the impact energy may be greater than the maximum that the capture mechanism can tolerate.

Also of note is the proximity of the contact points to the boundary of the zone that ensures compliance with the lateral misalignment requirement. This could be unsafe if in the real case the disturbances are greater than those simulated.

4.4.2.1 Open Valve Failure with Compensatory Action

The controller is unable to compensate for the disturbance torque generated by the open-valve thruster on its own. A compensating action is therefore required. The strategy adopted is similar to the close valve failure situation: acting on the thruster with opposite thrust components in order to cancel the disturbing torque. With a total of two non-operational thrusters, the force was distributed to the remaining ones. The thruster opposite the fourth that can make up for the moment is the fifth that has force components as follows:

$$Thruster\ 5\ force\ components: [\ f_x \quad f_y \ -f_z]$$

This case is disadvantageous from the point of view of consumption. However, it must be considered that while in the case under consideration the failure is assumed at the beginning of the approach, in real cases it could occur at closer distances from the Target and therefore cause less consumption.

The controller has been subjected the 60 Monte Carlo tests required to meet ECSS standards. The ranges considered are the same as above and are reported here:

$$48\ m < x < 52\ m$$

$$-2\ m < y < 2\ m$$

$$-2\ m < z < 2\ m$$

$$-0.1\ \frac{m}{s} < v_x < 0\frac{m}{s}$$

$$-0.01\ \frac{m}{s} < v_y < 0.01\ \frac{m}{s}$$

$$-0.01\ \frac{m}{s} <\ v_z < 0.01\ \frac{m}{s}$$

$$18\ kg < m_c < 22\ kg$$

Figure 74, Figure 75, Figure 76 and Figure 77 show that if the valve opposite the failing valve is also opened, the trajectory is similar to that of a close valve failure with compensating action. In fact, in the [H-bar, R-bar] plane the trajectory is perfect, while in the [V-bar, R-bar] plane there is an oscillation that almost reaches the limits of the cone, although without touching it. Also in this case, as in the case of close valve failure with compensating action, having lost two thrusters because both of them are always with open valve and therefore no longer usable for control, the performance of the controller decreases. This happens in particular in situations where the lateral velocities are comparable or even higher than the axial ones.

Again, a contribution is also due to the force of aerodynamic resistance which, given its high value in the last 10 metres and also given the loss of controller capacity, tends to accentuate trajectory deviation. In fact, it can be seen that the oscillations always push the trajectory towards the positive V-bar axis.

It is also noticeable that, even in the cases where the oscillations occur, the trajectory in the last few metres falls perfectly within the requirement, this time by a large margin. It arrives in both planes at almost exactly zero distance from the mating point.

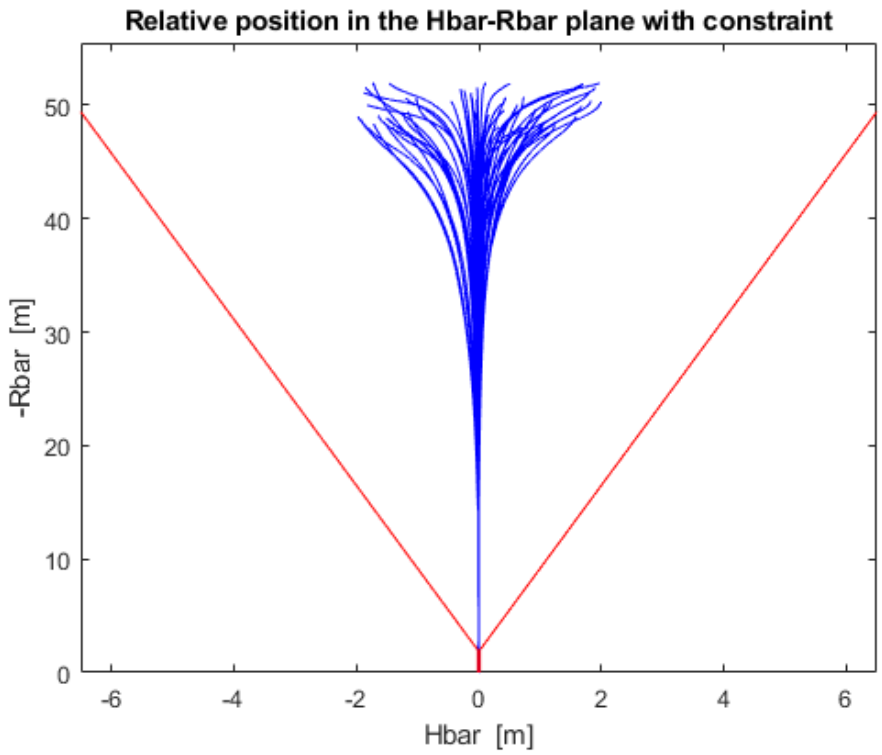

Figure 74 Trajectory in [H-bar, R-bar] plane for open valve failure for 60 Monte Carlo analysis

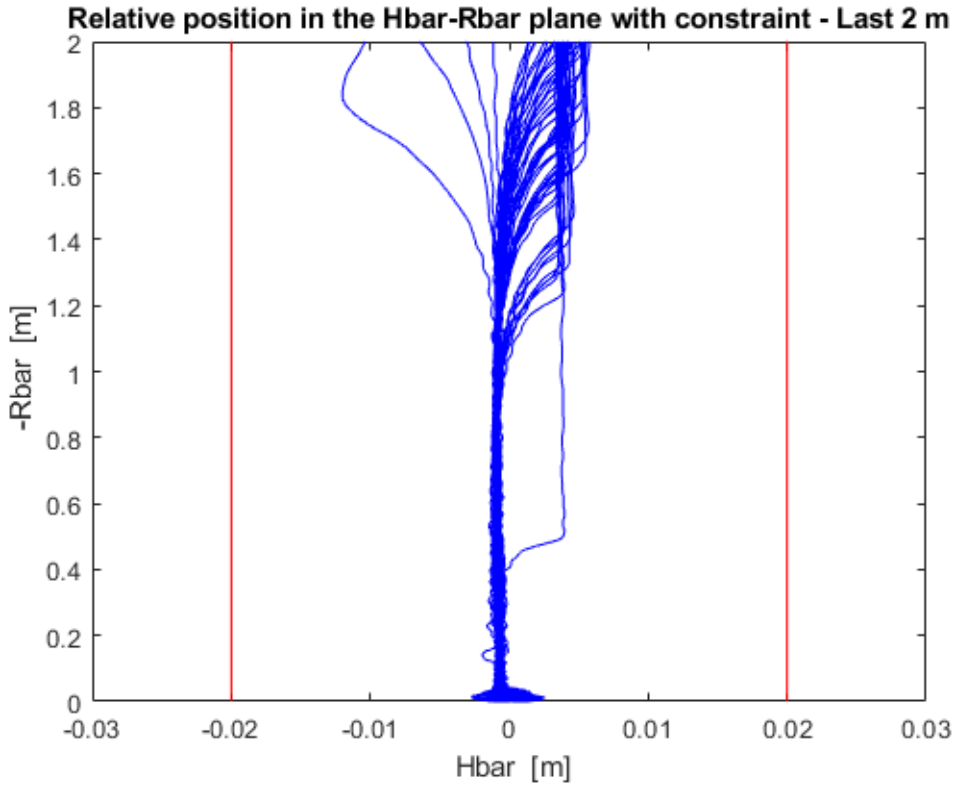

Figure 75 Zoom of trajectory in [H-bar, R-bar] plane for open valve failure for 60 Monte Carlo analysis

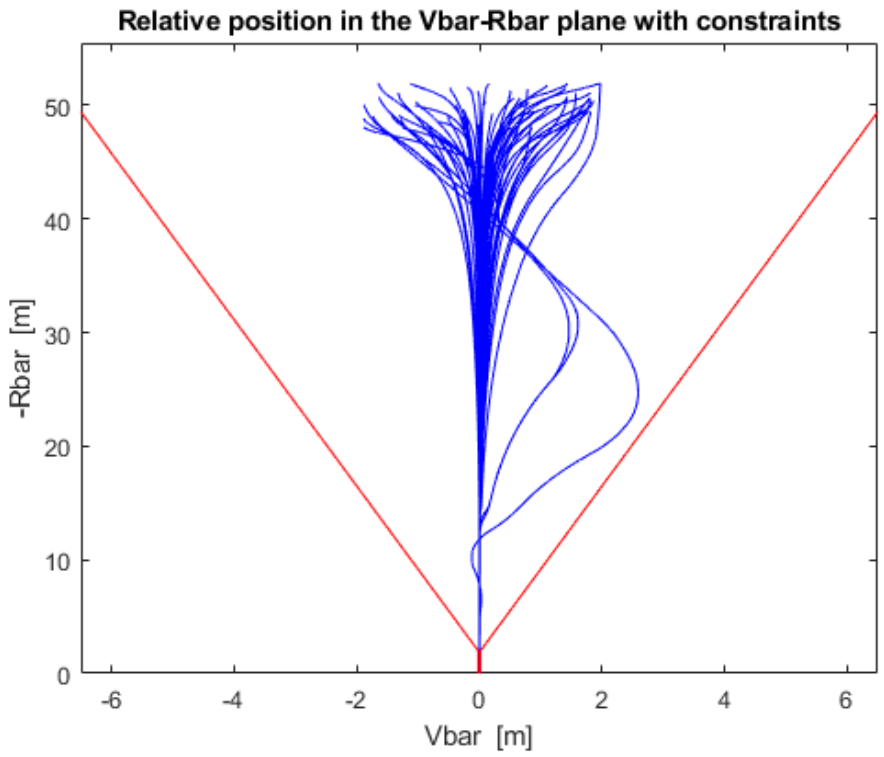

Figure 76 Trajectory in [V-bar, R-bar] plane for open valve failure for 60 Monte Carlo analysis

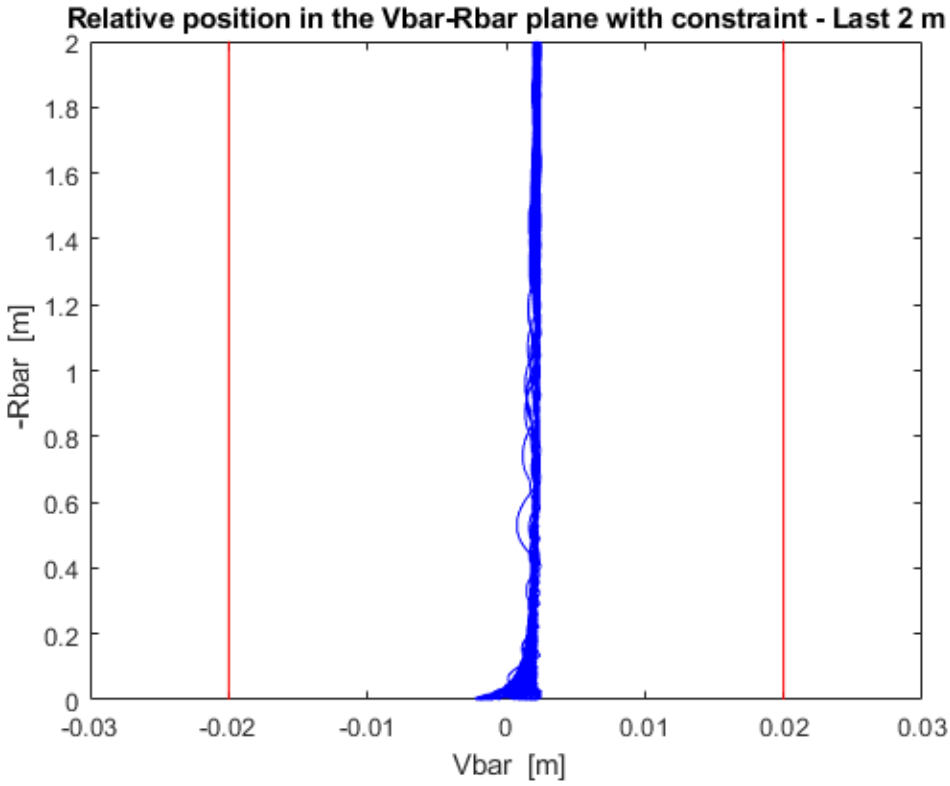

Figure 77 Zoom of trajectory in [V-bar, R-bar] plane for open valve failure for 60 Monte Carlo analysis

The 3D trajectory confirms that all the trajectories of the 60 Monte Carlo analyses fall within the cone and that in the last meters the lateral misalignment requirement (0.02 m) is met.

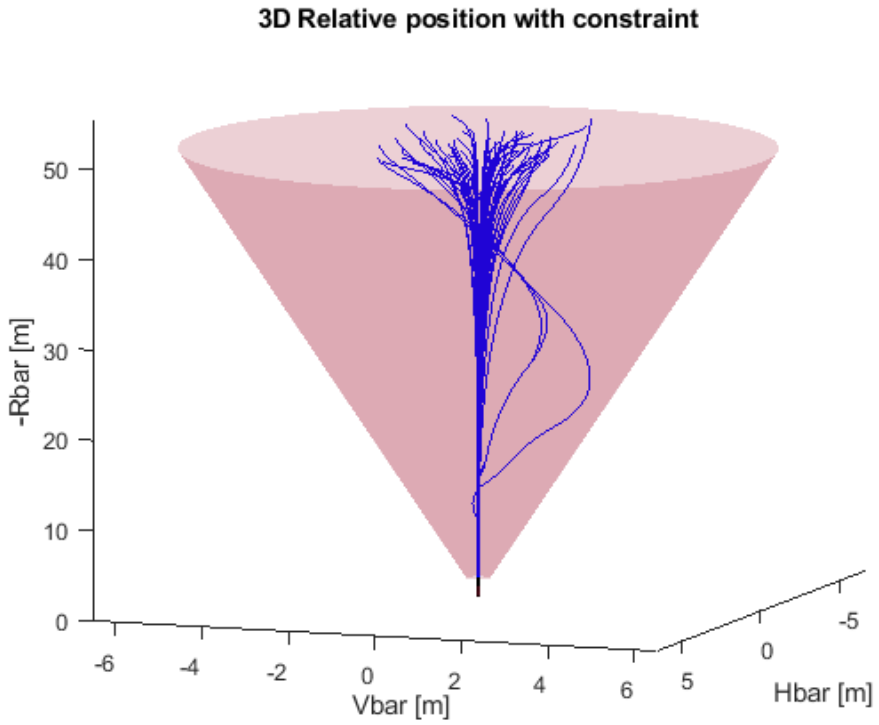

Figure 78 3D trajectory for open valve failure during 60 Monte Carlo analysis

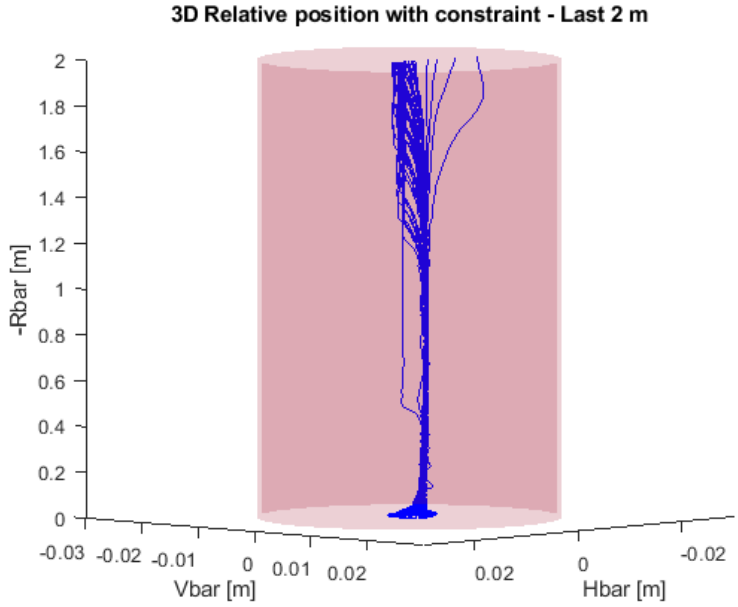

Figure 79 Zoom of trajectory for open valve failure during 60 Monte Carlo analysis

As seen from the previous figures, it also Figure 80 shows that the lateral misalignment requirement is met with a great deal of margin. It is also noted that, in this case, there is a great accuracy in the final position since all the points surround the mating point with distances from both axes well below 5mm.

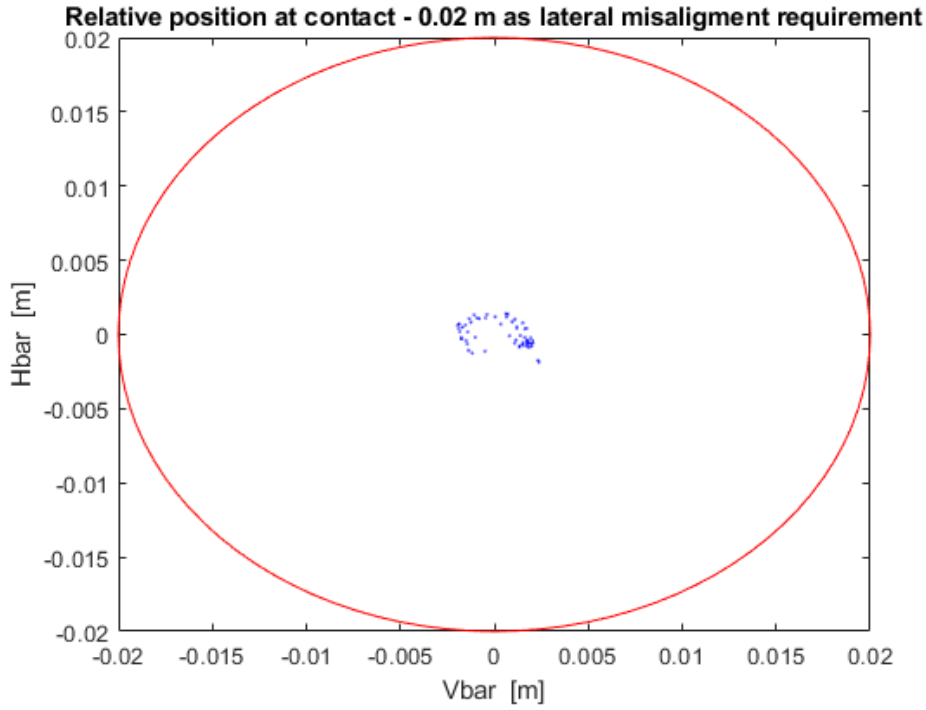

Figure 80 Position at contact for open valve failure

Figure 81 show the velocity profiles along the three axes. It can be seen that, the velocities have admissible values for the docking phase considered. In fact, they all reach zero and are therefore lower than the nominal case in which the one on R-bar is in the order of centimetres. This happens thanks to the compensating action performed so that the thrust given by the thruster with open valve is balanced by the compensator one and therefore the overall action is zero. Since in this case the actuation system works only with 2 thrusters instead of 4 for each direction, the maximum thrust is halved and therefore the times are longer as observed from the split axis. Moreover, also in this case the requirement that the entire trajectory must be carried out in a period of less than 10 minutes (i.e. 600s) is not met. This could lead to unfavourable lighting conditions or lack of coverage from ground stations.

Another disadvantage of this case is that having two thrusters constantly open the fuel consumption increases. It is therefore possible to think of having an escape manoeuvre to retry, once the failure has been resolved) to retry the approach.

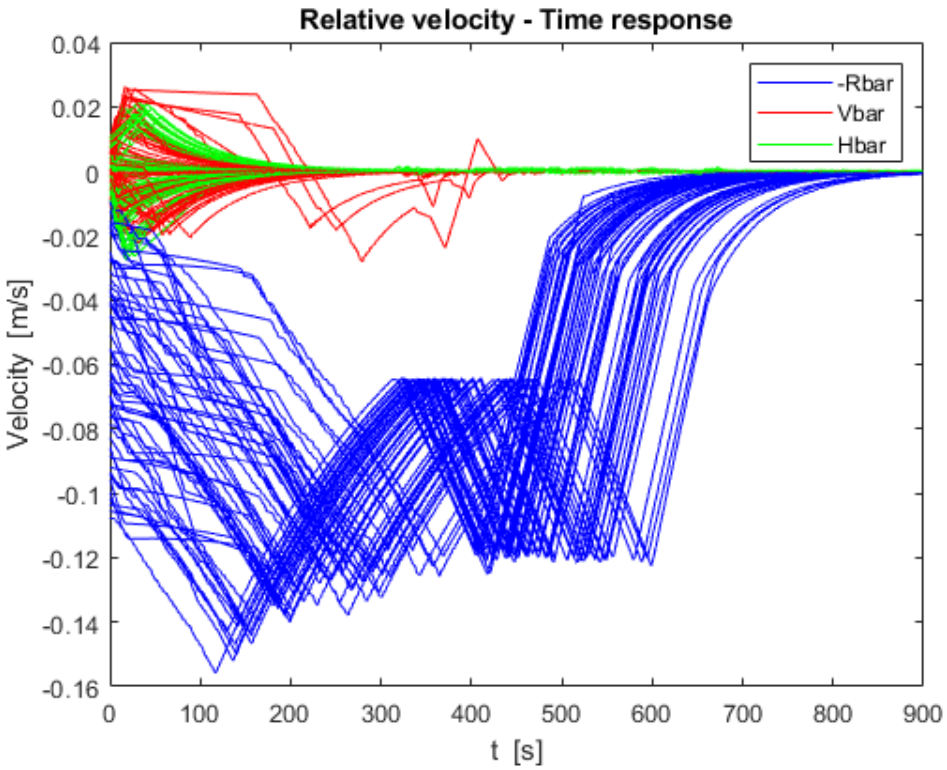

Figure 81 Velocity for open valve failure during 60 Monte Carlo analysis

In conclusion, in this chapter the performance of the controller has been analysed in conditions: nominal, nominal but with initial conditions changed through the robustness analysis, and in off-nominal conditions. While in nominal conditions the results are very satisfactory from every point of view and guarantee compliance with the requirements, in off-nominal conditions the performance decreases due to the limitations of the propulsion system. In the case of a close valve failure, the trajectory always falls within the cone limits if the valve of the thruster opposite to the failed one is also closed to and so in the case in which a compensatory action is performed and only within the velocity limits that have been established as a requirement that, at the beginning of the closing, the Chaser must have. In this case the actuating thrust for each thrust direction would be half of the nominal one which leads to an increase in docking time which may be unacceptable due to lighting conditions or ground coverage. In the case of open valve failure, with velocities in the ranges established, the trajectory is axial even without compensating action, but this leads to too high velocities at the contact which could not be supported by the capture mechanism. With a compensating action, the course of the trajectory and velocities are the same as in the case of close-valve failure with the worsening of the increase in propellant consumption as the valves of two thrusters are continuously open. It has also been observed that, in both the latter cases, the oscillatory trend towards V-var that only a few trajectories demonstrate can be linked to velocities along the R-bar axis that are lower or comparable with those along the lateral axes for which it could be necessary also establish a requirement on minimum velocity along R-bar.

5 Collision Avoidance: Results and discussion

The need to prevent collisions is fundamental in the case of proximity operations, especially if these involve docking with the Target. Preventive actions therefore become necessary if the requirements and constraints to which the Chaser must be subject cease to be respected. This chapter deals with the two different types of analysis carried out that fall under collision avoidance analysis.

- The first concerns the shutdown of the thrusters at a non-zero distance from the Target, this is desired in general because the jets exiting the thrusters can cause damage to the Target surfaces and especially, since in the case under consideration the Target is Space Rider, the fouling of other payloads.
- The second concerns escape manoeuvres that must be carried out if, during the approach, the cone constraint is violated. This can occur in the event of errors or failures (of the actuating system, navigation system, etc.). These manoeuvres must ensure sufficient clearance from the Target in the shortest possible time. Given the multiple nature of the need to execute an escape manoeuvre, they must be designed so that they can also be executed without active control.

5.1 Thruster Shutdown

In general, the shutdown of thrusters in the vicinity of the Target is designed because exhaust plumes the propulsion module (PM) could damage or foul their surfaces. In the case study, the S/C Chaser is SROC which, at the end of docking, re-enters the Space Rider cargo. The propulsion system of SROC, as discussed in the section 2.4.4 is of the cold gas type, so the exhaust plumes the eight thrusters are relatively cold. The shutdown is therefore not performed to avoid damaging the Target surfaces, but to avoid fouling the other payloads contained into the cargo.

Switching off the thrusters at a given distance also means that control is lost from that point on, making the motion of the S/C leader free and no longer controllable. This makes this phase very delicate. The whole GNC system must be designed to ensure that once the thrusters have been switched off, the SROC can reach the mating point with the required lateral misalignment of:

$$Lateral\ misalignment\ requirement: 0.02\ m$$

The objective of this analysis is to identify the distances, in proximity of the contact, in which the controller referred to in section 2.6 ensures compliance with the misalignment requirement. This must be checked against both the V-bar and H-bar directions.

Analyses have been carried out with the following assumptions in Table 6.

Table 6 Assumption for Thrusters Shutdown

Maximum PM shutdown distance [m]	2
Maximum PM shutdown distance [m]	0.1
Step between distances [m]	0.1

Mass [kg]	20

Initial conditions – Nominal scenario			
	R-bar	V-bar	H-bar
Position [m]	50	0	0
Velocity [m/s]	0	0	0

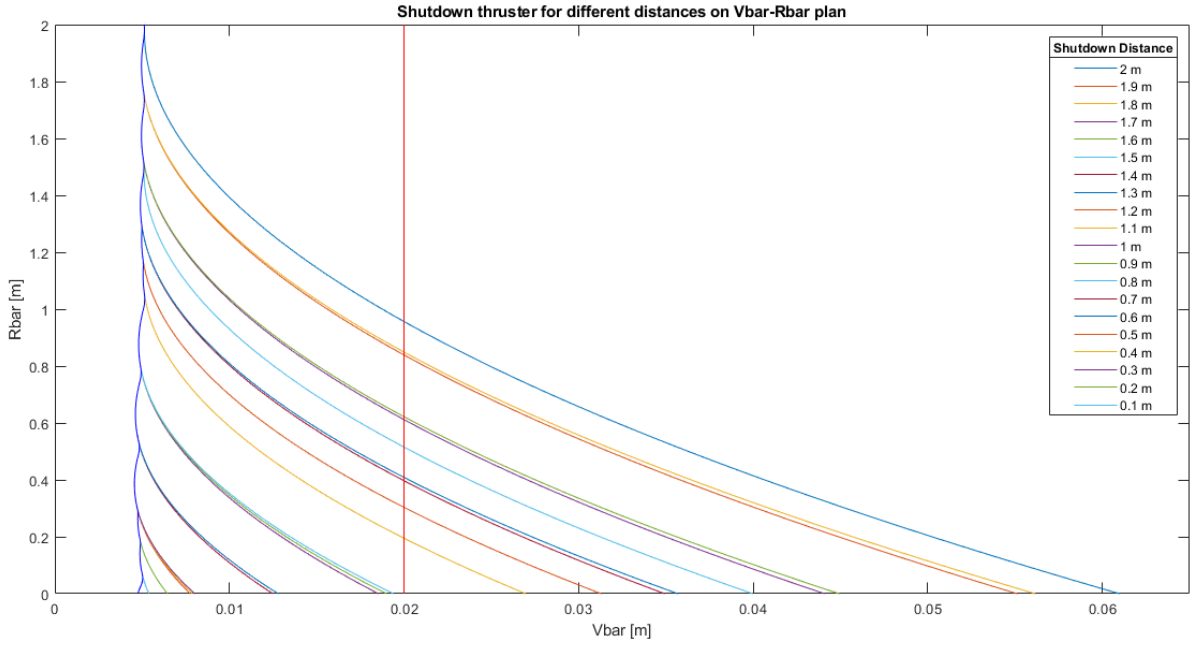

Figure 82 Trajectory after thrusters shutdown in [V-bar, R-bar] plane

Figure 82 shows that there is a drift of the trajectory along the V-bar axis once the PM has been deactivated. This is due to the drag that causes the CubeSat to decay. In fact, due to the different dimensions of the two spacecraft involved, the two ballistic coefficients have two orders of magnitude of difference. For this reason, in the last 10m of the trajectory, a factor equal to 100N has been added to the aerodynamic force acting on the Chaser, which causes this drift in the V-bar direction.

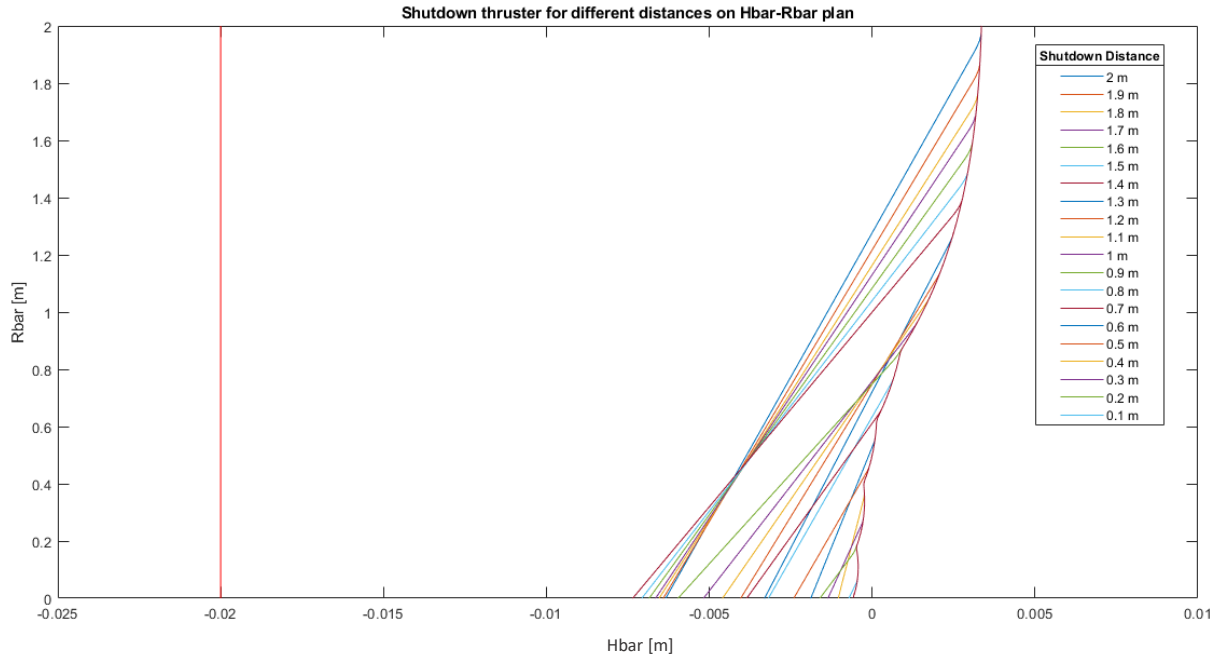

Figure 83 Trajectory after thruster shutdown in [H-bar, R-bar] plane

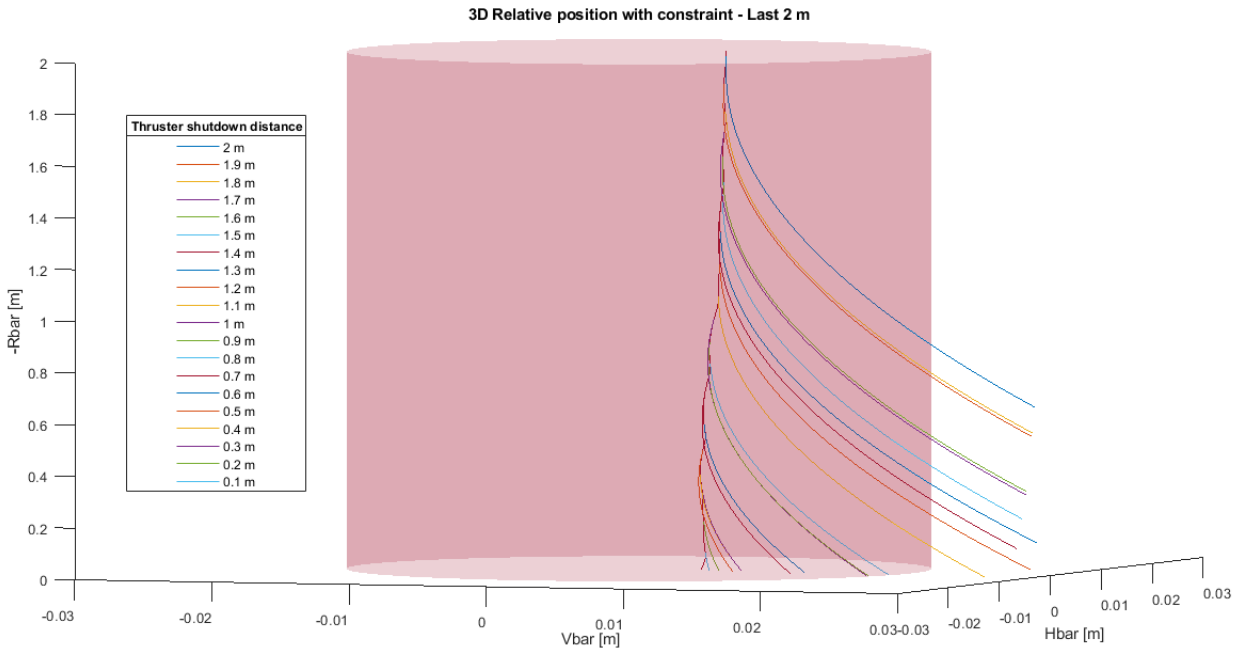

Figure 84 3D trajectory after thrusters shutdown

The results obtained are shown in Figure 82, Figure 83 and Figure 84. It can be seen that, in the plane [H-bar, R-bar] the requirement on lateral misalignment is always verified. In the plane [V-bar, R-bar] this is verified only for distances less than one meter. If the coupling is performed mechanically, the distance at which the

use of the thrusters is interrupted can be less than 50cm. In the case of magnetic coupling, this distance would be dangerous because the magnetic mechanism would interfere with the ADCS magnetometers, and this could lead to measurement errors that could prevent the mission from being achieved.

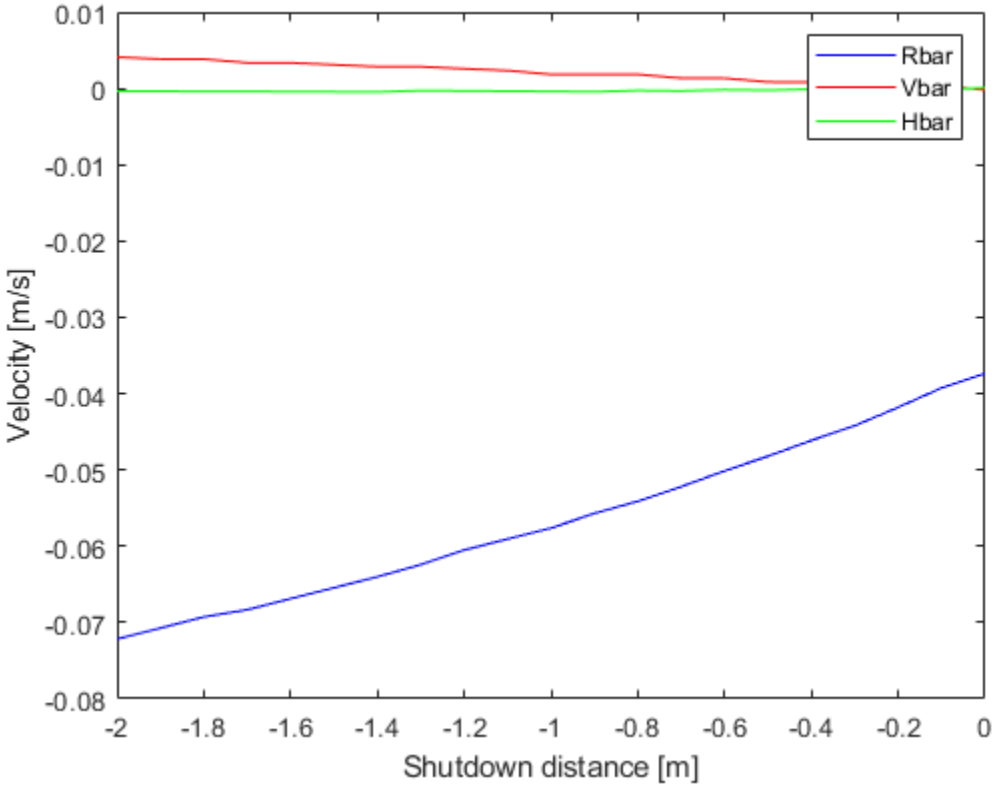

Figure 85 Velocity at contact for different shutdown distances

In Figure 85 which shows the velocity at the contact, it can be seen that the greater the thruster shutdown distance, the greater the contact velocity. The contact velocity requirement has been set equal to:

$$V_{contact} < 0.05\ m$$

which is respected for distances from the Target from 0.7m to 0.1 m. If greater distances have been chosen, the design of the docking mechanism would have to be modified so that it could absorb higher shock intensities.

5.2 Collision Avoidance Manoeuvre (CAM)

Collision avoidance manoeuvres are escape manoeuvres which aim to move the Chaser away from the Target in the shortest possible time and in the safest possible way for both vehicles involved. The objective

of this part of the thesis work is to design CAM that can secure the two Spacecraft involved and that can be executed for any condition that generates the need for CAM. When the possibility of a collision occurs, it is not necessarily known what causes it, so the safest solution is to move away as fast as possible (within the limits established by the thruster design) and to place to safety at a point that by requirement must be at a minimum distance of 2 km from the Target. Since the cause could also involve the AODCS such as damage or malfunction of the relative navigation cameras or Lidar, the operation of the GNC could also be compromised. For this reason, it was decided to use a classical approach that follows the one foreseen for the ISS approaches, that is to perform an open-loop CAM through a manoeuvre that used single command as simple as possible and that involves the minimum number of subsystems. For these reasons it has been decided to consider an impulsive manoeuvre. Moreover, since it might not be possible to analyse the cause of the collision possibility in a quick period of time, it is necessary to develop a strategy that can be applied to every dangerous situation and that for each of them respects the imposed requirements.

The requirements to be met are:

- Move up to at least 2 km away from the Target;
- Be passive safe for at least 24 hr.

The escape trajectory must therefore:

- Bring the CubeSat to a safe position where the fault or cause of fault can be identified and retry the docking manoeuvre;
- Being as economical as possible to allow the Chaser to retry the approach.

Since the Target, in the case under consideration is Space Rider, and SROC have different sizes and ballistic coefficients, they are subject to different drag. In particular, the Target is subject to a higher drag, which causes its orbit to decay earlier. If the Chaser during a CAM escaped towards positive V-bar there would then be another risk of impact due to this. For this reason, the manoeuvre must be carried out towards the negative V-bar axis.

The methodology used is summarised in the Figure 86 and consists in identifying the conditions under which a CAM may be necessary, identifying the worst-case, designing a manoeuvre that meets the requirements in the worst case and also in all the others. From the analyses carried out, considerations emerged such that the first results have been considered unsatisfactory leading to the identification of different strategies.

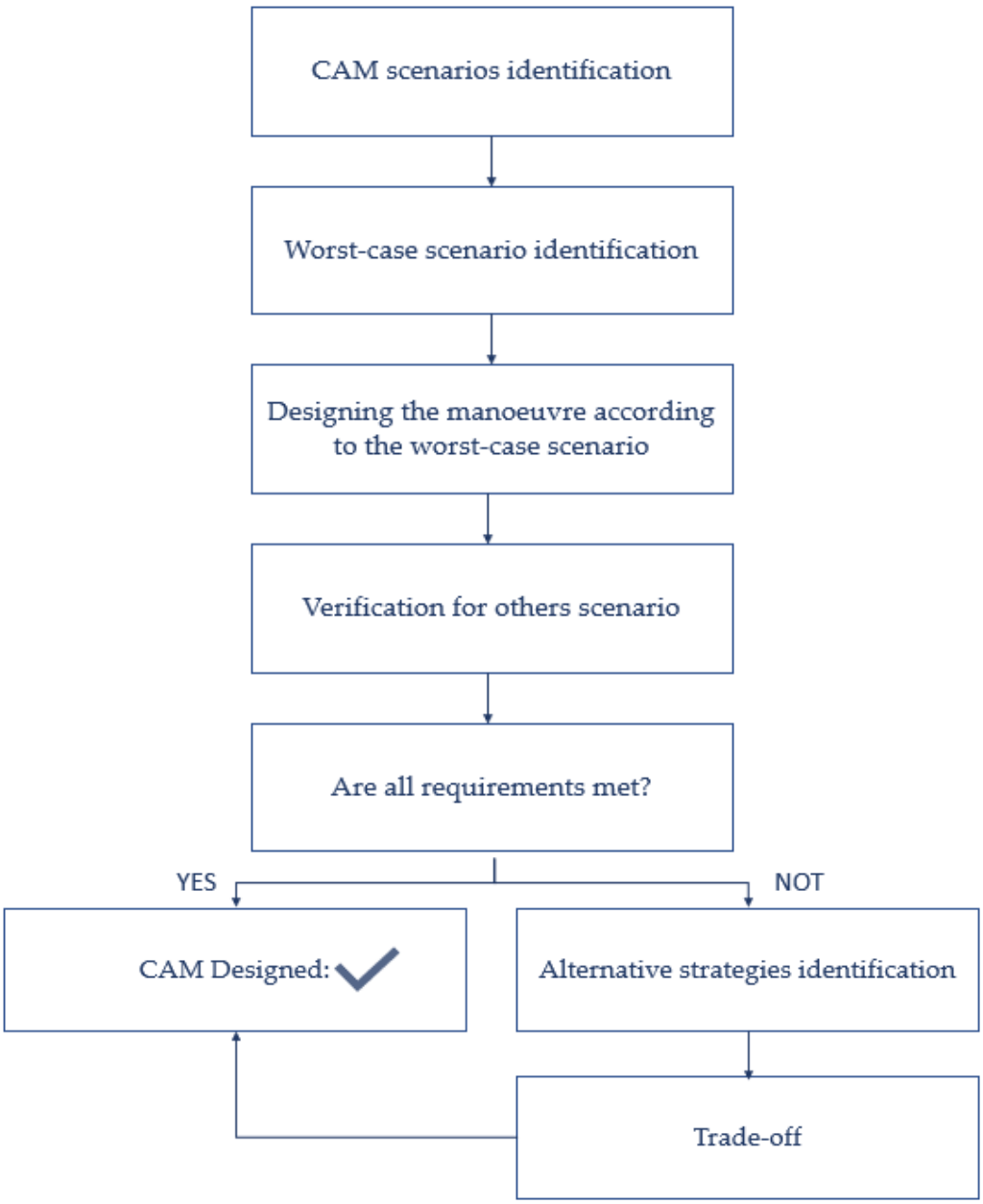

Figure 86 Methodology for CAM strategy definition

5.2.1 CAM scenarios identification and worst case

The main scenarios in which the need for CAM may be required are:

1) The nominal scenario, where it may become necessary due to:
    a. Errors that may lead to non-compliance with alignment or velocity requirements;
    b. Failures of the sensors and therefore the loss of the required accuracy and with the consequent possibility of not being within the tolerances on the lateral misalignment required at capture and, in addition, to the loss of performance of the GNC.
    c. It could also be required from the ground because the Target is not ready for coupling.

In this scenario the worst velocity conditions are reached around 30m as can be seen from the Figure 23 in the Section **Error! Reference source not found.**. This is the best-case scenario, as in nominal conditions the velocities are very low. Having low velocities means moving away faster or needing to give a shorter impulse and thus lower Delta-V and consumption with a greater probability of being able to retry the manoeuvre.

2) The off-nominal scenario which, in the analysis conducted, concern the occurrence of failures to the valves of the propulsion module. In particular, closed valve or open valve failures type have been dealt with. In this case it is necessary to differentiate the type of failure. Considering the closed-valve case, the velocities are lower than in the nominal case (see Figure 65), which leads to a lower control input than in the previous case, but there are also fewer thrusters available (3 out of 4 for each thrust direction), which means that the trajectory goes out of the cone for numerous combinations of initial conditions, if a compensating action is not performed. Even if this is executed, however, the docking phase will take longer. The open valve case, on the other hand, is worse than the previous cases due to the greater velocity of the Chaser during the trajectory caused by the non-closure of the valve (see **Error! Reference source not found.**), if a compensating action is not performed. Even in this case, there are only 3 out of 4 thrusters operating, which may be more complex to manage without a close-loop control system.

3) The last case considered is that in which the velocity requirements at the start of docking (i.e. 50m) are significantly outside the maximum allowed value. This is the case when, due to malfunctions during the trajectory between hold point 2 and the docking close-range rendezvous start point, an undesired and uncontrolled increase in velocities has occurred. It has been assumed that the velocity on R-bar is greater than the maximum considered during the Monte Carlo analyses but of the same order of magnitude (i.e. decimetres per second), and along V-bar and H-bar of one order of magnitude greater. In fact, it is the lateral velocities that cause exits from the safety cone because if the velocity along R-bar is an order of magnitude greater, the effect of an increase along the lateral one is controllable by the system. Since in this case the lateral velocities become of the same order of magnitude as the axial ones, the output of the control will be a much longer impulse than it would be in the previous cases, both along R-bar along which it will have a greater component, but also along V-bar. Even though this is a difficult scenario to realise, it is still important to consider it in order to really assume the worst conditions.

In addition, the effect of the aerodynamic drag will also have to be taken into account, making CAM in the V-bar-R-bar plane the worst case compared to those in the H-bar-R-bar plane. In fact, drag helps when violating the safety cone in the positive half-plane of V-bar, but opposes the manoeuvre in the opposite case.

5.2.2 Designing the manoeuvre according to the worst-case scenario

Considering scenario 3) as the worst case, conditions have been first simulated for it to occur. It has already been mentioned that the lateral velocity components must be comparable with the axial one, the higher the lateral components the sooner the violation of the cone constraint will occur (i.e. the trajectory is more curved). By varying the initial velocity conditions iteratively, the desired trajectories have been obtained. The initial conditions used are shown both to show how high the velocity must be, both axial and especially lateral for this scenario to occur. Also, as will be seen, the trajectories considered are only 4 in the negative

V-bar half-plane and 4 in the other. This is not only because it is an example, but also because in most of the trials performed, the controller was able to control the trajectory even at a velocity greater than that considered in the robustness analysis (see paragraph Robustness Analysis4.3) and make it executable. This gives an idea of the rarity with which such events can occur.

Since, as mentioned, along V-bar the worst case occurs due to the action of aerodynamic resistance, the trajectories exiting the safety cone towards the negative V-bar axis and those directed towards the positive V-bar axis are divided.

Table 7 Worst-Case CAM initial conditions

R-bar Distances		**Exit towards + V-bar**			**Exit towards - V-bar**		
		R-bar	**V-bar**	**H-bar**	**R-bar**	**V-bar**	**H-bar**
40 m	Position [m]	53	-8	8	53	8	8
	Velocity [m/s]	-0.1	0.2	0	-0.2	-0.2	0
30 m	Position [m]	52	-7	7	53	8	8
	Velocity [m/s]	-0.3	0.17	0	-0.25	-0.2	0
20 m	Position [m]	54	-7	7	54	7	7
	Velocity [m/s]	-0.35	0.08	0	-0.30	-0.18	0
15 m	Position [m]	52	-7	7	54	7	7
	Velocity [m/s]	-0.3	0.1	0	-0.38	-0.18	0
Mass [kg]		20					

These conditions give the trajectories in Figure 87.

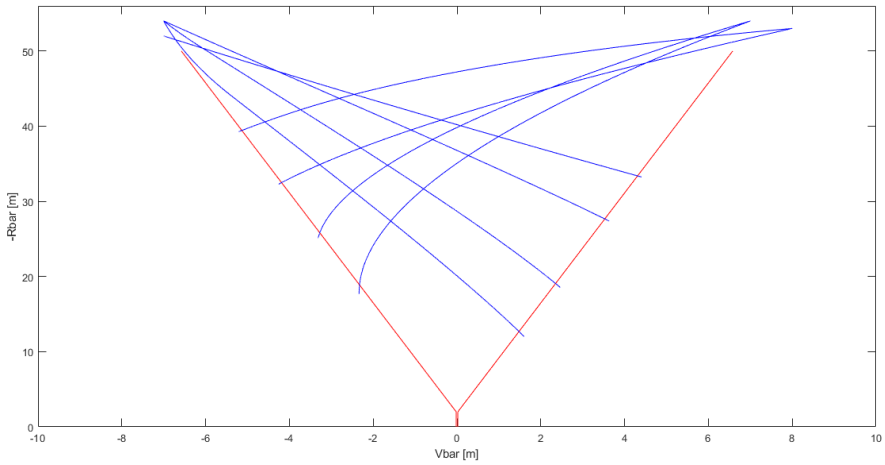

Figure 87 Worst-Case CAM initial trajectory [V-bar, R-bar] plane

The worst of which are those at 40m and 30m exiting towards negative V-bar axis. These have high velocity values along the R-bar axis (the maximum value considered along the nominal robustness analyses is 0.2 m/s), but also high velocity values in V-bar (the maximum value in the nominal robustness analyses is 0.03 m/s). Velocities along H-bar have been not considered, as anticipated, the worst conditions are for velocities along V-bar. Furthermore, the requirement for which the trajectory must be passive safe for 24 hr must be respected, but due to the computational cost a first estimate is performed considering as a requirement that for which it must be passive safe for at least two orbital periods (each orbital period is ~92 minutes). Based on these considerations the nominal impulse has been chosen. The impulse command must be such that it opposes motion along R-bar and that along V-bar. The first ensures that the Chaser moves away, the second causes an extension of the trajectory along the V-bar axis in such a way that it can reach a distance of at least 2 km. Iteratively, these values have been chosen to meet the requirements. The impulse, considering the thruster providing a maximum thrust of 35 mN, is:

$$\Delta v_{R-bar} = 0.44 \, \frac{m}{s}$$

$$\Delta v_{V-bar} = 0.18 \, \frac{m}{s}$$

Where Δv indicates the Delta-V along axial and lateral direction. The results obtained for this worst-case distance have been extended to all other worst-case distances along R-bar according to the initial conditions in the Table 7 giving the results in Figure 88 and the verification of the softened requirement on the two orbital periods in Figure 89.

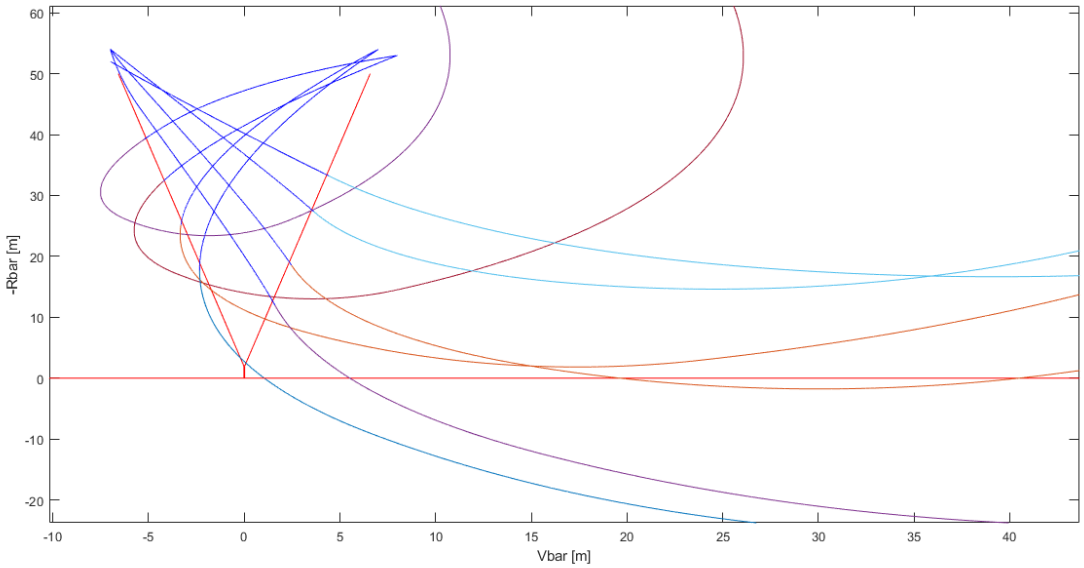

Figure 88 Worst-Case CAMs

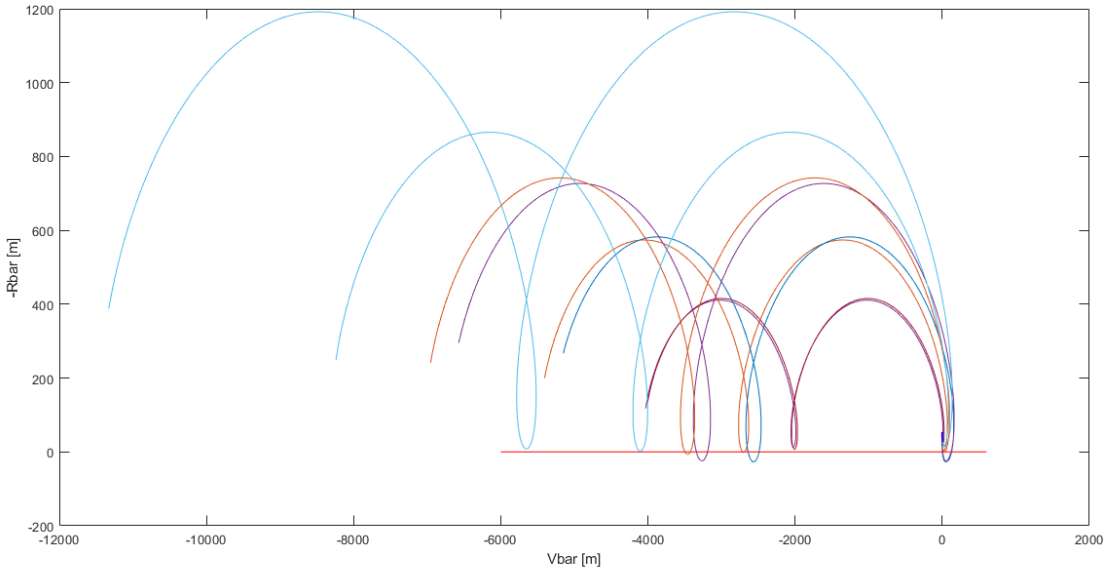

Figure 89 CAM trajectories in worst-case scenario in two orbital periods in [V-bar, R-bar] plane

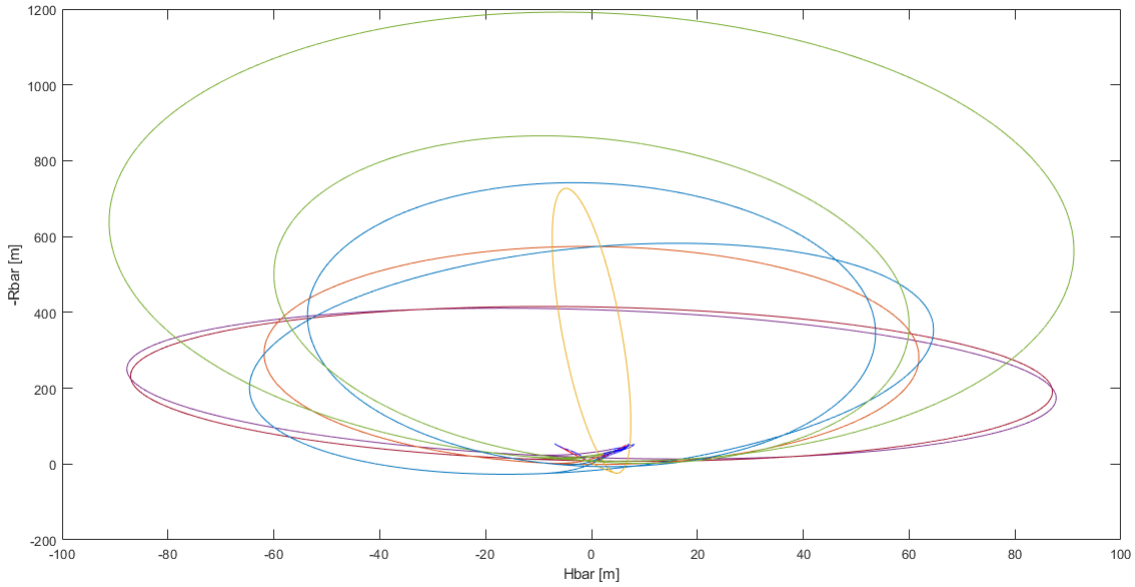

Figure 90 CAM trajectories in worst-case scenario in two orbital periods in [H-bar, R-bar] plane

It is noted that:

- all manoeuvres respect the constraint on the final position (> 2km);
- all manoeuvres are passive safe for at least 2 orbital periods;
- for R-bar distances of less than 20 metres, CAM is no longer possible. Even for longer V-bar pulses the situation does not change. This is due to the fact that, since the velocity is high (especially along V-bar), the pulses must be of longer duration in order to cancel or counteract it. Even by increasing the pulse duration in the moments following the start of CAM the manoeuvre still does not "feel" the whole pulse. Therefore, even by increasing the pulse duration, the situation does not improve after a certain threshold.

5.2.3 Verification of the manoeuvre for the other scenarios

In the previous paragraph it has been seen that the requirements are therefore met for the worst case for collision avoidance manoeuvres performed above 20m. Furthermore, as these velocities are much higher than the other cases considered (i.e. 1) and 2)), for this reason the CAMs will certainly be adaptable to them as well.

5.2.3.1 Nominal Scenario

First of all, the CAM thus designed is tested on the nominal scenario. In the nominal case (no failure) the maximum velocities are reached at the beginning of the trajectory, if it starts from nominal position and velocity as can be seen from the Figure 91. Maximum velocities correspond to the worst case for the CAM design in relation to the requirement that the final distance of the Target must be at least 2 km , because the velocities to be canceled and inverted will be greater.

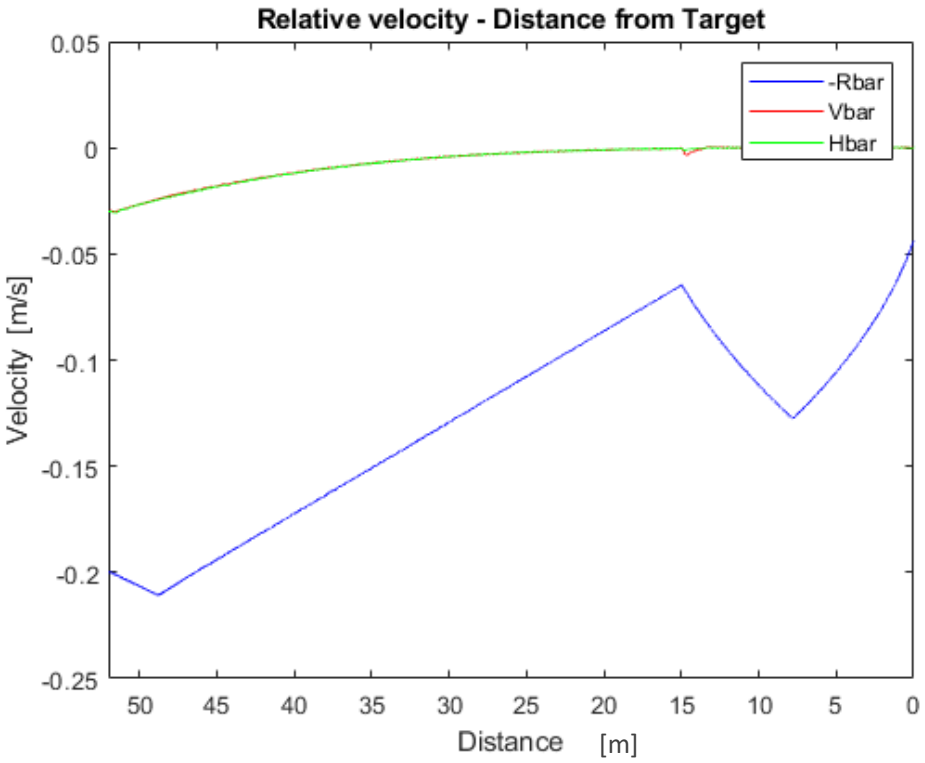

Figure 91 Velocity profiles during docking at different distances

The analyses have been carried out in the case of maximum velocities (i.e. worst case for the execution of CAM manoeuvres) and, in order to be conservative, initial velocity conditions equal to the maximum ones considered in the Monte Carlo analyses have been chosen. Therefore, the initial condition are:

Table 8 Initial Conditions for CAM in nominal scenario

	R-bar	**V-bar**	**H-bar**
Position [m]	52	2	2
Velocity [m/s]	-0.2	-0.03	-0.03
Mass [kg]	20		

The analyses have been performed from 45m to 5m with a 10m step. The results are shown in the Figure 92. Here, it should be noted that up to 10m the manoeuvres described in the previous paragraph are excellent as they move the Chaser away from the Target avoiding collisions. Given the high axial velocities even with longer pulses along the V-bar it is not possible to move away the satellite faster due to the propulsive limits. Higher pulses along the R-bar axis causes the opposite effect, that is to bend the trajectory even more touching the origin of the axes.

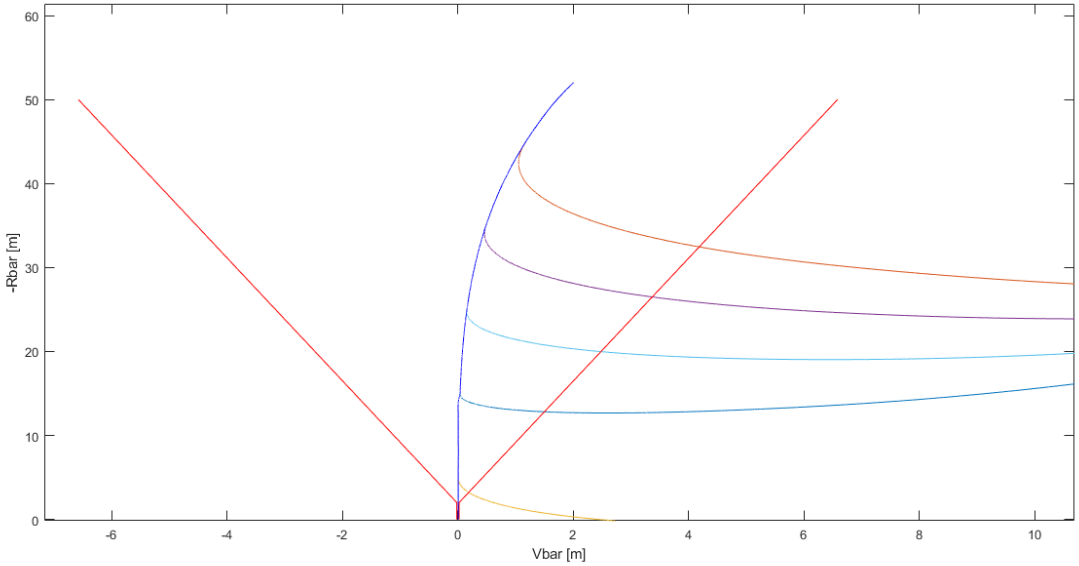

Figure 92 CAM trajectories in nominal scenario in [V-var, R-bar] plane

This behavior can be explained by looking at the figure again Figure 91. Here it can be seen that, the Chaser first decelerates and then accelerates up to a maximum velocity along the R-bar axis reached around 15m from the Target. From here a new deceleration begins which leads, at the end of the maneuver, to the verification of the velocity requirements at the contact. If a CAM is performed from 5m, the axial velocity is close to the second maximum, around -0.15m. This means that the maneuver designed previously does not verify the expected trend (i.e. does not cause a trajectory with a greater slope than the previous ones), but instead a worse behavior is obtained.

5.2.3.1.1 CAM from the cone limit with nominal velocity

A final case analysed within the nominal scenario (no failure), is that for which the escape manoeuvre is carried out when the Chaser is on the cone. This can happen for example due to navigation errors where the trajectory followed is not the one detected by the GNC. Also in this case the initial conditions considered are those of maximum velocities among those considered during the analysis in paragraph 4.3. Regarding position on cone, distances from the Target from 45m to 5m in steps of 10m, are considered.

Table 9 Initial conditions for CAM from cone in - Nominal scenario

R-bar Distances		**Exit towards + V-bar**			**Exit towards - V-bar**		
		R-bar	**V-bar**	**H-bar**	**R-bar**	**V-bar**	**H-bar**
45 m	**Position [m]**	45	5.92	5.92	45	-5.92	-5.92
	Velocity [m/s]	-0.19	0.02	0.02	-0.19	-0.02	-0.02

35 m	**Position [m]**	35	4.6	4.6	35	-4.6	-4.6
	Velocity [m/s]	-0.15	0.015	0.015	-0.15	-0.015	-0.015

25 m	**Position [m]**	25	3.15	3.15	25	-3.15	-3.15
	Velocity [m/s]	-0.108	0.002	0.002	-0.108	-0.002	-0.002

15 m	**Position [m]**	15	1.71	1.71	15	-1.71	-1.71
	Velocity [m/s]	-0.065	0.0003	0.0003	-0.065	-0.0003	-0.0003

5 m	Position [m]	5	0.4	0.4	5	-0.4	-0.4
	Velocity [m/s]	-0.105	0.0002	0.0002	-0.105	-0.0002	-0.0002

Mass [kg]	20

Executing, from these positions, the escape manoeuvre designated in the previous paragraphs gives the results shown in Figure 93.

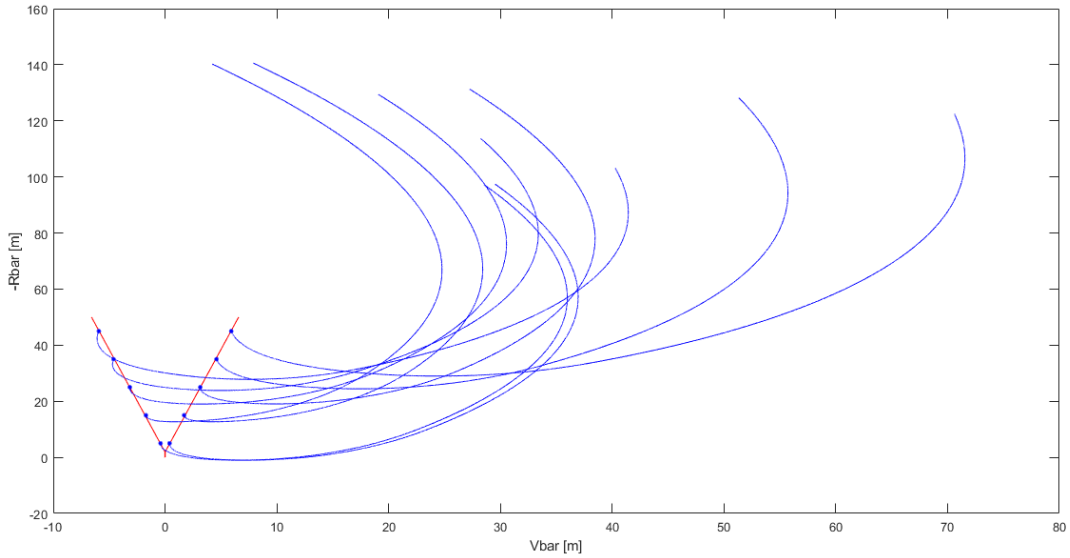

Figure 93 CAM from cone position in [V-bar, R-bar] plane

The same behaviour is observed as before. The CAMs are perfectly executable from any dance over 5m. To make the CAM executable even from such small distances, try a re-tuning of the controller would be needed so that the output velocity profile is strictly decreasing.

In Figure 94 and Figure 95 the trajectory for two orbital periods on the [V-bar, R-bar] and [H-bar, R-bar] planes are shown. It can be seen that, after just over an orbital period (~92 minutes) the trajectory intersects

the negative V-bar axis at a distance greater than 2km, after which it continues defining a series of loops. it is also noted that in the [H-bar, R-bar] plane it returns to the starting point cyclically, this represents an advantage in the case in which the approach must be retried to avoid consumption also along that direction.

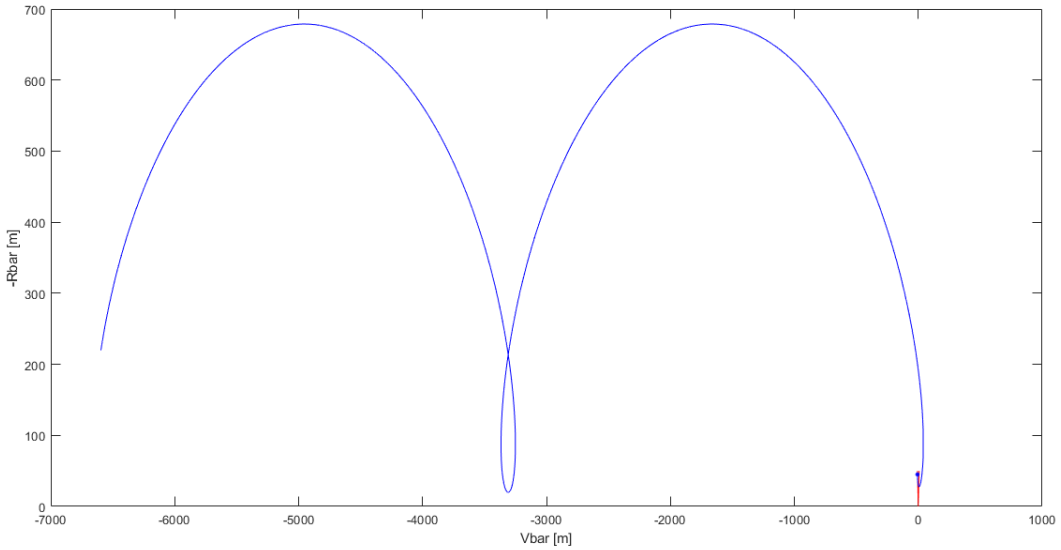

Figure 94 CAM from cone position in two orbital period in [V-bar, R-bar] plane

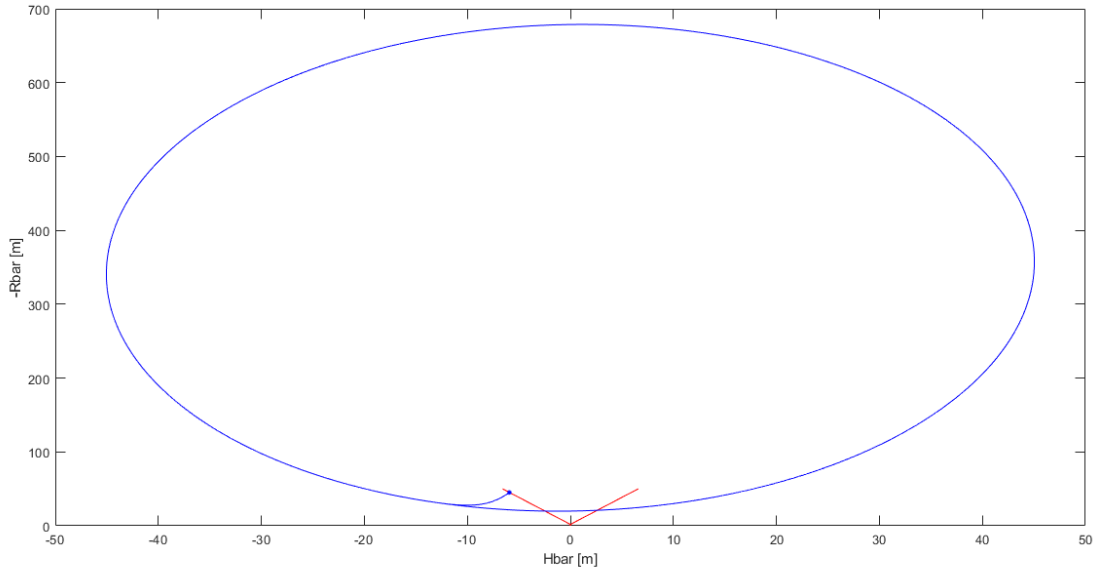

Figure 95 CAM from cone position in two orbital period in [H-bar, R-bar] plane

5.2.3.2 Close Valve Failure Scenario

Since, as mentioned, the worst conditions for the execution of the CAM occur for higher velocities, the worst ones used in the Monte Carlo simulations (see paragraph 4.4.1) are considered as input velocities, namely:

Table 10 Initial conditions for CAM - Close Valve Failure scenario

	R-bar	V-bar	H-bar
Position [m]	52	2	2
Velocity [m/s]	-0.2	-0.03	-0.03
Mass [kg]	20		

The results can be seen in Figure 96 and Figure 97 where the manoeuvre selected in previous paragraph is applied to different points of the trajectory, from 45m to 5 meters, with a step of 10m. It is assumed that the failure occurs at the beginning of the trajectory. Figures shown the CAMs during 10 minutes after they begin. The same considerations made previously are repeated, but in this case the manoeuvre can also be performed at 5m but touching the V-bar axis. However, this is outside the expected safety requirements.

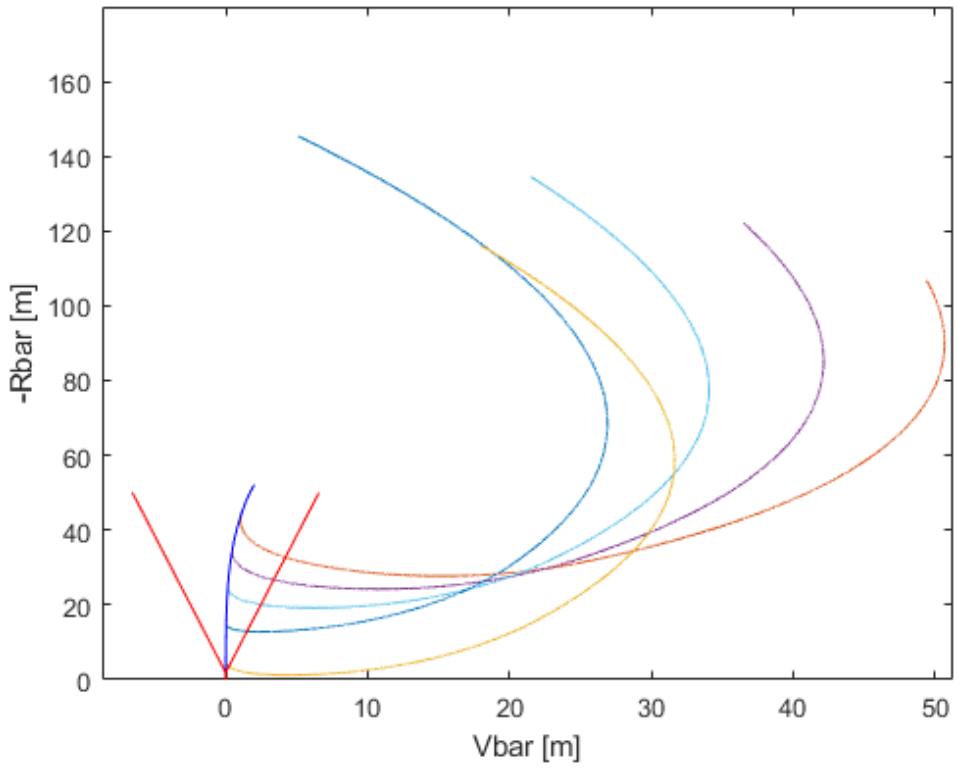

Figure 96 CAM in close valve scenario in [V-bar, R-bar] plane

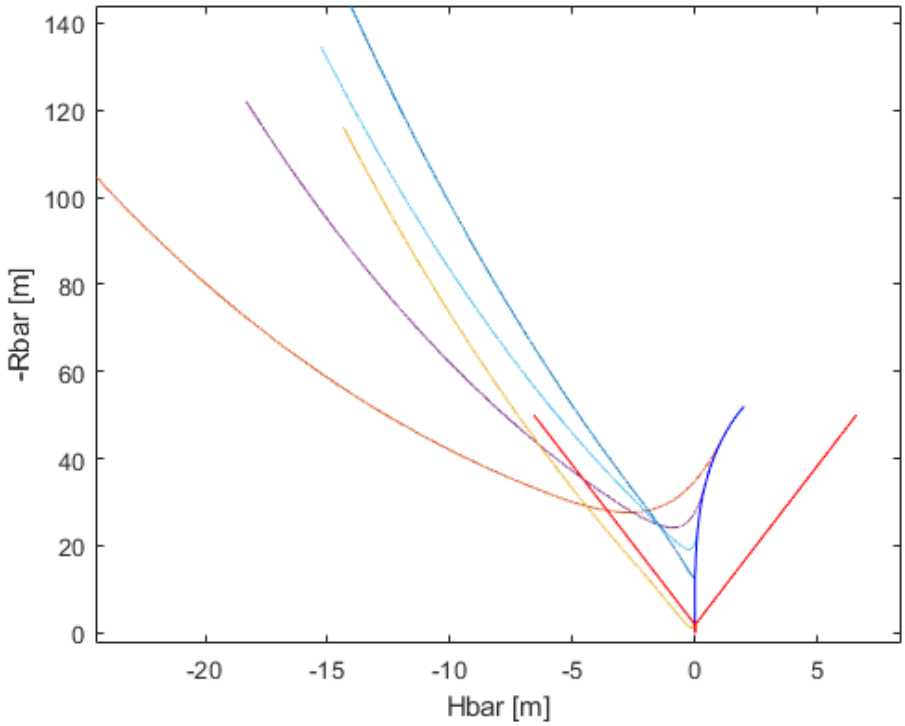

Figure 97 CAM in close valve scenario in [H-bar, R-bar] plane

Figure 98 it is a demonstration of the fact that the performance of the CAM at 5m is due to the high velocities at this distance. In fact, if the manoeuvre is performed at 2m where the axial velocity is half than at 5m, it is noted that the manoeuvre is possible. In particular, except for the first seconds after the CAM beginning in which the distance falls below 2m, subsequently it continues to increase, minimizing the probability of collision.

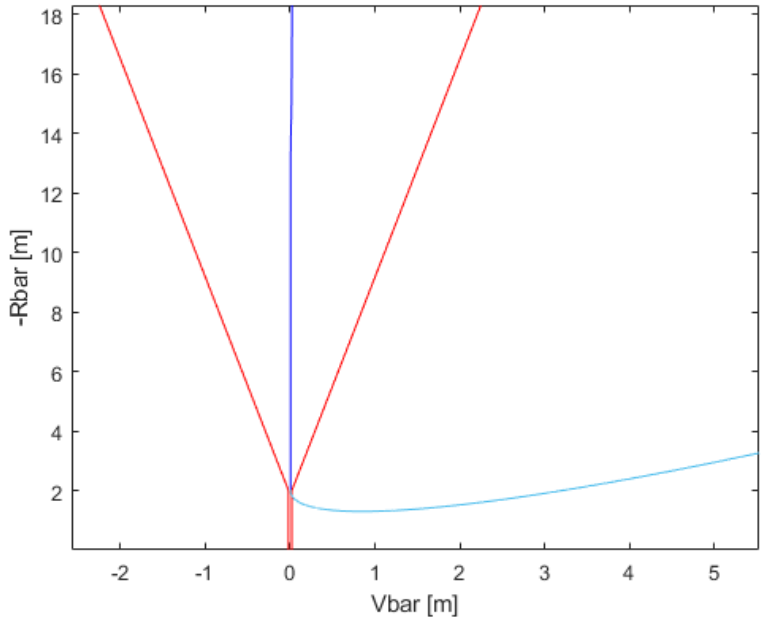

Figure 98 CAM close valve failure scenario from 2m in [V-bar, R-bar] plane

Considering the CAM started at the point of maximum velocity is at 40m, it has been demonstrated that the requirement that it must reach a minimum distance of 2 km and that it must be passive safe for at least 2 orbital periods is met . This can be seen in the Figure 99 and Figure 100.

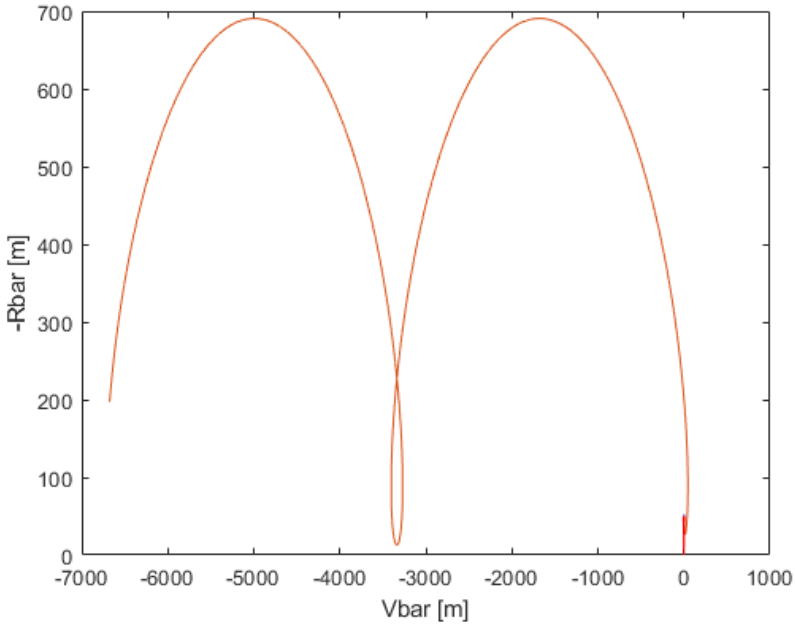

Figure 99 CAM in close valve scenario during two orbital period in [V-bar, R-bar] plane

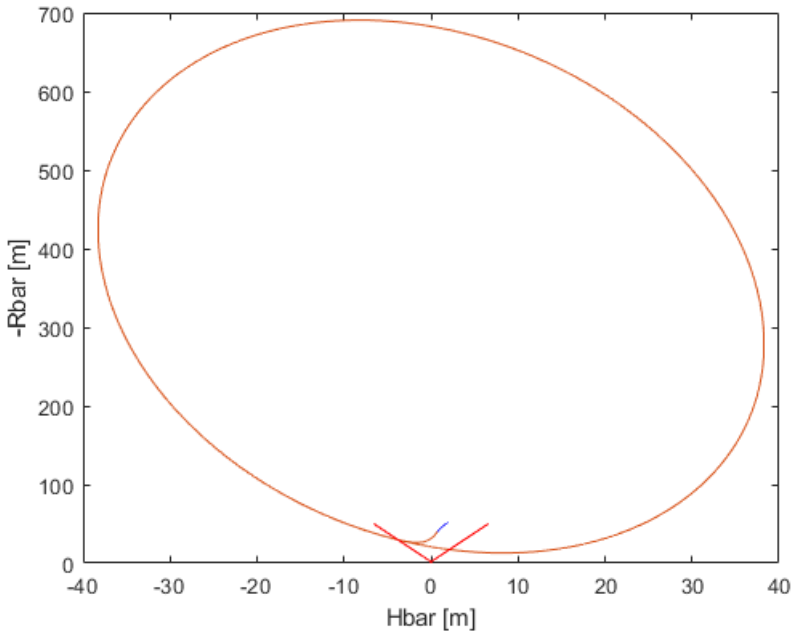

Figure 100 CAM in close valve scenario during two orbital period in [H-bar, R-bar] plane

5.2.3.3 Open Valve Failure Scenario

For the Open Valve Failure Scenario it can be done the same as for previous one. The highest velocities among those considered during the Monte Carlo analysis for all axes are considered such as to be more conservative.

Table 11 Initial conditions for CAM - Open Valve Failure scenario

	R-bar	**V-bar**	**H-bar**
Position [m]	52	2	2
Velocity [m/s]	-0.2	-0.03	-0.03
Mass [kg]	20		

The selected impulse collision avoidance manoeuvre is applied to different points of the trajectory, from 45 to 5 meters, with a step of 10m. In Figure 101 and Figure 102the CAMs are seen for the 10 minutes following their start. It is observed that the curves are lower than the previous ones. This is due to the higher velocities caused by the failures that oppose those of the escape manoeuvre.

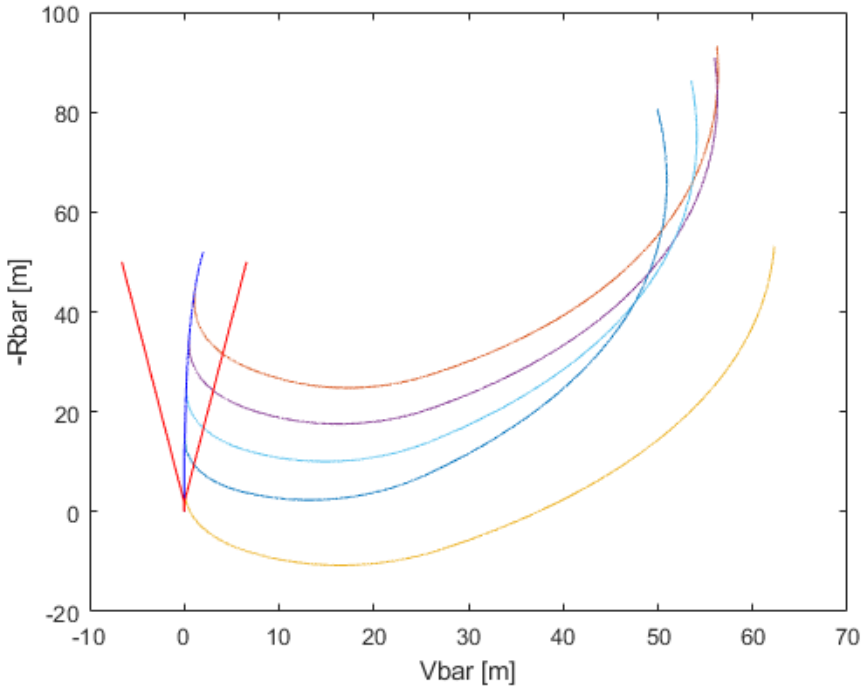

Figure 101 CAM open valve failure scenario in [V-bar, R-bar] plane

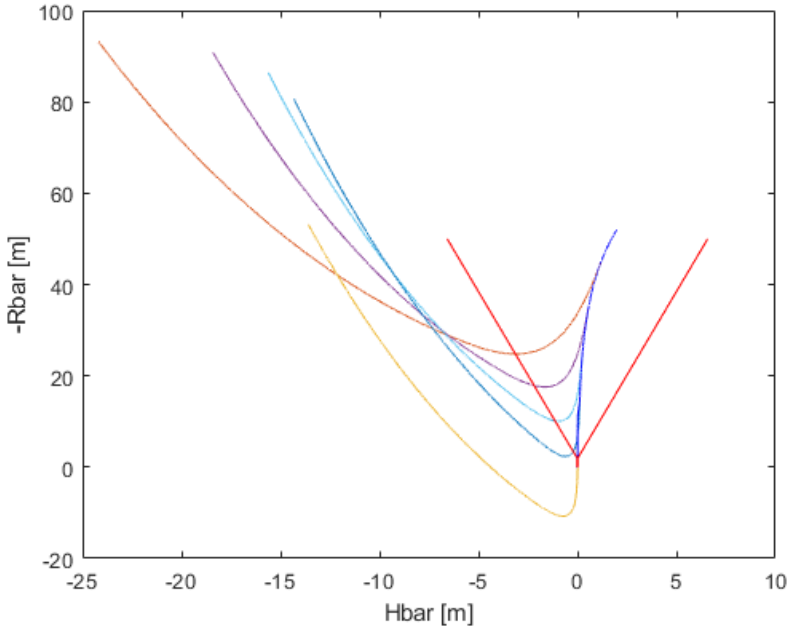

Figure 102 CAM open valve failure scenario in [H-bar, R-bar] plane

In this case, as can be seen, in this case the manoeuvre for distances on R-bar of 5m leads to a too slow departure which results in a collision. To avoid this situation without resorting to a re-tuning of the controller, different pulses have been tried. It is shown in Figure 103. In the instants immediately following the beginning of the CAM the behaviour is the same even for Delta-V much greater than those found

previously, because since the control impulse and consequently the actuation one last a certain period which must be high given the maximum thrust value available (i.e. 0.35 mN), the effects of the entire manoeuvre after a few tens of seconds.

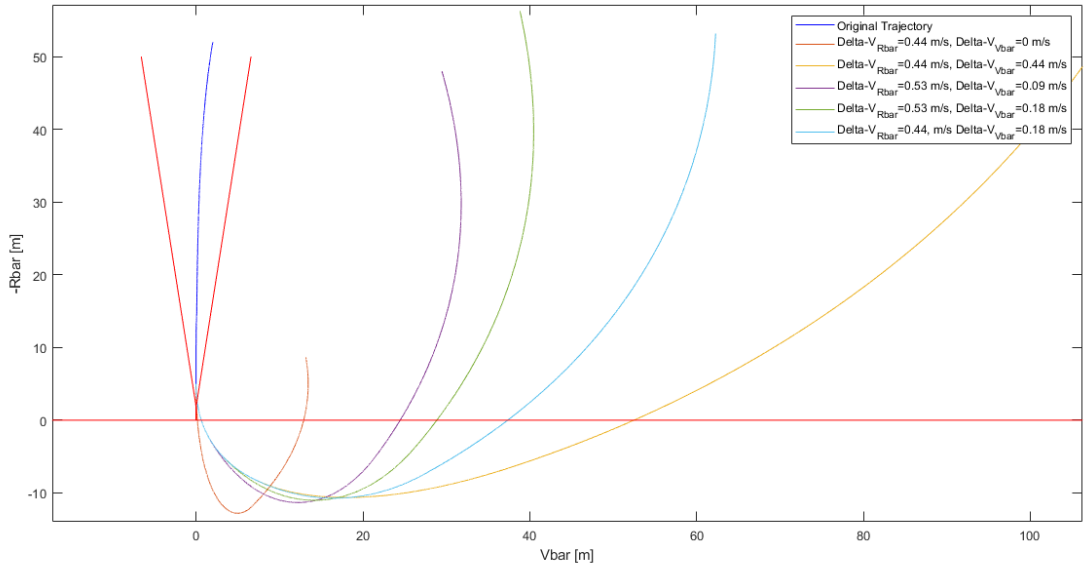

Figure 103 Different Delta-V manoeuvre in CAM open valve failure scenario at 5m

It should be noted that this is the worst condition in the case of open valve failure. In fact, it has been hypothesized that the failure occurs at 50m and that this is found only in the points examined. Therefore, in the case of CAM at 5m it was assumed that for 45m it is not detected. A more realistic case consists in the detection of the failure in a period closer to that in which it occurs. For example, it is assumed that it occurs at 10m and the system detects it at 5m. In Figure 104 and Figure 105 the results are shown.

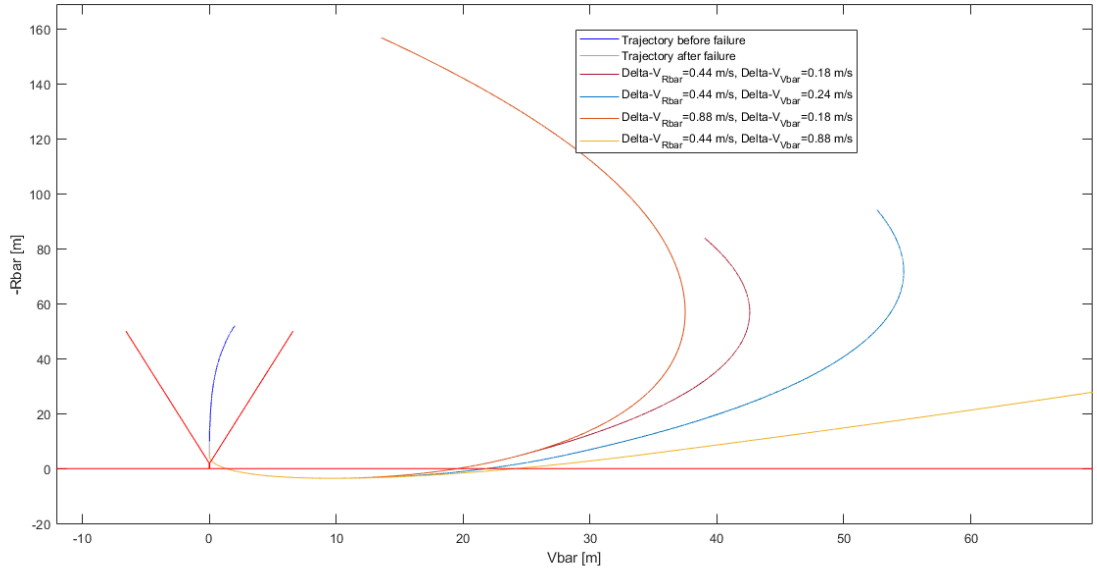

Figure 104 CAM open valve failure scenario, failure at 10m, CAM stats at 5m for different Delta-V in [V-bar, R-bar] plane

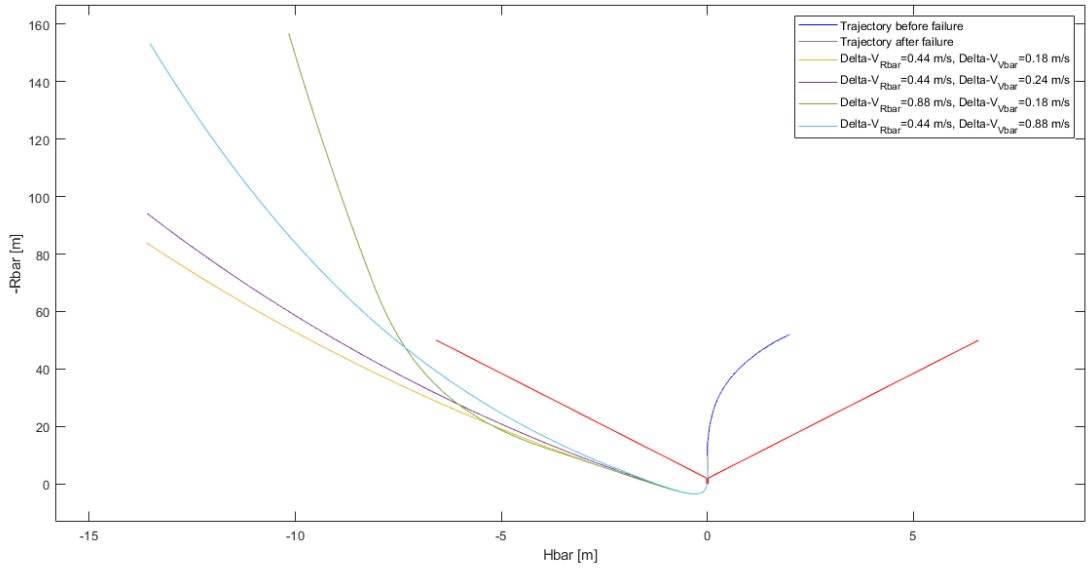

Figure 105 CAM open valve failure scenario, failure at 10m, CAM stats at 5m for different Delta-V in [H-bar, R-bar] plane

Even considering a more real case in which the failure occurs at 10m and the increase in velocity given by the opening of the valve which remains continuously open is identified at 5m is considerable, such that the Chaser at 5m has lateral velocities in the order of 10^{-5} m/ s but axial of -0.13 m / s. This means that the collision cannot be avoided at this distance.

5.2.4 24 hours Passive Safe Requirement

One of the requirements to be met for Collision Avoidance Manoeuvres is that the trajectory must be passive safe for at least 24 hours if a CAM is performed. In all the previous paragraphs this requirement has only been verified by considering two periods (i.e. about 3 hours) due to the computational cost, but it has been seen that the trajectory is formed by a string of loops towards the negative V-bar axis so this led to the assumption that the trajectory is passive safe for 24 hr. But this might not be true because of the aerodynamic resistance which, especially at the altitudes in question (i.e. 400 km) has a strong action causing the satellite to decay. This requirement has thus been verified using another software: STK. By simulating the same propulsion system as the one under study and the same initial conditions, it has been seen that the trajectory proceeds towards the negative V-bar axis, as had been demonstrated by the results of the analyses, and continues this motion for at least 24 hr.

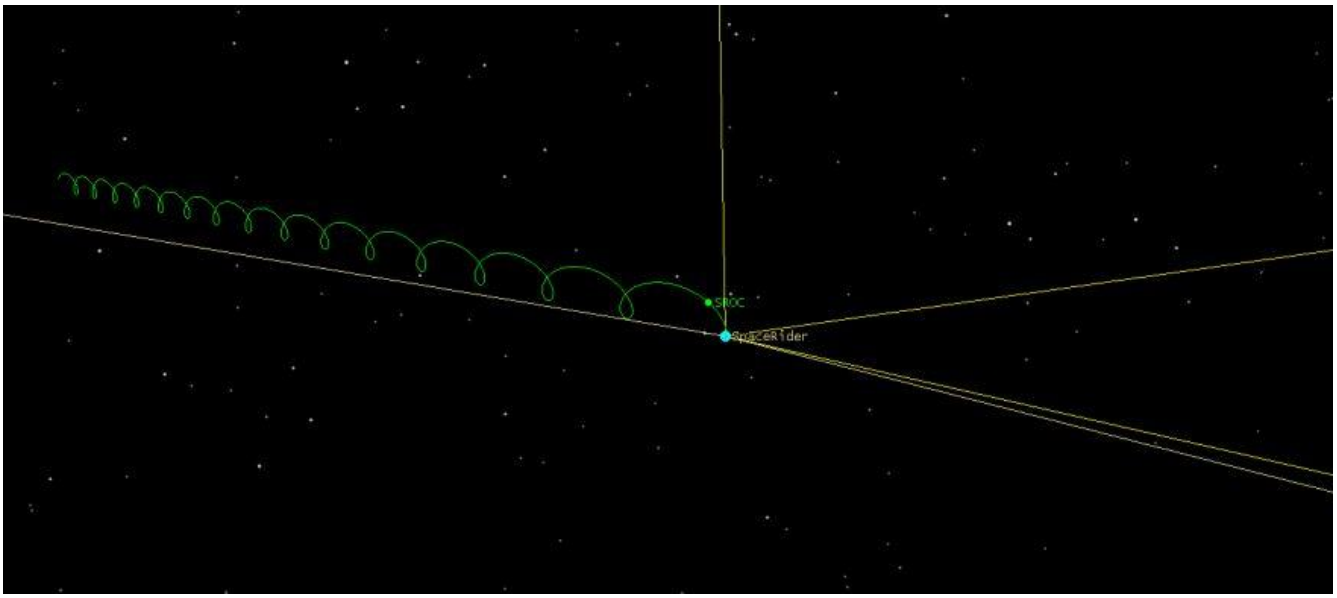

Figure 106 24 Hr Passive Safe Requirement Respected

5.2.5 Identification of alternative strategies

The search for a new strategy based on the designed one but which can improve it, derives from the results of the paragraph 5.2.2. It has been seen that in the worst-case scenario there is the impossibility to perform CAM below 20m (depending on the V-bar half-plane on which the cone is violated), and therefore the loss of safety for a third of the trajectory. Furthermore, all the results obtained for the other scenarios considered velocities greater than those that from the proposed requirement in Section 4.4.1.1 should have been at the beginning of the docking phase.

This leads to the identification of a different strategy. It has been said that this scenario is caused by the high velocities at the start of docking. Just as there is control over position through the cone constraint, one can consider control over the velocity profile. If at the entrance of the cone, i.e. at 50m, the velocity requirements are not met, the implementation of a CAM can be considered. This would have the advantage of increased

safety since there would not be the problem of not being able to perform CAM at close range to the Target (i.e. <20m) due to high velocities.

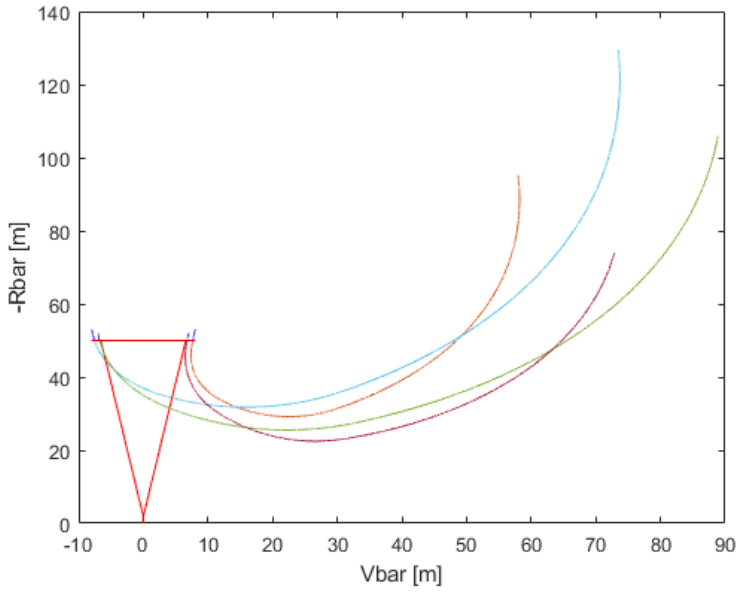

Figure 107 Alternative CAM strategy in [V-bar, R-bar] plane

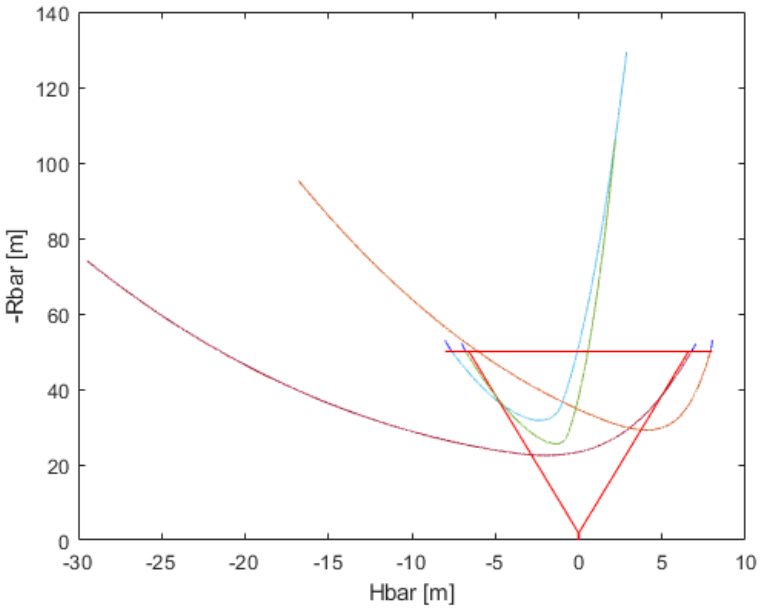

Figure 108 Alternative CAM strategy in [H-bar, R-bar] plane

Another solution could be to establish ranges of distances along R-bar in which different impulsive manoeuvres could be used. This would lead to a greater optimisation of resources and would be adaptable also to the case of navigation errors (within a certain range) since each position would fall in a range to which a unique CAM corresponds.

A further development could be to make CAM only partially open-loop. This could be done by dividing the manoeuvre into two phases, the first open-loop, like the ones analysed, which stops when the distance on R-

bar exceeds a threshold value (e.g. the distance at which the keep-out zone ends, in the case of SROC at 100m). From this point, if the type of failure or malfunction has been detected (even if not resolved), the trajectory may continue in a different way depending on the type of damage detected. If it also involves the GNC (failure in the navigation department, etc.) it is possible to proceed with the open-loop CAM as seen so far; if, instead, the GNC is entirely usable, it is possible to proceed with a close-loop trajectory based on a feedback control that can be, for example, the one used in the fly-around docking phase (not yet implemented in the system), for example an LQR or a simple PID. It is not recommended to use the NMPC in this case because the dynamics implemented in the controller plant on which the predictions are based is linearised, this is a simplification that cannot be used unless in the vicinity of the Target (a few meters).

an example of CAM divided into two phases has been performed. The first is an open-loop trajectory interrupted a distance greater than 100m and the second is a close-loop manoeuvre with a PID controller up to 2km.

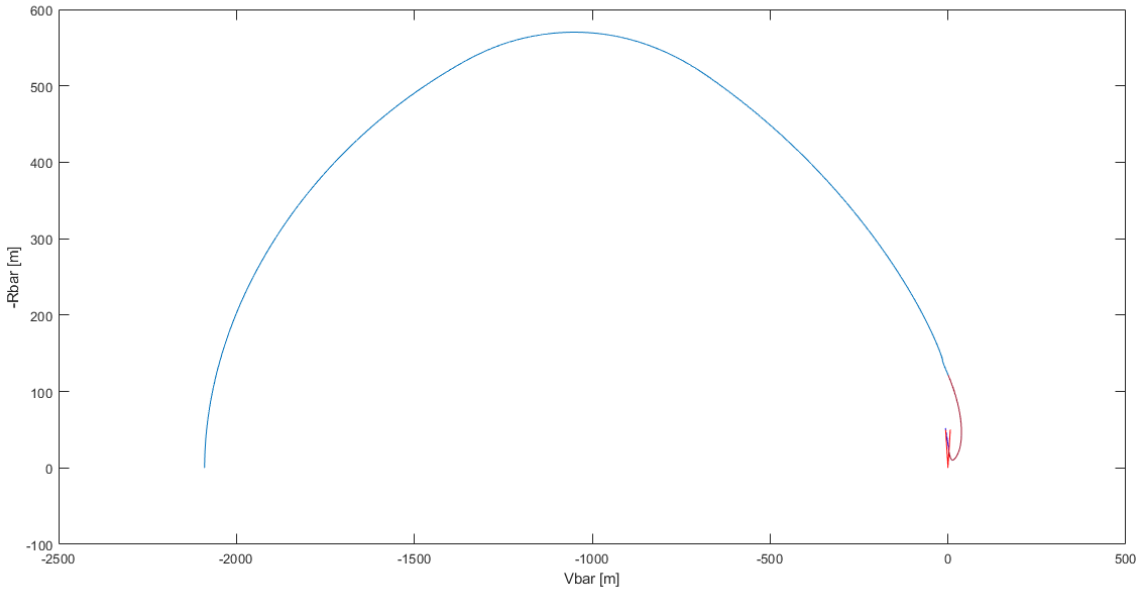

Figure 109 Close-loop CAM example

Finally, it should be noted that the simulations have been performed considering the maximum velocities to which the controller was subjected in the robustness analysis, to consider worse conditions.

6 Conclusions

The purpose of this study was to obtain a guidance and control model capable of performing a docking manoeuvre in accordance with the requirements under nominal conditions and in the presence of a failure. Furthermore, an automatic collision avoidance system has been implemented to perform escape manoeuvres in the event of a violation of the trajectory constraints or in any other event that compromises spacecraft safety.

The first part has assessed the capabilities of the orbital controller based on the Nonlinear Predictive Model. A set of optimal parameters has been identified in order to obtain an excellent control of the trajectory during the last meters of the approach. A set of Monte Carlo analyses demonstrated the robustness of the controller in the nominal scenario and the compliance with the requirements on the final position, velocity and trajectory constraint even in the event of disturbances.

In the presence of a failure, oscillations of the trajectory occur even if compensating actions are implemented. Therefore, a requirement on initial velocities has been established such that the constraints imposed can be respected and docking can be achieved even with a failed thruster.

Therefore, a requirement on the initial velocities was established such that, if respected, docking can occur even with a failure of the propulsion system. It has also been observed that a minimum axial velocity requirement may also be necessary at the start of docking so that the trajectory, again in the event of failure, has an axial profile without oscillations. Nevertheless, due to the decreased performance of the propulsion system in the event of a thruster failure, the duration of the manoeuvre increases. In this scenario escape manoeuvres may be necessary if the best illumination and coverage for communications with ground station.

The second part of the thesis focused on collision avoidance situations. In particular, two studies have been conducted. The first one concerns thruster shutdown in the last meters of the trajectory to avoid exhaust plumes fouling the other payloads of the mothercraft. In this regard, it has been demonstrated that the lateral misalignment constraint is always fulfilled for distances less than or equal to 1m. This makes coupling possible through a magnetic or mechanical mechanism. It was also observed that increasing the thruster shutdown distance increases the velocity at the mating point, therefore the lateral misalignment requirement is met for distances less than 0.7m. When the coupling mechanism will be definitively chosen a trade-off can be performed to choose whether to turn off the thrusters at greater distances from the Target but also accepting higher contact velocities and therefore higher energies released at the impact or instead maintain the current requirements.

Finally, Collision Avoidance Manoeuvre has been studied. Starting from the identification of the worst-case in which it may occur, the manoeuvre has been designated in order to be easily executable and to require the minimum number of subsystems involved. The Collision Avoidance Manoeuvre performance has been evaluated under nominal conditions, thruster failure events, and safety constraint violations showing that it can be performed up to distances greater than 5m from the Target because of an increase in the axial velocity makes the manoeuvre less performant around this distance. Several strategies have been studied to improve the model. A possibility could be to combine the constraint on the trajectory with an additional one on the velocity profile or considering a close-loop system to be enabled if the failure does not affect the operation of the GNC. All these strategies can be explored further in the future of the project.

7 Reference

[1] J. R. Kopacz, R. Herschitz, J. Roney, Small satellites an overview and assessment, Acta Astronautica, Volume 170, 2020, Pages 93-105, https://doi.org/10.1016/j.actaastro.2020.01.03 4.

[2] Nichele, F., Villa, M. and Vanotti, M. (2018), "Proximity operations - autonomous space drones", in Proceedings of the 4S Symposium, May, Sorrento (Italy)

[3] Corpino S., Stesina F. (2020), Inspection of the cis-lunar station using multi-purpose autonomous Cubesats, Acta Astronautica, Volume 175, 2020, Pages 591-605, https://doi.org/10.1016/j.actaastro.2020.05.053 .

[4] Nastasi K., Thomas D., Tetreault K., Elliott I., Black J., Real-Time Optimal Control, & Tracking of Autonomous Micro-Satellite Proximity Operations, AIAA SPACE 2016 13 - 16 September 2016, Long Beach, California, https://doi.org/10.2514/6.2016-5617

[5] Richard-Noca, M. et al. (2016), "Developing a reliable capture system for Cleanspace one", in Proceedings of the International Astronautical Congress, Guadalajara, September

[6] S Corpino, F Stesina, D Calvi, L Guerra, (2020), Trajectory analysis of a CubeSat mission for the inspection of an orbiting vehicle, Advances in aircraft and spacecraft science, Vol 7(3), pp 271-290, https://doi.org/10.12989/aas.2020.7.3.271

[7] C. Pirat, F. Ankersen, R. Walker, V. Gass, (2018), Vision Based Navigation for Autonomous Cooperative Docking of CubeSats, Acta Astronautica, Volume 146, 2018, Pages 418-434, https://doi.org/10.1016/j.actaastro.2018.01.059.

[8] R. Opromolla, G. Fasano, G. Rufino, M. Grassi, A review of cooperative and uncooperative spacecraft pose determination techniques for close-proximity operations, Progress in Aerospace Sciences, Volume 93, 2017, Pages 53-72, https://doi.org/10.1016/j.paerosci.2017.07.001.

[9] F. Sansone, A. Francesconi, L. Olivieri and F. Branz, "Low-cost relative navigation sensors for miniature spacecraft and drones," 2015 IEEE Metrology for Aerospace (MetroAeroSpace), 2015, pp. 389-394, hhttps://doi.org/10.1109/MetroAeroSpace.2015.7180688.

[10] F. Branz, L. Olivieri, F. Sansone, A. Francesconi, (2020), Miniature docking mechanism for CubeSats, Acta Astronautica, Vol. 176, pp 510-519, https://doi.org/10.1016/j.actaastro.2020.06.042

[11] V. P. Legostayev and I. P. Shmyglevskiy, "Control of space vehicles rendezous at the stage of docking," Automatica, vol. 7, no. 1, pp. 15–24, Jan. 1971. [Online].
Available: http://www.sciencedirect.com/science/article/pii/0005109871900756

[12] H. Park, S. Di Cairano, and I. Kolmanovsky, "Model predictive control of spacecraft docking with a non-rotating platform," IFAC Proc. Volumes, vol. 44, no. 1, pp. 8485–8490, 2011. [Online].
Available: http://www.sciencedirect.com/science/article/pii/S1474667016449736

[13] Q. Li, J. Yuan, B. Zhang, and C. Gao, "Model predictive control for autonomous rendezvous and docking with a tumbling target," Aerospace Science and Technology, vol. 69, pp. 700–711, Oct. 2017. [Online].
Available: http://www.sciencedirect.com/science/article/pii/S1270963817301293

[14] Yang H. (2021) Manned Rendezvous and Docking Technology. In: Manned Spacecraft Technologies. Space Science and Technologies. Springer, Singapore. https://doi.org/10.1007/978-981-15-4898-7_6

[15] Copot, C.; Muresan, C.I.; Beschi, M.; Ionescu, C.M. A 6DOF Virtual Environment Space Docking Operation with Human Supervision. Appl. Sci. 2021, 11, 3658. https://doi.org/10.3390/app11083658

[16] R. Murtazin, N. Sevastiyanov, N. Chudinov, Fast rendezvous profile evolution: From ISS to lunar station, Acta Astronautica, Volume 173, 2020, Pages 139-144, https://doi.org/10.1016/j.actaastro.2020.04.032

[17] Arantes Jr. G., Komanduri A., Martins Filho L. S. (2011), "Guidance for rendezvous maneuvers involving non-cooperative spacecraft using a fly-by method," in Proceedings of 21st International Congress of Mechanical Engineering, Natal, Brazil, October

[18] S. Ueda and A. Noumi, "Precise Rendezvous Guidance in Low Earth Orbit via Machine Learning," 2019 SICE International Symposium on Control Systems (SICE ISCS), 2019, pp. 27-32, doi: 10.23919/SICEISCS.2019.8758738.

[19] Li, Peng, Zheng H. Zhu, and S. A. Meguid. (2016) "State dependent model predictive control for orbital rendezvous using pulse-width pulse-frequency modulated thrusters." Advances in Space Research. DOI: 10.1016/j.asr.2016.04.022

[20] Di Cairano, S. Park, H. Kolmanovsky (2012) "Model Predictive Control Approach for Guidance of Spacecraft Rendezvous and Proximity Maneuvering", *Int. Journal of Robust and Non Linear Control*, vol 22, DOI: 10.1002/rnc.2827

[21] Corpino, S. et al. (2017) “Control of a Noncooperative Approach Maneuver Based on Debris Dynamics Feedback”, Journal of Guidance, Control, and Dynamics, 41(2), pp. 431–448. doi: 10.2514/1.G002685.
[22] Calafiore G., Fagiano L., “Robust model predictive control via scenario optimization”, IEEE Tran. Autom Control, vol 58, no 1, pp 219- 246, Jan 2013
[23] Bowen J., Villa M., Williams A. (2015), CubeSat based Rendezvous, Proximity Operations, and Docking in the CPOD Mission, In proceedings of Small Satellite Conference Logan, Utah August
[24] C. Pirat, F. Ankersen, R. Walker and V. Gass (2020), "H-infinity and mu-Synthesis for Nanosatellites Rendezvous and Docking," in IEEE Transactions on Control Systems Technology, vol. 28, no. 3, pp. 1050-1057, doi: 10.1109/TCST.2019.2892923.
[25] M. Mammarella et al. (2020), "An Offline-Sampling SMPC Framework With Application to Autonomous Space Maneuvers," in IEEE Transactions on Control Systems Technology, vol. 28, no. 2, pp. 388-402, doi: 10.1109/TCST.2018.2879938.
[26] CubeSat Market by Size (0.25U to 1U, 1 to 3U, 3U to 6U, 6U to 12U, 12U and Above), Application (Earth Observation & Traffic Monitoring, Science Technology and Education, Space Observation, Communication, and Others), End User (Government and Military, Commercial, and Non-profit Organizations), and Subsystem (Payloads, Structures, Electrical Power Systems, Command and Data Handling, Propulsion Systems, Attitude Determination and Control Systems, and Others): Global Opportunity Analysis and Industry Forecast, 2020–2027. https://www.alliedmarketresearch.com/cubesat-market-A09399
[27] W.Fehse, “Automated Rendezvous and Docking of Spacecraft”.

Acknowledgements

A few years ago, reading an in-depth study of the Space Shuttle's thermal protection system for “materials for aerospace applications” course, I fell in love and decided that I would continue my study in space subjects. A few years later, I have been the opportunity to participate in this thesis project and be a member of the SROC Mission. I would like to thank my supervisors Sabrina Corpino and Fabrizio Stesina for the opportunity to take part in this project and for all that I have learnt from working with them.

I would also like to thank my all family and particularly to my mother for her patience and tenacity, the friends who have been close to me, from near and far, and above all the person who has supported me the most along this journey, my partner in adventures and my love.